Charles University in Prague
First Faculty of Medicine

Study program: Biomedical Informatics

Mgr. Pavel Šanda

Information processes in neurons

Informační procesy v neuronech

PhD Thesis

Thesis advisor: Doc. RNDr. Petr Lánský DrSc.
Institute of Physiology,
Academy of Sciences of the Czech Republic

Prague, 2012

Declaration

I declare that I have written this thesis on my own and listed all used sources. I also declare that the work has not been used to obtain another or the same university degree. I agree with the permanent archiving of the electronic version of the thesis in the database project Theses.cz in order to allow systematic similarity check of the qualification works.

Prohlášení

Prohlašuji, že jsem závěrečnou práci zpracoval samostatně a že jsem řádně uvedl a citoval všechny použité prameny a literaturu. Současně prohlašuji, že práce nebyla využita k získání jiného nebo stejného titulu.

Souhlasím s trvalým uložením elektronické verze mé práce v databázi systému meziuniverzitního projektu Theses.cz za účelem soustavné kontroly podobnosti kvalifikačních prací.

V Praze, 26.6.2012

Pavel Šanda

Identification Record

SANDA, Pavel. Information processes in neurons. Prague, 2012. 76 pages. PhD Thesis. Charles University in Prague, 1st Faculty of Medicine, Dept. of Computational Neuroscience FGU AS CR. Supervisor Petr Lansky.

Identifikační záznam

ŠANDA, Pavel. Informační procesy v neuronech. [Information processes in neurons.] Praha, 2012. 76 stran. Dizertační práce. Univerzita Karlova v Praze, 1. lékařská fakulta, Oddělení početních neurověd FGÚ AVČR. Vedoucí práce Petr Lánský.

I would like to thank my supervisor Petr Lansky for the support he provided during all the research. My thanks go also to Petr Marsalek for all his help.

I am also grateful to various institutions in Prague and abroad which allowed me to stay and perform the research work.

The thesis is based on 5 published papers (detailed in the section *List of publications* on page 38), the following chapters give extended introduction and context for the whole work.

Information processes in neurons

Contents

List of Abbreviations

IF integrate-and-fire model

LIF leaky integrate-and-fire model

ISI Interspike interval

ITD interaural time difference

MSO medial superior olive

CN cochlear nucleus

L/MNTB lateral/medial nucleus of trapezoid body

1 Introduction

Starting with the work of Santiago Ramón y Cajal, neuronal cells in the brain were recognized as independent units which communicate via the contact of axons to dendrites and the body of nerve cells, and create neuronal circuits through branching of their fibers (Ramon y Cajal, 1899), English translation Ramon y Cajal (1995).

Simultaneously to Cajal's morphological findings, a larger group of scientists discovered the existence of action potentials (impulses, spikes) traveling through nerve fibers. Since these impulses are similar in duration and shape, this naturally lead to the binary all-or-none concept. As part of what would be later called the *neuronal doctrine,* Cajal proposed unidirectional transmission of nerve impulses from dendrites through soma to axon and called it the law of dynamic polarization.

In the same way as Cajal postulated the neuron as a basic anatomical unit, McCulloch and Pitts postulated the neuron as a basic unit of information processing and used the all-or-none concept for modeling nervous activity on the basis of logical calculus. In their seminal work a formal model of the neuron was formulated and it was even indicated that a network of such formal neurons is Turing-complete (McCulloch and Pitts, 1943).

With experimental research developing, such level of formal description of information processing in a neuron was no more adequate. No later than in 1959 it was observed that many electrical events on the membrane are of a continuous nature and that there exists some background spontaneous activity (Bullock, 1959). The following decades added new findings, which were either beyond neuronal doctrine or even contradicting it and the whole picture became more complicated (Bullock et al., 2005). Similarly the question *where* and on *which scale* (or level of description) information processing takes place became problematic. For example glia cells were found to communicate with each other via transmitters and gap junctions (Fields and Stevens-Graham, 2002), chemical synapses between glia cells and neurons were found as well (Bergles et al., 2000). Thus, it is possible that there is parallel information processing going on at slower time scales.

1.1 Level of description

Another ambiguity stems from the choice of the proper level of description. We can distinguish the level of large neural networks, simple circuits, individual neurons, the sub-cellular level, membranes and the underlying biochemistry. Traditionally the community around artificial neuronal networks does not use a detailed description of neurons and is satisfied with abstract models not much different from the original McCulloch-Pitts neuron. This abstraction would be hardly acceptable for the community studying the features of single neurons and their membrane for its drastic simplification since it would be impossible to mimic many of the effects observed in physiological experiments. However, it does not automatically follow that a more detailed description opens up a better understanding of the system as a whole.

One such example is Hopfield's work on the neural network for content-addressable memory (Hopfield, 1982). According to the critics of this paper, the neurons should have continuous input-output relations, moreover real neurons and circuits have integration time delays due to the capacitance of the neuronal membrane. Therefore, the time evolution of the state of such systems should be represented by a continuous time representation. In his response Hopfield showed that the important properties of the original model remain intact when these two simplifications of the model are eliminated (Hopfield, 1984).

On the other hand, a more detailed model can completely change the way how information processing is implemented. For example in order to compute a certain formula from logical calculus, the classical McCulloch-Pitts approach needs to assemble a circuit from neurons in a similar fashion as when logical gates are assembled in modern digital computers. However, when we stop to look at a neuron as a simple one-point integrator of incoming signal and make a detailed model of a branching dendritic tree, we get a very different picture of possible computations within a single neuron only. Decomposing the dendritic tree of the neuron into subunits (Koch et al., 1982) shows that the combination of a specific branching topology,

and the precise timing of excitatory and inhibitory inputs implements the approximation of logical gates (AND NOT, OR, AND) and even multiplicative arithmetical operations. Since all logical operations can be defined via AND and AND NOT gates, any logical operation can be synthesized by local circuits consisting of synapses between the dendrites of two or more neurons (Koch et al., 1983).

However, the discussion about the level of detail and precision in the modeling of information flow inside the nervous system does not necessarily end at the level of membrane biophysics. In a series of papers Hjelmfelt showed that even enzymatic reactions inside cells can be interpreted as information processing and he also showed that it is possible to construct a universal Turing machine based on such reactions (Hjelmfelt et al., 1991; Hjelmfelt and Ross, 1992, 1993).

While the advantages of a more detailed description are clear, there is also a price to be paid. Firstly, more details of the model usually require more parameters and it is often hard or even impossible to obtain such parameters from experimental setup. Secondly, a more detailed description might be intractable from a mathematical point of view, and no deeper insight about the dynamics of the system can be obtained. Thirdly, when we are interested in dynamics of large scale networks, the simulation of detailed models can be very demanding on the computational power.

To sum up, there is no "proper" level of description unless we take into account the aim and context of the study. In the rest of the text we will have a look at the class of simplified models of the neuronal membrane. Then we will inquire into possible encoding schemes of the action potential sequences ("*spike-trains*") generated by the neurons (or by their models respectively). Finally we will focus on the problem of spatial hearing and the different neuronal coding mechanisms used to explain animal sensitivity of sound localization.

2 Integrate and Fire neuronal model

2.1 Types of Integrate and fire model

Three basic types of models of a single neuron can be distinguished - digital (all-or-none) and continuous, which can be subsequently modeled either as a single point in a space or with more unit compartments simulating morphology of the real neuron and its branching structure (Segev, 1992). We shall focus on the single-point continuous models only.

Generally, the family of continuous models is described by an electrical circuit representing the iso-potential patch of a membrane. The simplified model of a neuron membrane as an electrical circuit consisting of capacitor with leak was first proposed by Lapicque (1907), translation and review Lapicque (2007); Brunel and van Rossum (2007). It was, however, before the mechanisms of the action potential firing were understood and the first formulations of the whole *leaky-integrate-and-fire* (LIF) model appeared later (Stein, 1965; Knight, 1972).

The most simple version of the model circuit consists of capacitor C only (representing lipid layers of the membrane) and is called *perfect integrator* (Koch, 2005). Membrane voltage $V(t)$ can be written in this case as

$$C\frac{dV(t)}{dt} = I(t)\,, \tag{1}$$

where $I(t)$ represents the current from synaptic input at time t (or intracellular electrode). The spiking mechanism is missing in this model and it is usually described just as a complete reset after certain voltage threshold S is reached; switch through which the accumulated voltage is discharged would implement such behaviour inside electrical circuit.

If the neuronal membrane consists only of a twofold lipid layer, the voltage would increase no matter how slowly the incoming current arrives since the membrane functions as a perfect insulator. In biological reality the membrane contains also proteins which form specific channels through which various ions can flow and leak the charge. In such case the voltage on the membrane does not integrate as above and additional resistor R

implementing this leakage is added in parallel to capacitor in the electric circuit thus forming *leaky-integrate-and-fire* (or *forgetful*) model. The current through the resistor follows Ohm's law and the equation (1) can be rewritten as

$$C\frac{dV(t)}{dt} + \frac{V(t)}{R} = I(t)\,. \tag{2}$$

Again, the voltage is integrated in subthreshold regimen (see section 2.2) and once threshold S is reached, voltage is reset to its initial value and integration starts anew.

Specific integrate-and-fire (IF) models which employ spike generation as integral and emergent part of the model have been proposed, for example by Fitzhugh (1961) who suggested simplification of the Hodgkin-Huxley model (see below) and Nagumo et al. (1962) who formulated a corresponding electronic circuit. The system is described by two coupled differential equations and its advantage compared to the Hodgkin-Huxley model is that the mathematical properties can be understood quantitatively.

Because of the random nature of incoming synaptic signal, a stochastic version of integrate-and-fire model has been developed. Initial work was done by Gerstein and Mandelbrot (1964) who used random walk to mimic excitatory and inhibitory input pulses. The random walk counterpart of the leaky model has been formulated by Stein (1965, 1967). Subsequently, a continuous model can be obtained as a limit case thus obtaining *Ornstein-Uhlenbeck* model (Uhlenbeck and Ornstein, 1930; Ricciardi and Sacerdote, 1979), which can be written as the equation

$$C\frac{dV(t)}{dt} + \frac{V(t)}{R} - C\sigma\xi(t) = I(t)\,, \tag{3}$$

where ξ represents white noise from the synaptic input and σ its variability.

A plethora of integrate-and-fire model variants can be found in a recent review of Burkitt (2006a,b).

As a side note we shall remember that apart from the phenomenological models above, more biologically plausible models exist including a channel based biophysical description. Outstanding among there is the description

by Hodgkin-Huxley who formulated their model after a long series of experiments on the giant squid axon (Hodgkin and Huxley, 1952). Total membrane current I can be written as a sum of ionic currents on the membrane and capacitave current

$$C\frac{dV(t)}{dt} + I_{Na}(t) + I_K(t) + I_{leak}(t) = I(t)\,, \tag{4}$$

where the sodium I_{Na} and potassium I_K ionic currents are determined by the driving potential via Ohm's law. For a full description of the equations left and its parameters see Hodgkin and Huxley (1952). While being closer to the physiological reality, the Hodkgin-Huxley model cannot be analyzed analytically, has lots of parameters and its simulations require high computational resources. On the other hand, simplified IF models are both easier to analyze and simulate, fewer parameters are needed to be estimated from the data.

2.2 The parameters of LIF

Because IF models have been widely employed in neuronal modeling, there is always question whether these models are sophisticated enough to mimic the behaviour of biological neurons (Feng, 2001). Despite of wide usage of IF models in the theoretical literature there has never been an attempt to check IF models accuracy and assumption against intracellular recordings of the membrane voltage (the traditional attempts were more focused on the interspike intervals (ISI) statistics obtained from extracellular recordings). In a couple of papers we compared *in-vivo* intracellular neuronal recordings and stochastic variant of LIF model (3)

$$\frac{dV(t)}{dt} = -\beta(V(t) - x_0) + \mu + \sigma\xi(t),\, V(0) = x_0 \tag{5}$$

with few modifications, namely we assume that input μ is constant in time and the process starts at the resting level x_0. The (constant) parameters C, R form the so-called membrane time constant $\tau = RC$, which we use here inversely as $\beta = \frac{1}{RC}$ to conform with notation used later in our work

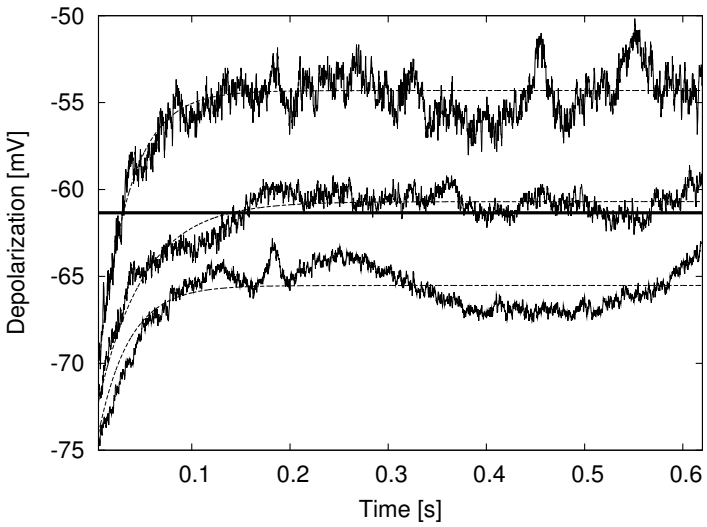

Figure 1: Three basic regimes of neuronal firing. From top to bottom we successively see the schematic evolution of a membrane potential in the suprathreshold/threshold/subthreshold regimen. Spike generation upon reaching the threshold S (thick solid line) is not considered. Thin dotted lines converge to asymptotic mean depolarization. We can see that in case of subthreshold regimen additional noise is the only way how the membrane potential can reach the threshold.

and let the reader directly delve into it. As in other LIF models spike is not intrinsic part of description and membrane potential is reset to x_0 whenever $V(t)$ reaches the threshold S.

Parameters of such model are traditionally divided into those, which depend on membrane properties (β – inverse of the membrane time constant, S – threshold, x_0 – resting level) and those, which depend on the input signal (μ – mean signal, σ – signal variability).

The asymptotic mean depolarization derived from (5) as $E(V(\infty)) = x_0 + \mu/\beta$ determines three regimes of neuronal firing (see Fig. 1):

- the subthreshold regimen ($\mu/\beta \ll S - x_0$) with Poissonian firing. As the asymptotic mean depolarization does not reach the threshold the firing depends on the noise and without it the neuron would remain silent.

- the threshold regimen ($\mu/\beta \approx S - x_0$), where the distribution of ISIs is positively skewed and resembles for example Gamma distribution.

- the suprathreshold regimen ($\mu/\beta \gg S - x_0$), where the firing is almost regular and ISI histogram resembles normal distribution. The noise plays a limited role in this range of parameters.

Initially, in Lansky et al. (2006), we obtained parameters and compared different estimation methods for the spontaneous part[1] of the recordings and checked basic assumptions of the model. We found, that in general the data are consistent with the model. The spontaneous part is in subthreshold noise-driven regimen and ISIs are exponentially distributed, which suggests they are generated in accordance with Poisson process. There were, however, also inconsistencies with the model. The model assumes that spectra of the input signal should be flat, while we found characteristic hump around the frequency of 2200 Hz in data, which was subsequently eliminated by filtering. Next, the subthreshold regime requires the asymptotic depolarization far below the threshold. In our case the asymptotic threshold is below the threshold, but it is less than two-standard-deviations envelope. The model also assumes a fixed value of the reset depolarization x_0, which did not hold, the effect of this discrepancy for the model performance is negligible, however.

In the second analysis (Lansky et al., 2010), we compared activity and estimated parameters for spontaneous and stimulated part of the recordings and discussed their firing regimes. The simulation based on the estimated parameters fits well with the course of the membrane depolarization (see Fig. 2). The parameters dependent on the input signal μ and σ were larger than in spontaneous part and the overall firing regimen is suprathreshold as expected. Despite the assumptions that x_0 is not dependent on input signal our data shows that its value is actually influenced by the stimulation.

To summarize, external stimulation affects input parameters and thus

[1]The recordings contained spontaneous activity of the neurons in auditory pathway and stimulated activity triggered by acoustic signal.

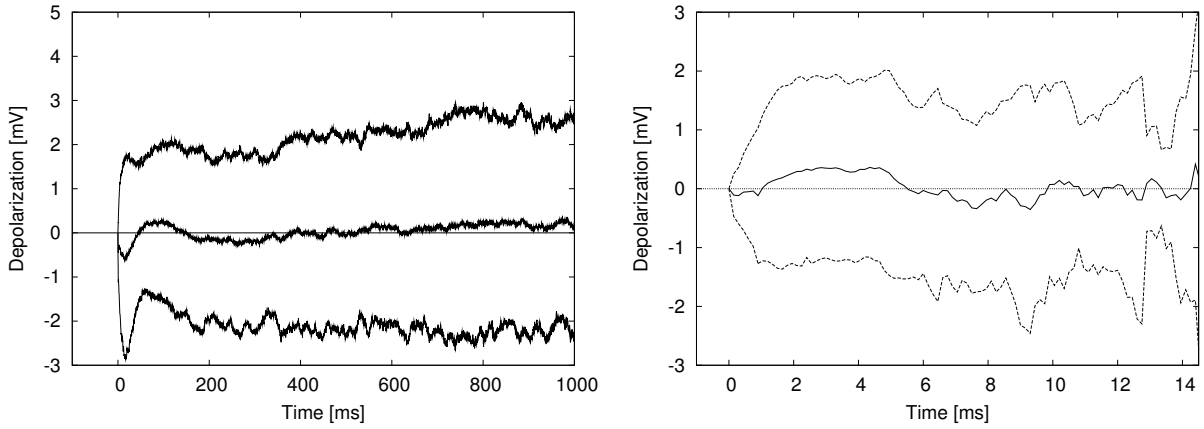

Figure 2: The accuracy of the model simulation compared with the recorded data. The simulation of the model (5) used parameters estimated from the data. The middle line shows the mean difference of the membrane potential between simulations and experimental recordings, while the surrounding lines are 2 standard-deviations envelope. In ideal case we would obtain flat line at 0. Left panel is comparison of the spontaneous part of the record, right panel shows comparison of (acoustically) stimulated part of the record. Different time axis is due to the fact that stimulation brings the neuron to the suprathreshold regime where interspike intervals are much shorter.

time evolution of membrane voltage in (5) and it has direct consequence on the ISI statistics, since the stimulated intervals will be generally much shorter.

The currently dominating opinion is that for neural coding is important just occurrence of the spike (in time), neither its shape nor the membrane evolution between spikes. From this point of view, the evolution details of the membrane potential are not important, what matters is the time when the potential reaches the threshold for firing and the question is whether such simplified models can reliably predict occurrence of spiking times. The ability to predict spiking behaviour has been shown for particular types of neurons in this class of models (Kistler et al., 1997; Keat et al., 2001; Jolivet et al., 2006; Kobayashi et al., 2009). It needs to be emphasized that in order to strengthen the predictive power of spiking models, the dynamics of threshold was included in the IF description, see (Jolivet et al., 2008a,b).

3 Neural code

3.1 Types of neural code

Let us now abstract from the underlying spiking mechanisms and focus only on the resulting sequence of spikes. Such spike train is often considered as a code through which information is conveyed across the neural system. Beginning with the pioneering work of Lord Adrian who showed the relation between the frequency of spikes of frog muscle receptors and the stretching the muscle with different weights (Adrian and Zotterman, 1926), the idea of firing *rate code* became the textbook model of neural coding.

This idea suggests that there is continuous function $f(t)$ according to which resulting spike train is produced, more precisely $p = \int_{t_0}^{t_0+\Delta t} f(t)dt$ determines the number of spikes expected to occur in the interval $[t, t+t_0]$. In case Δt is sufficiently small so that $p \leq 1$ we can interpret p as a probability that the spike occurs in $[t, t+t_0]$. Of course such rate function is not directly visible and we experimentally observe only realization of spikes sampled from f. The conventional way of estimating such background rate

function is recording multiple trials with identical stimuli and average the rate over all recorded trials into post-stimulus time histogram (PSTH, Gerstein and Kiang (1960)). Another approach which has the advantage of creating smooth function even for single recorded trial is kernel smoothing (Nawrot et al., 1999).[2] In this method the spike train is convolved with kernel of a particular shape (usually gaussian one) and (band)width. Common problem of both PSTH and kernel based method is ad-hoc choice of the histogram bin-size/kernel bandwidth which results in different firing rate estimates. In series of papers Shimazaki and Shinomoto (2007, 2010) suggested method for determining optimal width, based on the assumption that the underlying spike generation process is Poissonian. We employed the kernel optimization method for the analysis of experimental recordings of olfactory neurons and found it computationally demanding. In order to speed up the bandwidth determination we analyzed the algorithm and transformed it into the parallel one which thanks to its speed-up in the supercomputer environment allowed online interactive work with the data. The details are covered in Šanda (2010), the analysis of the data was not yet published.

The relationship between the mean firing rate and stimulus intensity has been established (Fuortes, 1958; Matthews, 1964; Grüsser et al., 1968), more recent examples of firing rate codes are from the monkey visual cortex neurons, where the spike count correlates with motion discrimination performance (Britten et al., 1992; Celebrini and Newsome, 1994) or stimulus identity (Desimone et al., 1984). For some time it was assumed that such code captures all relevant information because the firing-rate coding scheme was robust against unreliability and noise observed in neuronal activity. Later decades brought experimental findings which showed that what was often considered as erratic behaviour (McCulloch, 1959) was rather misunderstanding of the code transmitted (Barlow, 1972) and neurons can be thought as a reliable unit of transmission – as an outstanding example Sakitt

[2]There is a group of methods employing Bayesian inference for the firing rate estimation which we will not pursue here. For recent review and comparison of various methods see Cunningham et al. (2009).

(1972) showed that even single spike in certain critical sensory neuron can lead to conscious experience.

In an influential workshop report by Perkel and Bullock (1968) it was concluded that one should not expect universal coding principle independent of the context and an extensive list of possible neuronal codes was given. Experimental evidence of codes which depend on precise timing of individual spikes started to appear at that time (Segundo et al., 1963; Chung et al., 1970; Richmond et al., 1987). Moreover, it was shown that spiking mechanism can be very reliable (Bryant and Segundo, 1976; Mainen and Sejnowski, 1995). Subsequently the term *temporal coding* was coined for the situation when precise timing of spikes matters, however, a precise definition is missing and the term may be used to refer to different concepts.

One important concept is that of synchronous firing across neurons at the same time leading to the coherent firing of spatially distributed neurons (Bialek et al., 1991), possibly connected to oscillations (Eckhorn et al., 1988; Gray et al., 1989). Although a vast body of work focuses on the visual system, this type of coding has been found both in auditory (deCharms and Merzenich, 1996) and in olfactory systems (Wehr and Laurent, 1996; Laurent et al., 1996; Perez-Orive et al., 2002). Compared to rate coding where fundamental operation would be the temporal integration, basic operation for this type of code would be coincidence detection for spikes coming from different inputs. Such summation based on the activity of synchronized inputs would be more effective than code based on the firing rate (Singer and Gray, 1995).

Another concept of temporal coding is represented by the notion that specific time intervals between spikes may code some information, proposed as early as in Lorente de Nó (1939), experimentally confirmed in Strehler and Lestienne (1986); similar coding via temporal patterns has been found as well (Eskandar et al., 1992). Yet another specific type of this code can be based on the first spikes and its latencies (VanRullen and Thorpe, 2002).

There is also recent evidence of the so called *sparse coding*. It refers to the idea that sensory information can be encoded by only a small number of neurons within population or sparse activity of a single neuron (Olshausen

and Field, 2004). One notable example is from the primary auditory cortex where DeWeese et al. (2003) showed that a neuron can produce a single spike in a response to sound stimuli with very high reliability. Except experimental evidence in other sensory systems (Vinje and Gallant, 2000; Perez-Orive et al., 2002), there is also a body of theoretical work showing that sparse coding increases the capacity of associative memories, makes the representation of signal easier to transmit and is efficient in terms of energy consumption (Levy and Baxter, 1996). The relation between dense spatial-temporal code and sparse code has been discussed in Theunissen (2003), from another point of view (Földiák and Young, 1995) sparse coding can be seen as a compromise between global activity of a whole neuron population and single *grandmother*-like cell (Gross, 2002).

Another type of coding given by topographic position of a neuron is not characterized by the type of neural firing activity but by the spatial position of the active neuron in the brain tissue alone. An example of such "code" is the mapping human anatomy in motor cortex (Penfield and Boldrey, 1937; Nakamura et al., 1998) or representation of sound source spatial azimuth in nucleus laminaris in birds (Carr and Konishi, 1988).

From the point of view of the whole network more codes can be used simultaneously (Huxter et al., 2003) and even single spike train can encode multiple features, for example Keat et al. (2001) shows how three different features – *what*, *when*, *how much*, are assembled into waveform shape, precise latency and firing rate of action potentials. Another example is our proposal of a neural circuit computing sound azimuth in mammals (Sanda and Marsalek, 2012) which uses a combination of topographic code (auditory nerve fibers are sensitive to narrow range of frequencies), time coding (coincidence detection of appropriate spikes from ipsi- and contra-later fibers) and rate code (capturing the final azimuth), details are depicted in section 3.3.1.

After introducing basic types of neural code we will focus on a particular topic of binaural hearing, where most types of the aforementioned codes occur in parallel.

3.2 Spatial hearing

In order to determine the direction of a sound source the neural circuit needs to compute azimuth and elevation of the sound source given then input signal. The important auditory cues are interaural time differences (ITD[3]), interaural intensity differences (IID) and spectral content of the signal. While the visual information can severely modulate auditory responses and is important in the development and calibration of the (auditory) space representations, the neural circuit in auditory pathway responsible for spatial hearing is capable of highly accurate localization predictions based on the auditory cues only (King, 2009). Thus we will focus on the computational processing of auditory cues occurring in initial parts of auditory pathway.

Historically two mechanisms of localization in the horizontal plane were proposed by Békésy (von Békésy, 1930; van Bergeijk, 1962) and Jeffress (1948). Von Békésy model assumes neurons in unspecified brain nucleus on which fibers from left and right ear converge. The first arriving signal from left/right (L/R) defines tuning of the neuron (*channel)* to be L or R respectively. L/R signals traveling through the nucleus tune the whole population of the neurons and higher centers integrate the number of L/R-tuned neurons. In parallel more intensive stimuli from one side is able to excite larger population of neurons tuned to that side. The final azimuth is determined by the ratio of L/R tuned neurons.

Later and more widespread concept of delay lines (Jeffress, 1948) assumes array of neurons each acting as a coincidence detector for the signal from left and right side. The axonal fibers have systematically different lengths so that additional time needed for the action potential to traverse fiber from one side exactly compensates ITD. Thus each neuron is tuned to narrow sector of the azimuthal space and the array of such neurons create a whole topographical map of the azimuthal space (see Fig. 3).

The research on barn owls (Carr and Konishi, 1990) (and similarly later

[3]Sound arrives at different times on the left and right ear. This difference defines ITD and is dependent on the sound source position and the head size.

in chicken (Overholt et al., 1992; Köppl and Carr, 2008) and emu (MacLeod et al., 2006)) convincingly showed that Jeffress delay lines are employed in birds and although it is known that binaural hearing evolved independently in different species (birds, reptiles and mammals in particular) the Jeffress model became textbook model for binaural hearing. Last decade, however, brought controversy over the mechanism of binaural hearing in mammals.

3.3 Neural code for spatial hearing of mammals

Experimenting and theorizing about the mechanism of (human) spatial hearing dates back to the psychoacoustic works of Thompson (1882) and Rayleigh (1907) who formalized the duplex theory. In this theory low frequency sounds are localized by ITD while high frequency sounds by IID. In general contours this distinction holds even nowadays, anatomical and physiological findings confirmed this distinction on physiological and anatomical level (Yin, 2002; Tollin, 2003). Additionally, research showed that spectral cue is actively used for sound source elevation (Davis et al., 2003; Oertel and Young, 2004). There seems to be agreement on the general mechanism of IID processing (roughly speaking subtraction of excitatory signal from ipsilateral side and inhibitory signal from contralateral side (Covey et al., 1991)). The mechanisms of ITD processing particularly in low frequencies is a matter of discussions and poses open problem upon which will we focus from now on.

3.3.1 Low frequency ITD cues and modeling

While the anatomical evidence for delay lines in birds is solid, there is a weak anatomical evidence for delay lines in mammals. Moreover there are contradictions in physiological recordings on small mammals, which show rather broadly tuned neurons (channels) and bring back the attention to the Békésy concept (McAlpine et al., 2001; McAlpine and Grothe, 2003).[4]

[4]Another distinct concept of cochlear traveling wave was proposed to account for the existing experimental data, but we would not pursue any details here (Joris et al., 2006).

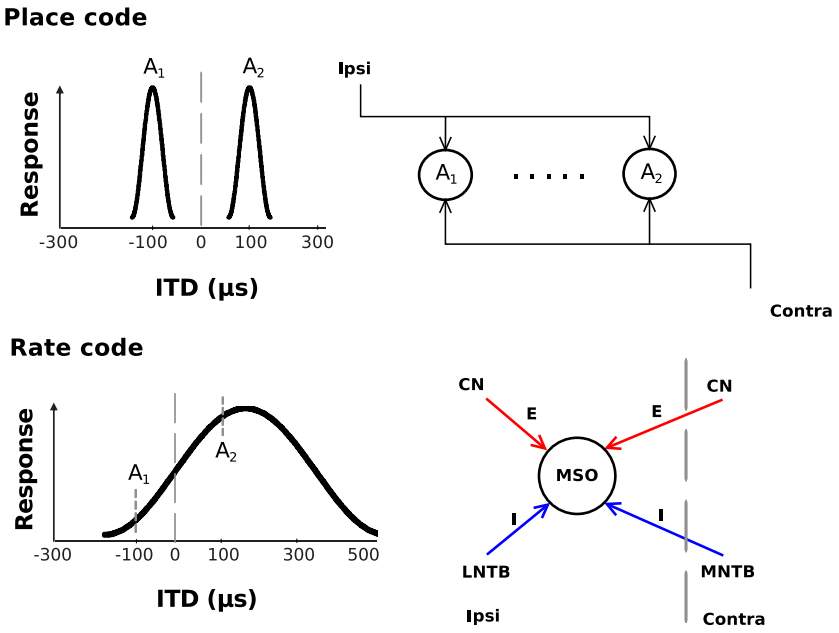

Figure 3: Different concepts explaining ITD sensitivity in spatial hearing. The place code proposed by Jeffress consists of topographical ordered set of neurons (top-right). Each neuron functions as coincidence detector and receives ipsi- and contralateral axonal input. As we move along the array of neurons the axonal delay from ipsilateral side gets longer and vice-versa for the contralateral side. Because the neurons work as coincidence detectors the difference in axonal length must exactly counter-balance ITD delay. In consequence each ITD value activates (ideally) single neuron. On top-left we can see the profile of neuronal firing (ITD *tuning-curves*) — for two distinct ITD values A_1, A_2 two different neurons maximally fire at short range around A_1/A_2 respectively. On contrary the concept of rate code suggests that neurons do have approximately similar broad response curves (bottom-left) and thanks to specific excitation/inhibition mechanism (bottom-right, we show mammalian anatomical wiring at MSO neuron) the firing response of binaural neuron gradually changes as we move along different ITD values. The difference between two azimuths A_1, A_2 is represented by the different firing rates of the neuron. Because critical encoding is employed in the slope part of the tuning curve (in our scheme the part between the A_1 and A_2) it is sometimes called also slope-encoding.

In series of experiments the key role of synaptic inhibition on the first binaural neuron in MSO was elucidated (Brand et al., 2002; Grothe, 2003; Pecka et al., 2008). The key finding is that synaptic inhibition on the critical neuron shifts maximum of the broad ITD curve out of physiological range relevant for the animal. It was suggested that azimuth is in this case encoded in the slope part within physiological range of the ITD curve (see Fig. 3) by the firing rate of binaural neuron. Marsalek and Lansky (2005) took this concept and proposed stochastic model for the spike interaction in this first binaural neuron.

We continued in this direction and simulated such stochastic circuit in (Sanda and Marsalek, 2012). Our aim was twofold. First, to build circuit representing the whole auditory pathway up to the first binaural neuron, endow it with small number of parameters and then explore the parameter space in order to understand the circuit dynamics. Second, to compare the performance of such neuron with known results in psychophysics by employing the concept of ideal observer located at the final stages of the circuit — such observer measures time consumed by the circuit until reliable azimuth estimate is reached.

There are currently two areas of spatial hearing research which usually do not coincide much. Either electro-physiological recording of critical (MSO) neurons on small rodents which provides knowledge about the shape of ITD tuning curves and let us theorize about the neural code used. Or psychophysical experiments on human subjects, which provide us information about spatial accuracy and measurements about minimal time needed for solid azimuth estimate. Providing electro-physiological recording from human subjects or psychological estimates of sound location from small rodents is difficult task from obvious reasons. Our model connects these two separated fields of research.

The first part of the model we proposed can be seen as formalization of available anatomical and physiological data, while the second "observer" part directly connects its result with psychophysics.

As a short summary the model is able to reproduce the shape and position of ITD tuning curves known from experiments as well as inhibition

related results causing tuning curve shift. We identified the main parameter responsible for this shift as coincidence window width. Next, we found that certain amount of jitter actually improves efficiency of the circuit and explored more thoroughly impact of jitter on time efficiency of the circuit in Šanda (2011). Thanks to the observer module and data from psychophysics we estimated value of minimal number of parallel circuits needed to reproduce psychoacoustic experiments.

The actual number of parallel fibers and their convergence on critical neurons is not exactly known and technical difficulties of physiological recordings in MSO neurons do not provide sufficient experimental data to decide the underlying mechanism even after decades of research. Mathematical modeling can thus elucidate restrictions of suggested mechanisms which can be checked by additional experiments.

4 Conclusions

It is widely believed that information processing in and between neurons is mediated by action potentials (spikes) traveling along the neuronal membrane. This process can be described at different levels — starting from detailed biochemical models of membrane, continuing to its phenomenological models (integrate-and-fire models being the typical example) and ending with very abstract models, in which only spike times are considered.

One particular description was chosen — stochastic LIF model — and compared with *in-vivo* intracellular activity of neuron (such analysis has not been done before, only either extracellular or *in-vitro* data are usually available). We estimated parameters of the LIF model and tested in numerical simulations (based on the estimated parameters) how model predictions correspond to the real neuron. Additionally we characterized the difference between spontaneous and acoustically stimulated behavior of the neuron. To conclude, it was found that

- generally, the data are consistent with the model
- in the spontaneous part of the record:

  - asymptotic depolarization is below threshold and neuron is in subthreshold noise-driven regimen
  - ISIs distribution suggests Poisson process
  - there are also inconsistencies between the data and model (or its assumptions):
    * spectra of the input signal should be flat, while we found one dominant frequency
    * the reset depolarization is not a fixed value
    * experimental and modeled ISI distributions do not coincide exactly

- in the stimulated part of the record:
  - firing regimen is suprathreshold
  - parameters representing input take larger values in stimulated part of the recording
  - experimental and modeled ISI distribution coincide
  - inconsistencies with the model assumptions:
    * reset depolarization is influenced by stimulation

As expected, we found that stimulation brings neuron into suprathreshold regimen which causes the average ISI to be shorter than it is in the spontaneous neuronal firing. This observation brings us directly to the more abstract level of description, where we analyze spike trains without considering exact membrane voltage between the spikes. In other words, we ask how the external stimulus is *encoded* in the spike train emitted by neurons.

There are many such neuronal codes described in the literature and we focused on the open problem of neural mechanisms responsible for spatial hearing in mammals. Several theories (which are actually a mixture of different codes) explaining the experimental findings were proposed and we modeled a specific variant of so called slope-encoding model. Stochastic neuronal circuit mimicking auditory pathway up to the first binaural neuron was constructed. Considering this circuit we were able to:

- reproduce of standard results found in experiments (ITD tuning curves)
- identify the role of parameters responsible for ITD timing shift (coincidence window)
- describe parameter responsible for efficiency of coding (jitter)
- estimate minimal number of parallel circuits needed to reproduce results obtained psychoacoustic experiments on binaural hearing.

References

E.D. Adrian and Y. Zotterman. The impulses produced by sensory nerve-endings: Part 2. The response of a single end-organ. *Journal of Physiology*, 61:151–171, 1926.

H.B. Barlow. Single units and sensation: a neuron doctrine for perceptual psychology. *Perception*, 1:371–394, 1972.

D.E. Bergles, J.D.B. Roberts, P. Somogyi, and C.E. Jahr. Glutamatergic synapses on oligodendrocyte precursor cells in the hippocampus. *Nature*, 405:187–191, 2000.

W. Bialek, F. Rieke, R.R. De Ruyter Van Steveninck, and D. Warland. Reading a neural code. *Science*, 252:1854–1857, 1991.

A. Brand, O. Behrend, T. Marquardt, D. McAlpine, and B. Grothe. Precise inhibition is essential for microsecond interaural time difference coding. *Nature*, 417:543–547, 2002.

K.H. Britten, M.N. Shadlen, W.T. Newsome, and J.A. Movshon. The analysis of visual motion: a comparison of neuronal and psychophysical performance. *Journal of Neuroscience*, 12:4745–4765, 1992.

N. Brunel and M.C.W. van Rossum. Lapicque's 1907 paper: from frogs to integrate-and-fire. *Biological Cybernetics*, 97:337–339, 2007.

H.L. Bryant and J.P. Segundo. Spike initiation by transmembrane current: a white-noise analysis. *Journal of Physiology*, 260:279–314, 1976.

T.H. Bullock. Neuron doctrine and electrophysiology. *Science*, 129:997–1002, 1959.

T.H. Bullock, M.V.L. Bennett, D. Johnston, R. Josephson, E. Marder, and R.D. Fields. The neuron doctrine, redux. *Science*, 310:791–793, 2005.

A.N. Burkitt. A review of the integrate-and-fire neuron model: I. Homogeneous synaptic input. *Biological Cybernetics*, 95:1–19, 2006a.

A.N. Burkitt. A review of the integrate-and-fire neuron model: II. Inhomogeneous synaptic input and network properties. *Biological Cybernetics*, 95:97–112, 2006b.

C. E. Carr and M. Konishi. Axonal delay lines for time measurement in the owl's brainstem. *Proceedings of the National Academy of Sciences USA*, 85:8311–8315, 1988.

C.E. Carr and M. Konishi. A circuit for detection of interaural time differences in the brain stem of the barn owl. *Journal of Neuroscience*, 10: 3227–3246, 1990.

S. Celebrini and W.T. Newsome. Neuronal and psychophysical sensitivity to motion signals in extrastriate area MST of the macaque monkey. *Journal of Neuroscience*, 14:4109–4124, 1994.

S.H. Chung, S.A. Raymond, and J.Y. Lettvin. Multiple meaning in single visual units. *Brain, Behaviour and Evolution*, 3:72–101, 1970.

E. Covey, M. Vater, and J.H. Casseday. Binaural properties of single units in the superior olivary complex of the mustached bat. *Journal of Neurophysiology*, 66:1080–1094, 1991.

J.P. Cunningham, V. Gilja, S.I. Ryu, and K.V. Shenoy. Methods for estimating neural firing rates, and their application to brain-machine interfaces. *Neural Networks*, 22:1235–1246, 2009.

K.A. Davis, R. Ramachandran, and B.J. May. Auditory processing of spectral cues for sound localization in the inferior colliculus. *Journal of the Association for Research in Otolaryngology*, 4:148–163, 2003.

R.C. deCharms and M.M. Merzenich. Primary cortical representation of sounds by the coordination of action-potential timing. *Nature*, 381:610–613, 1996.

R. Desimone, T.D. Albright, C.G. Gross, and C. Bruce. Stimulus-selective properties of inferior temporal neurons in the macaque. *Journal of Neuroscience*, 4:2051–2062, 1984.

M.R. DeWeese, M. Wehr, and A.M. Zador. Binary spiking in auditory cortex. *Journal of Neuroscience*, 23:7940–7949, 2003.

R. Eckhorn, R. Bauer, W. Jordan, M. Brosch, W. Kruse, M. Munk, and H.J. Reitboeck. Coherent oscillations: A mechanism of feature linking in the visual cortex? *Biological Cybernetics*, 60:121–130, 1988.

E.N. Eskandar, B.J. Richmond, and L.M. Optican. Role of inferior temporal neurons in visual memory. I. Temporal encoding of information about visual images, recalled images, and behavioral context. *Journal of Neurophysiology*, 68:1277–1295, 1992.

J. Feng. Is the integrate-and-fire model good enough? – a review. *Neural Networks*, 14:955–975, 2001.

R.D. Fields and B. Stevens-Graham. New insights into neuron-glia communication. *Science*, 298:556–562, 2002.

R. Fitzhugh. Impulses and physiological states in theoretical models of nerve membrane. *Biophysical Journal*, 1:445–466, 1961.

P. Földiák and M.P. Young. Sparse coding in the primate cortex. In Arbib M.A., editor, *The handbook of brain theory and neural networks*, pages 895–898. MIT Press, Cambridge, MA, 1995.

M.G. Fuortes. Electric activity of cells in the eye of Limulus. *American Journal of Ophthalmology*, 46:210–223, 1958.

G.L. Gerstein and N.Y.S. Kiang. An approach to the quantitative analysis of electrophysiological data from single neurons. *Biophysical Journal*, 1: 15–28, 1960.

G.L. Gerstein and B. Mandelbrot. Random walk models for the spike activity of a single neuron. *Biophysical Journal*, 4:41–68, 1964.

C.M. Gray, P. König, A.K. Engel, and W. Singer. Oscillatory responses in cat visual cortex exhibit inter-columnar synchronization which reflects global stimulus properties. *Nature*, 338:334–337, 1989.

C.G. Gross. Genealogy of the "Grandmother Cell". *The Neuroscientist*, 8: 512–518, 2002.

B. Grothe. New roles for synaptic inhibition in sound localization. *Nature reviews neuroscience*, 4:540–550, 2003.

O.J. Grüsser, U. Grüsser-Cornehls, and MD Licker. Further studies on the velocity function of movement detecting class-2 neurons in the frog retina. *Vision Research*, 8:1173–1185, 1968.

A. Hjelmfelt and J. Ross. Chemical implementation and thermodynamics of collective neural networks. *Proceedings of the National Academy of Sciences USA*, 89:388–391, 1992.

A. Hjelmfelt and J. Ross. Mass-coupled chemical systems with computational properties. *Journal of Physical Chemistry*, 97:7988–7992, 1993.

A. Hjelmfelt, E.D. Weinberger, and J. Ross. Chemical implementation of neural networks and Turing machines. *Proceedings of the National Academy of Sciences USA*, 88:10983–10987, 1991.

A.L. Hodgkin and A.F. Huxley. A quantitative description of membrane current and its application to conduction and excitation in nerve. *Journal of Physiology*, 117:500–544, 1952.

J.J. Hopfield. Neural networks and physical systems with emergent collective computational abilities. *Proceedings of the National Academy of Sciences USA*, 79:2554–2558, 1982.

J.J. Hopfield. Neurons with graded response have collective computational properties like those of two-state neurons. *Proceedings of the National Academy of Sciences USA*, 81:3088–3092, 1984.

J. Huxter, N. Burgess, and J. O'Keefe. Independent rate and temporal coding in hippocampal pyramidal cells. *Nature*, 425:828–832, 2003.

L.A. Jeffress. A place theory of sound localization. *Journal of Comparative and Physiological Psychology*, 41:35–39, 1948.

R. Jolivet, A. Rauch, HR Lüscher, and W. Gerstner. Integrate-and-Fire models with adaptation are good enough: predicting spike times under random current injection. *Advances in Neural Information Processing Systems*, 18:595–602, 2006.

R. Jolivet, R. Kobayashi, A. Rauch, R. Naud, S. Shinomoto, and W. Gerstner. A benchmark test for a quantitative assessment of simple neuron models. *Journal of Neuroscience Methods*, 169:417–424, 2008a.

R. Jolivet, F. Schürmann, T.K. Berger, R. Naud, W. Gerstner, and A. Roth. The quantitative single-neuron modeling competition. *Biological cybernetics*, 99:417–426, 2008b.

P.X. Joris, B. Van de Sande, D.H. Louage, and M. Van Der Heijden. Binaural and cochlear disparities. *Proceedings of the National Academy of Sciences USA*, 103:12917–12922, 2006.

J. Keat, P. Reinagel, R.C. Reid, and M. Meister. Predicting every spike: A model for the responses of visual neurons. *Neuron*, 30:803–817, 2001.

A.J. King. Visual influences on auditory spatial learning. *Philosophical Transactions of the Royal Society B: Biological Sciences*, 364:331–339, 2009.

W.M. Kistler, W. Gerstner, and J.L. Hemmen. Reduction of the Hodgkin-Huxley equations to a single-variable threshold model. *Neural Computation*, 9:1015–1045, 1997.

B.W. Knight. Dynamics of encoding in a population of neurons. *Journal of General Physiology*, 59:734–766, 1972.

R. Kobayashi, Y. Tsubo, and S. Shinomoto. Made-to-order spiking neuron model equipped with a multi-timescale adaptive threshold. *Frontiers in Computational Neuroscience*, 3, 2009.

C. Koch. *Biophysics of computation: information processing in single neurons*. Oxford University Press, USA, 2005.

C. Koch, T. Poggio, and V. Torres. Retinal ganglion cells: a functional interpretation of dendritic morphology. *Philosophical Transactions of the Royal Society of London. B, Biological Sciences*, 298:227–263, 1982.

C. Koch, T. Poggio, and V. Torre. Nonlinear interactions in a dendritic tree: localization, timing, and role in information processing. *Proceedings of the National Academy of Sciences USA*, 80:2799–2802, 1983.

C. Köppl and C.E. Carr. Maps of interaural time difference in the chicken's brainstem nucleus laminaris. *Biological cybernetics*, 98:541–559, 2008.

P. Lansky, P. Sanda, and J. He. The parameters of the stochastic leaky integrate-and-fire neuronal model. *Journal of Computational Neuroscience*, 21:211–223, 2006.

P. Lansky, P. Sanda, and J. He. Effect of stimulation on the input parameters of stochastic leaky integrate-and-fire neuronal model. *Journal of Physiology-Paris*, 104:160–166, 2010.

L. Lapicque. Recherches quantitatives sur l'excitation électrique des nerfs traitée comme une polarisation. *Journal de Physiologie et de Pathologie Générale*, 9:620–635, 1907.

L. Lapicque. Quantitative investigations of electrical nerve excitation treated as polarization. *Biological Cybernetics*, 97:341–349, 2007.

G. Laurent, M. Wehr, and H. Davidowitz. Temporal representations of odors in an olfactory network. *Journal of Neuroscience*, 16:3837–3847, 1996.

W.B. Levy and R.A. Baxter. Energy efficient neural codes. *Neural Computation*, 8:531–543, 1996.

R. Lorente de Nó. Transmission of impulses through cranial nerve nuclei. *Journal of Neurophysiology*, 2:402–464, 1939.

K.M. MacLeod, D. Soares, and C.E. Carr. Interaural timing difference circuits in the auditory brainstem of the emu (*Dromaius novaehollandiae*). *Journal of comparative neurology*, 495:185–201, 2006.

Z.F. Mainen and T.J. Sejnowski. Reliability of spike timing in neocortical neurons. *Science*, 268:1503–1506, 1995.

P. Marsalek and P. Lansky. Proposed mechanisms for coincidence detection in the auditory brainstem. *Biological Cybernetics*, 92:445–451, 2005.

P.B. Matthews. Muscle spindles and their motor control. *Physiological Reviews*, 44:219–288, 1964.

D. McAlpine and B. Grothe. Sound localization and delay lines - do mammals fit the model? *Trends in Neurosciences*, 26:347–350, 2003.

D. McAlpine, D. Jiang, and A.R. Palmer. A neural code for low-frequency sound localization in mammals. *Nature Neuroscience*, 4:396–401, 2001.

W.S. McCulloch. Agatha Tyche of nervous nets-the lucky reckoners. In *Mechanization of Thought Processes: Proceedings of a Symposium held at the National Physical Laboratory*, volume 2, pages 611–634. HMSO, London, 1959.

W.S. McCulloch and W. Pitts. A logical calculus of the ideas immanent in nervous activity. *Bulletin of Mathematical Biology*, 5:115–133, 1943.

J. Nagumo, S. Arimoto, and S. Yoshizawa. An active pulse transmission line simulating nerve axon. *Proceedings of the IRE*, 50:2061–2070, 1962.

A. Nakamura, T. Yamada, A. Goto, T. Kato, K. Ito, Y. Abe, T. Kachi, and R. Kakigi. Somatosensory homunculus as drawn by MEG. *Neuroimage*, 7:377–386, 1998.

M. Nawrot, A. Aertsen, and S. Rotter. Single-trial estimation of neuronal firing rates: from single-neuron spike trains to population activity. *Journal of Neuroscience Methods*, 94:81–92, 1999.

D. Oertel and E.D. Young. What's a cerebellar circuit doing in the auditory system? *Trends in Neurosciences*, 27:104–110, 2004.

B.A. Olshausen and D.J. Field. Sparse coding of sensory inputs. *Current Opinion in Neurobiology*, 14:481–487, 2004.

E.M. Overholt, E.W. Rubel, and R.L. Hyson. A circuit for coding interaural time differences in the chick brainstem. *Journal of neuroscience*, 12:1698–1708, 1992.

M. Pecka, A. Brand, O. Behrend, and B. Grothe. Interaural time difference processing in the mammalian medial superior olive: the role of glycinergic inhibition. *Journal of Neuroscience*, 28:6914–6925, 2008.

W. Penfield and E. Boldrey. Somatic motor and sensory representation in the cerebral cortex of man as studied by electrical stimulation. *Brain*, 60: 389–443, 1937.

J. Perez-Orive, O. Mazor, G.C. Turner, S. Cassenaer, R.I. Wilson, and G. Laurent. Oscillations and sparsening of odor representations in the mushroom body. *Science*, 297:359–365, 2002.

D.H. Perkel and T.H. Bullock. Neural coding. *Neurosciences Research Program Bulletin*, 6:221–350, 1968.

S. Ramon y Cajal. *Textura del sistema nervioso del hombre y los vertebrados.* Imprenta y Librería de Nicolás Moya, Madrid, 1899.

S. Ramon y Cajal. *Histology of the nervous system of man and vertebrates.* Oxford University Press, NY, 1995.

L. Rayleigh. On our perception of sound direction. *Philosophical Magazine*, 13:214–232, 1907.

L.M. Ricciardi and L. Sacerdote. The Ornstein-Uhlenbeck process as a model for neuronal activity. *Biological Cybernetics*, 35:1–9, 1979.

B.J. Richmond, L.M. Optican, M. Podell, and H. Spitzer. Temporal encoding of two-dimensional patterns by single units in primate inferior temporal cortex. I. Response characteristics. *Journal of Neurophysiology*, 57:132–146, 1987.

B. Sakitt. Counting every quantum. *Journal of Physiology*, 223:131–150, 1972.

P. Šanda. Speeding up the algorithm for finding optimal kernel bandwidth in spike train analysis. *European Journal for Biomedical Informatics*, 6: 73–75, 2010.

P. Šanda. Jitter effect on the performance of the sound localization model of medial superior olive neural circuit. *European Journal for Biomedical Informatics*, 7:51–54, 2011.

P. Sanda and P. Marsalek. Stochastic interpolation model of the medial superior olive neural circuit. *Brain Research*, 1434:257–265, 2012.

I. Segev. Single neurone models: oversimple, complex and reduced. *Trends in Neurosciences*, 15:414–421, 1992.

J.P. Segundo, G.P. Moore, L.J. Stensaas, and T.H Bullock. Sensitivity of neurones in Aplysia to temporal pattern of arriving impulses. *Journal of Experimental Biology*, 40:643–667, 1963.

H. Shimazaki and S. Shinomoto. A method for selecting the bin size of a time histogram. *Neural Computation*, 19:1503–1527, 2007.

H. Shimazaki and S. Shinomoto. Kernel bandwidth optimization in spike rate estimation. *Journal of Computational Neuroscience*, 29:171–182, 2010.

W. Singer and C.M. Gray. Visual feature integration and the temporal correlation hypothesis. *Annual Review of Neuroscience*, 18:555–586, 1995.

R.B. Stein. A theoretical analysis of neuronal variability. *Biophysical Journal*, 5:173–194, 1965.

R.B. Stein. Some models of neuronal variability. *Biophysical Journal*, 7: 37–68, 1967.

B.L. Strehler and R. Lestienne. Evidence on precise time-coded symbols and memory of patterns in monkey cortical neuronal spike trains. *Proceedings of the National Academy of Sciences USA*, 83:9812–9816, 1986.

F.E. Theunissen. From synchrony to sparseness. *Trends in Neurosciences*, 26:61–64, 2003.

S.P. Thompson. On the function of the two ears in the perception of space. *Philosophical Magazine*, 13:406–416, 1882.

D.J. Tollin. The lateral superior olive: A functional role in sound source localization. *Neuroscientist*, 9:127–143, 2003.

G.E. Uhlenbeck and L.S. Ornstein. On the theory of the Brownian motion. *Physical Review*, 36:823–841, 1930.

W.A. van Bergeijk. Variation on a theme of Bekesy: a model of binaural interaction. *Journal of the Acoustical Society of America*, 34:1431–1437, 1962.

R. VanRullen and S.J. Thorpe. Surfing a spike wave down the ventral stream. *Vision Research*, 42:2593–2615, 2002.

W.E. Vinje and J.L. Gallant. Sparse coding and decorrelation in primary visual cortex during natural vision. *Science*, 287:1273–1276, 2000.

G. von Békésy. Zur theorie des hörens. über das Richtungshören bei einer Zeitdefferenz oder Lautstärkenungleichheit der beiderseitigen Schalleinwirkungen. *Physikalische Zeitschrift*, pages 824–835, 1930.

M. Wehr and G. Laurent. Odour encoding by temporal sequences of firing in oscillating neural assemblies. *Nature*, 384:162–166, 1996.

T. Yin. Neural mechanisms of encoding binaural localization cues in the auditory brainstem. In Fay R.R. Oertel D., Popper A.N., editor, *Integrative functions in the mammalizan auditory pathway*, pages 99–159. New York: Springer-Verlag, 2002.

List of publications

Reviewed journals with impact factor

1. Lansky, P. and Sanda, P. and He, J., The parameters of the stochastic leaky integrate-and-fire neuronal model, Journal of Computational Neuroscience, 21:211–223, 2006. (Journal IF: 2.325)

2. Lansky, P. and Sanda, P. and Weiss, M., Modeling the influence of non-adherence on antibiotic efficacy: application to ciprofloxacin, The International Journal of Clinical Pharmacology and Therapeutics, 45:438–447, 2007. (Journal IF: 1.189)

3. Lansky P. and Sanda, P. and He J., Effect of stimulation on the input parameters of stochastic leaky integrate-and-fire neuronal model, Journal of Physiology - Paris, 104:160–166, 2010. (Journal IF: 3.030)

4. Sanda P. and Marsalek P., Stochastic interpolation model of the medial superior olive neural circuit, Brain Research, Brain Research, 1434:257–265, 2012. (Journal IF: 2.623)

Reviewed journals without impact factor

5. Šanda P., Speeding up the Algorithm for Finding Optimal Kernel Bandwidth in Spike Train Analysis, European Journal for Biomedical Informatics, 6:73–75, 2010.

6. Šanda P., Jitter Effect on the Performance of the Sound Localization Model of Medial Superior Olive Neural Circuit, European Journal for Biomedical Informatics, 7:51–54, 2011.

Reprints of published papers

The research papers 1, 3-6 represent the main part of the thesis, the preceding text gives extended introduction and context for the whole work. The research paper 2 is out of the thesis scope and is not included in the thesis. The reprints of the papers are attached below.

J Comput Neurosci
DOI 10.1007/s10827-006-8527-6

The parameters of the stochastic leaky integrate-and-fire neuronal model

Petr Lansky · Pavel Sanda · Jufang He

Received: 24 November 2005 / Revised: 23 March 2006 / Accepted: 28 March 2006 / Published online: 28 July 2006

Abstract Five parameters of one of the most common neuronal models, the diffusion leaky integrate-and-fire model, also known as the Ornstein-Uhlenbeck neuronal model, were estimated on the basis of intracellular recording. These parameters can be classified into two categories. Three of them (the membrane time constant, the resting potential and the firing threshold) characterize the neuron itself. The remaining two characterize the neuronal input. The intracellular data were collected during spontaneous firing, which in this case is characterized by a Poisson process of interspike intervals. Two methods for the estimation were applied, the regression method and the maximum-likelihood method. Both methods permit to estimate the input parameters and the membrane time constant in a short time window (a single interspike interval). We found that, at least in our example, the regression method gave more consistent results than the maximum-likelihood method. The estimates of the input parameters show the asymptotical normality, which can be further used for statistical testing, under the condition that the data are collected in different experimental situations. The model neuron, as deduced from the determined parameters, works in a subthreshold regimen. This result was confirmed by both applied methods. The subthreshold regimen for this model is characterized by the Poissonian firing. This is in a complete agreement with the observed interspike interval data.

Keywords Leaky integrate-and-fire model · Ornstein-Uhlenbeck neuronal model · Parameters estimation · Spontaneous firing

Action Editor: Nicolas Brunel

P. Lansky (✉) · P. Sanda
Institute of Physiology,
Academy of Sciences of the Czech Republic,
Prague, Czech Republic
e-mail: lansky@biomed.cas.cz

J. He
Department of Rehabilitation Sciences,
The Hong Kong Polytechnic University,
Hung Hom, Kowloon, Hong Kong

Introduction

Application of mathematical methods in neuroscience is based on construction of models aiming to mimic real objects. The models range from phenomenological mathematical models to very detailed biophysical models. From a biophysical point of view, the models of a single neuron reflect the electrical properties of its membrane via electric circuit description. Such circuit models can be written in terms of differential equations for the membrane voltage. Reducing these models, we can obtain integrate-and-fire types of model, which are reviewed in detail in most computational neuroscience monographs (Tuckwell, 1988; Koch, 1998; Dayan and Abbot, 2001; Gerstner and Kistler, 2002). These models are sometimes criticized for their too drastic simplification of reality (e.g., Segev, 1992). Simultaneously, the opposite opinion appears. For example, Kistler et al. (1997) claim that the integrate-and-fire model with a properly selected threshold, after reduction of the Hodgkin-Huxley four dimensional model, predicts 90 percent of the spikes correctly. Independently from this discussion, we observe that the number of papers devoted to the integrate-and-fire model, or at least employing it, is very high.

The simplest "realistic" neuronal model is the deterministic leaky integrate-and-fire model (Lapicque model, RC-circuit). It assumes that the membrane depolarization can

be described by a circuit with a generator, a resistor and a capacitor in parallel. It has to be stressed that while the electrical representation is related to a small isopotential patch of neuronal membrane, the mathematical variable (the voltage) reflects an abstract representation of a complete neuron. This is another simplification based on neglecting the spatial properties of a neuron. There are attempts to overcome this situation (e.g., Pinsky and Rinzel, 1994; Rodriguez and Lansky, 2000) but still the single-point models dominate most of the applications. Due to the simplicity of the deterministic leaky integrate-and-fire model, the action potential generation is not an inherent part of the model as in more complex models and a firing threshold has to be imposed. The model neuron fires whenever the threshold is reached and then the voltage is reset to its initial value. This means that in the electrical circuit representation a switch is added to the circuit. The reset following the threshold crossing introduces a strong nonlinearity into the model. For a constant input the model neuron remains silent, never reaching the threshold (subthreshold regimen), or fires at constant intervals (suprathreshold regimen).

The experimental data recorded from very different neuronal structures and under different experimental conditions suggest a presence of stochastic variables in neuronal activity. We may assume that there is a random component, generally regarded as noise, contained in the incoming signal. The other source of noise can be the neuron itself where a random component is added to the signal. Unfortunately, there is no clear distinction between noise contained in the signal and the system noise. A phenomenological way how to introduce stochasticity into the deterministic leaky integrate-and-fire model is simply by assuming an additional noise term. If the noise is not further specified, but assumed to be Gaussian and white, then the model is well known in physical literature as an Ornstein-Uhlenbeck model (e.g., Gardiner, 1982) and this model has been widely used in neuroscience literature (Tuckwell, 1988; Koch, 1998; Dayan and Abbot, 2001; Gerstner and Kistler, 2002). An alternative way to end up with the Ornstein-Uhlenbeck model is by diffusion approximation of the model with discontinuous trajectories (Stein, 1965). An advantage of this approach is that a direct interpretation of the parameters appearing in the Ornstein-Uhlenbeck neuronal model is available (Lansky, 1997).

Models without specified parameters remain only a tool for qualitative comparison and thus finding methods for estimation is equally important as model construction. The lack of methods for parameters identification had been noticed for a long period (e.g., Tuckwell and Richter, 1978; Brillinger and Segundo, 1979). In general, the traditional approaches were more frequently focused on interspike interval (ISI) distribution. Keat et al. (2001) as well as Paninski et al. (2004) developed methods based on extracellular recordings in vivo conditions with known input to the system. Estimation methods from in vitro voltage recordings for known input were presented by Stevens and Zador (1998), Rauch et al. (2003), Le Camera et al. (2004), Jolivet et al. (2006), Paninski et al. (2004). None of these papers treats comparison of the Ornstein-Uhlenbeck model with in vivo spontaneous activity. The likely reason is that, using the model, only interspike intervals (ISIs) were usually predicted and thus the attempts to identify the model parameters were based on observation of ISIs. Such a task is enormously complicated and leads to rather difficult numerical and mathematical problems (Inoue et al., 1995; Shinomoto et al., 1999; Ditlevsen and Lansky, 2005).

We aimed to study the estimation methods in the Ornstein-Uhlenbeck model, their stability and reproducibility. In the first Section we summarize the properties of the model. Then the methods for the estimation of its parameters are given and details of data acquisition presented. Simultaneously, the assumptions of the model are tested. Finally the parameters of the model are estimated and the obtained results are discussed. We restricted the study on a single neuron under spontaneous activity conditions. To extend the results on several neurons and different experimental conditions is possible, but beyond the scope of this article.

Model and its properties

The Ornstein-Uhlenbeck model of membrane depolarization is formally given by the stochastic differential equation,

$$dX(t) = (-\beta(X(t) - x_0) + \mu)dt + \sigma dW(t)\,, X(0) = x_0, \quad (1)$$

where dW represents increments of a standard stochastic Wiener process (Brownian motion), and $\beta > 0$ characterizes the spontaneous decay of the membrane depolarization in the absence of input to the resting level x_0. The drift coefficient μ reflects the local average rate of displacement due to the neuronal input and local variability is represented by the infinitesimal variance σ (the variability of the neuronal input). The spikes are not an intrinsic part of the model but are generated when the membrane depolarization $X(t)$ reaches for the first time the firing threshold S, which is an additional parameter. Then, the depolarization is reset to the resting level, x_0, and the process of input "integration" starts anew. We should keep in mind that also the reset level, x_0, represents an additional parameter of the model. Thus the model is fully described by Eq. (1) with its five parameters: β, μ, σ, S and x_0. As said, the ISIs are identified in model (1) with the first-passage times of the process $X(t)$ across the boundary S,

$$T = \inf\,(t > 0,\ X(t) \geq S > x_0)\ . \tag{2}$$

Due to the complete reset in defining ISI by Eq. (2) and due to the constant input μ, the ISIs form a renewal process, which means that ISIs are independent and identically distributed random variables. Formula (1) can be rewritten in a form often seen in engineering applications using the term white noise,

$$\frac{dX(t)}{dt} = -\beta(X(t) - x_0) + \mu + \sigma\xi(t)\,, X(0) = x_0\,, \tag{3}$$

with the same interpretation of the parameters as above, only the white noise $\xi(t)$ is a formal derivative of the Wiener process with respect to time. For a fixed time t, $X(t)$ given by (1) or (3) is a Gaussian random variable. In absence of the threshold S and if σ tends to zero, we can solve the differential Eq. (3). The solution is identical with the mean value of the stochastic depolarization given by Eq. (1)

$$E(X(t)) = x_0 + \frac{\mu}{\beta}(1 - \exp(-\beta t)) \tag{4}$$

and the variance of $X(t)$ is

$$Var(X(t)) = \frac{\sigma^2}{2\beta}(1 - \exp(-2\beta t))\,. \tag{5}$$

The position of the asymptotic depolarization $E(X(\infty)) = x_0 + \mu/\beta$ determines regimes of firing of the Ornstein-Uhlenbeck model. For $\mu/\beta \gg S - x_0$, the suprathreshold regimen, the firing is almost regular and ISI histogram resembles normal distribution. The noise plays a limited role in this range of parameters. For $\mu/\beta \approx S - x_0$, the distribution of ISIs is positively skewed and resembles Gamma distribution. In the subthreshold regimen, $\mu/\beta \ll S - x_0$ the firing becomes Poissonian. Here, the noise plays a crucial role and without it the neuron would remain silent. This last regimen is important for this study, as will be seen. Of course, the signs "$\gg$" and "$\ll$" are relative to the asymptotic variance $Var(X(\infty)) = \sigma^2/2\beta$. More details on the Ornstein-Uhlenbeck neuronal model can be found, for example, in Tuckwell (1988) or in Ricciardi and Lansky (2003).

The description of the process via Eq. (3) is apparently an intuitive extension of the deterministic approach. Its advantage is in giving a method for a computer simulation of the process sample trajectories (Kloeden and Platen, 1992). The simplest discrete-time approximation of (3) is a stochastic analogue of the Euler scheme for ordinary differential equations,

$$X_{i+1} = X_i - \beta(X_i - x_0)h + \mu h + \sigma\epsilon_i\,, X_0 = x_0\,, \tag{6}$$

where h denotes the time step of simulation, X_i (i = 1,2, ...) are the simulated values of the process, and ϵ_i are independent and normally distributed random variables, $\epsilon_i \sim N(0, h)$. The increments ϵ_i in (6) can be replaced by $\pm\sqrt{h}$ selecting these values with equal probability $^1/_2$, which substantially decreases the simulation time (Tuckwell and Lansky, 1997). This was the procedure applied to simulate the membrane depolarization in this study. Apparently, the parameters β, σ, μ and x_0 have to be determined for the simulation procedure. If the ISIs are to be simulated, then in addition, the firing threshold S is required. As mentioned, the spikes in the model are generated when the membrane depolarization $X(t)$ reaches, for the first time, the firing threshold S. While the simulation of the trajectories X contains no systematic bias, it is not true for the simulation of the first passage times (Lansky and Lanska, 1994). It is systematically overestimated and this effect has to be minimized.

Two basic types of data can be used for the identification of the parameters appearing in Eq. (1). In the first of them only the ISIs are available, which means the realizations of the random variable defined by Eq. (2). If this is the case, then the situation is complicated and the solution can be achieved only under some additional assumptions. For example, it has to be assumed that the firing threshold and the resting level are known. In the second situation, which is investigated here, the membrane depolarization is recorded between the generation of spikes. To specify the firing threshold and reset level seems to be a simpler task than to estimate the remaining parameters of the model. We should simply record what was the reset after the end of an action potential and what was the final value of the depolarization when it started. However, we will see that the situation is not so simple and also these two parameters need to be estimated. A method of estimating the remaining parameters was proposed more than two decades ago (Lansky, 1983). Thus the novelty of this paper is mainly in application of the method to real intracellular data. For an extensive methodological review of estimation methods in stochastic diffusion processes, for which Eq. (1) is a special case, see Prakasa Rao (1999).

The aim of this article is primarily determination of the values of the parameters β, σ and μ. The question is whether these parameters are stable over a long period or whether they vary in short time ranges. Whereas σ and μ are input parameters and thus are assumed to change whenever the input to a neuron has changed, model (1) assumes that β is a property of the membrane (in the same way as S and the reset level) and these three intrinsic parameters should be stable. However, these are only assumptions which have never been confirmed. Thus, initially we estimate the parameters separately for each ISI.

Methods

(a) Estimation from a single interspike interval

The records of the depolarization within single ISI permit us to estimate β, μ and σ. Theoretically also two additional parameters S and x_0 could be determined, but as we will see, for that purpose more realizations of the ISIs are necessary.

Let us assume that in one ISI the membrane depolarization $X_i = x_i$ is sampled at $N+1$ points ($i = 0, \ldots, N$) at steps h at times $t_i = ih$ (the notation is complicated for non equal sampling step but the results are analogous). Then the formulas for the estimation of the parameters by the maximum likelihood method are

$$\hat{\beta} = \frac{1}{h} \frac{\sum_{j=0}^{N-1} x_j^2 - \sum_{j=0}^{N-1} x_{j+1} x_j + (x_N - x_0)\overline{x}}{\sum_{j=0}^{N-1} x_j^2 + \overline{x}^2 N}, \tag{7}$$

$$\hat{\mu} = \frac{x_N - x_0}{T} + \hat{\beta}\bar{x} \tag{8}$$

and

$$\hat{\sigma} = \frac{1}{T} \sum_{j=0}^{N-1} (x_{j+1} - x_j + x_j h\hat{\beta} - h\hat{\mu})^2, \tag{9}$$

where $\overline{x} = \frac{1}{N}\sum_{j=0}^{N} x_j$, $T = Nh$. These formulas are discrete-time variants of the formulas based on the assumption that the depolarization is continuously recorded in between the spikes.

Formula (4) suggests that the method of moments can also be used. Then, we minimize the functional

$$L(\beta, \mu) = \sum_{j=1}^{N} (x_j - x_0 - \frac{\mu}{\beta}(1 - \exp(-\beta j h)))^2 \tag{10}$$

with respect to the parameters β and μ by a regression method. It is obvious that efficiency of this method depends on the distance of x_0 from the asymptotic depolarization μ/β. An increase of β relatively to h also handicaps the method.

Another method for estimate of the noise amplitude is

$$\hat{\sigma}' = \frac{1}{T} \sum_{j=0}^{N-1} (x_{j+1} - x_j)^2. \tag{11}$$

This estimate follows from theoretical results established by Feigin (1976). Comparing Eqs. (9) and (11), we can see that for $h \to 0$ in (9) we end up with Eq. (11). We will compare all these estimation methods.

(b) Estimation from several interspike intervals

In this situation, if we assume that the parameters remain stable over several ISIs we can use the extension of three estimates as were formally proposed by Lansky (1983). That method takes into account the length of ISIs and in some sense shorter ISIs contribute to the estimates less than longer ones. Here we use a slightly different approach. We estimate the parameters for each ISI separately. Then, the global estimates are representative over ISI counts not the total length of the record. Further, and it is the main reason, in this way we also get some information about the dependency of the values on the lengths of ISI and their position in the record. The global record can be characterized by representative values of β_M, μ_M and σ_M , in our case we use medians (denoted by index M) of the estimated values.

If several ISIs are available, then in addition to the parameters mentioned in the previous Section, also the threshold S and the reset value x_0 can be estimated. For this purpose we simply use the medians of the values observed for each ISI.

Animal preparation for the intracellular recordings

Guinea pigs served as subjects for the intracellular recording experiments. Anaesthesia was initially induced with pentobarbital sodium (Nembutal, Abott, 35 mg/kg, ip) and maintained by supplemental doses of the same anaesthetic (about 5–10 mg/kg/hr) during the surgical preparation and recording. Throughout the recording, an electrocorticograph was monitored to assess the level of anaesthesia. The subject was mounted in a stereotaxic device following the induction of anaesthesia. A midline incision was made in the scalp and a craniotomy was performed to enable vertical access to the MGB in the right hemisphere (He, 2003; Xiong et al., 2003; Yu et al., 2004). The head was fixed with two stainless steel bolts to an extended arm from the stereotaxic frame using acrylic resin. The left ear was then freed from the ear bar, so that the subject's head remained fixed to the stereotaxic device without movement.

Cerebrospinal fluid was released at the medulla level through an opening at the back of the neck. The animal was artificially ventilated. Both sides of the animal's chest were opened, and its body was suspended to reduce vibrations of the brain caused by intra-thoracic pressure. The experimental procedures were approved by the Animal Subjects Ethics Sub-Committee of The Hong Kong Polytechnic University.

A glass-pipette as the recording electrode, filling it with 0.5M KCl (pH 7.6, 0.05M Tris HCl buffer) was used. The resistance of the electrode ranged between 40–90 M . The electrode was advanced vertically from the top of the brain by a stepping motor (Narishige, Tokyo, Japan). After the electrode was lowered to a depth of 4–5 mm, the cortical exposure was sealed using low-melting temperature paraffin.

When the electrode was near or in the target area, it was slowly advanced at 1 or 2 μm per step.

Data collection

Upon penetrating the membrane of a cell, the electrode detected the negative membrane potential. After amplification, the membrane potential as well as the auditory stimulus were stored in the computer with the aid of commercial software (AxoScope, Axon). The direct current (DC) level of the recording electrode was frequently checked and set to zero during the experiments. The DC level after each recording was used to compensate for the membrane potential of some neurons. Neurons showing a resting membrane potential lower than -50 mV and spontaneous spikes (if any) of larger than 50 mV were included in the present study. Single neuron data were selected for this article. The membrane potential was recorded (in 100 mV) with time step $h = 0.00015\,[\mathrm{s}] = 0.15\,[\mathrm{ms}]$, for period $0-501$ [s]. Accompanying the values of the membrane potential is the stimulus level. For the purpose of this study we selected only ISIs which were entirely outside the stimulation period.

Detection of spikes and determination of S and x_0

The parameter estimation method is based on the observation of the membrane depolarization between spikes. Therefore the spikes have to be removed from the data but it is not entirely obvious which part of the records can be included in the estimation procedure. At first, we detect the spikes and then we judge their beginnings and their ends. In this way ISIs are fixed. The least problematic is spike detection. The level for this purpose was experimentally chosen at the value of -35.5 [mV] (note that this is not the firing threshold S, but a value to detect spikes in continuous sampling of the voltage), see Fig. 1(a).

From visual inspection of the data it is clearly difficult to decide where exactly to start and to end the spikes, and hence to decide which data to include in the parameter estimation procedure. It follows from this inspection that for detected spikes the width of the spike as well as the voltage where ISI starts, are not always the same. This is in contrast with the assumptions of model (1). The consequences are summarized in the Discussion. Determining x_0 by the minimum voltage after detected spike failed due to the large fluctuations of these values. The final solution, which was adopted, was that all data were transformed by a moving average (over 6 values) and the minimum in "the valley" after a spike is considered to be start of an ISI. This procedure was confirmed by the following analysis (see next Section). To find this minimum, at first "the valley" has to be defined.

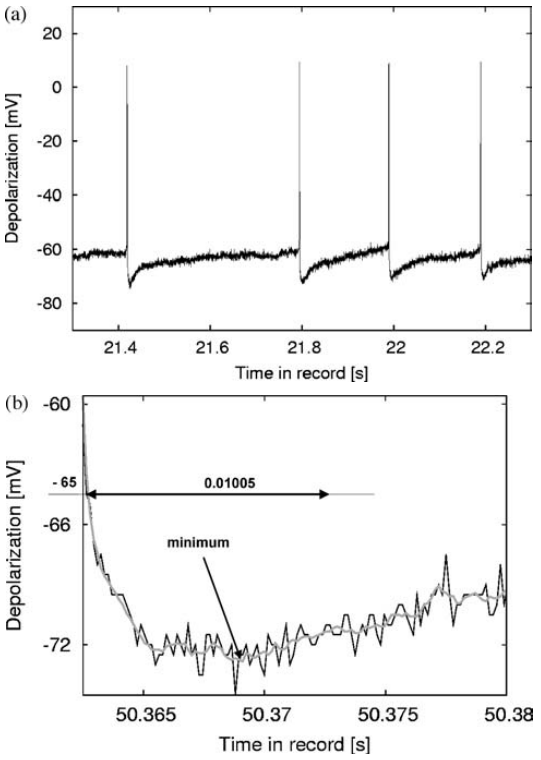

Fig. 1 Example of data used for the estimation of the parameters. (a) The spikes are not initiated at the same values and the end is not uniquely defined. (b) Schematic illustration of ISI initial point detection (for details see text). Gray line is the moving average over six observations given by black line

Its start is fixed at the moment when the depolarization reaches the value of -65.5 [mV] for the first time after spike generation. Its end is the time point 0.01005 [s] after its beginning. In this region the minimum depolarization is sought for (see Fig. 1(b)).

Defining the end of each ISI was not so problematic and we took the point 0.01005 [s] before detected spike, i.e., before the voltage reaches -35.5 [mV]. For threshold determination, we took the last point with decreasing depolarization before the spike detection (in other words, the depolarization only increases to the top of the spike after this point).

Model assumptions—Frequency analysis

When we tried the maximum-likelihood estimates directly from the raw data we got the results which are illustrated in Fig. 2 in a typical example.

It obvious that the simulated trajectory differs from the recorded one in several respects. The former reaches the steady-state much faster and the amplitude of the noise is

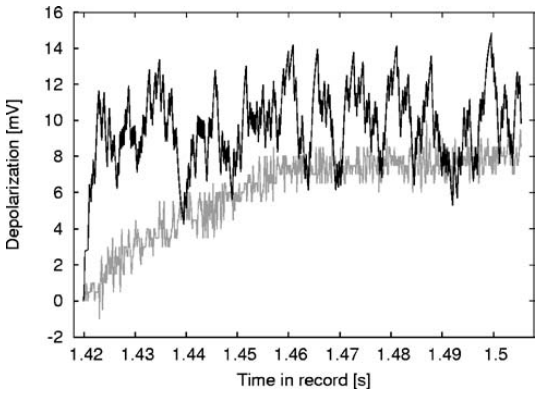

Fig. 2 Example of membrane potential trajectories, experimental (gray) and simulated (black) using the parameters estimated by the maximum likelihood method from the original data

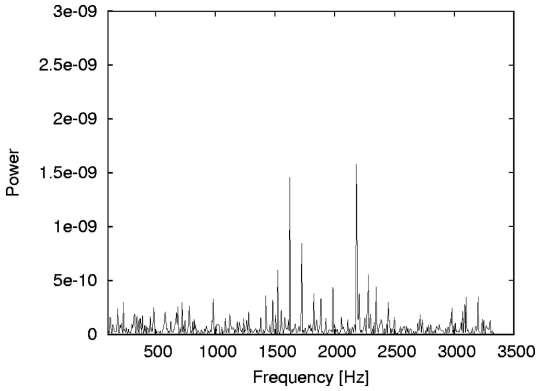

Fig. 3 Example of spectral decomposition of the data

much higher. Further, it seems that the noises is not of the same type. This suggests that the assumptions of the model should be checked. The assumptions imply that the spectra of the data should not contain a dominant frequency (white noise contains all the frequency components equally). We performed a spectral decomposition of several parts of the data and always found dominant frequency at 2180 [Hz]. An example of spectral density obtained from the data is in Fig. 3. In this example there is also high peak at 1600 [Hz].

The source of this high frequency noise is not clear and to avoid its influencing the results, all the values of the membrane depolarization were transformed by a moving average over a time window of six steps. To eliminate this high frequency noise we tried two strategies (moving averages, averages over non overlapping time windows). The second strategy appeared as inferior to the moving averaging. The success was judged from the fit of the estimates to those obtained from the regression of the data to an exponential function (4), see formula (10). In the example, on the interval (20.4201–20.54955) [s], statistical regression gives $\mu = 0.341$ [V/s] and $\beta = 21.036$ [1/s]. The results of the maximum likelihood estimate after computing moving averages are given in Table 1.

Table 1 Example of dependence of maximum likelihood estimates on number of steps in moving average procedure

Number of steps	Estimate σ	Estimate μ	Estimate β
1	0.071	1.954	170.80
2	0.038	0.785	62.17
3	0.024	0.454	33.03
4	0.017	0.370	24.90
5	0.014	0.355	23.06
6	0.011	0.343	21.58
7	0.011	0.331	20.53
8	0.009	0.329	20.10
9	0.007	0.317	19.04
10	0.007	0.310	18.59

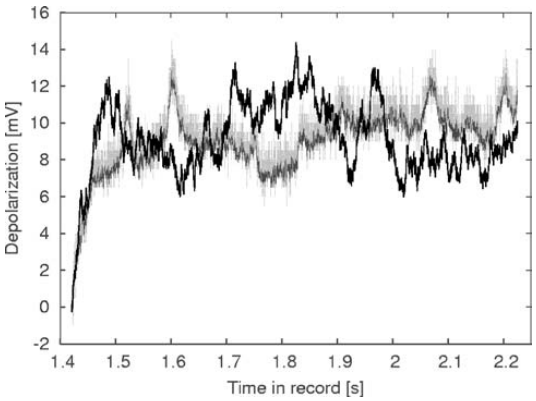

Fig. 4 Example of membrane potential trajectories, experimental (light gray), filtered (dark gray) and simulated (black) using the parameters estimated from the filtered data. Filtering decreased the amplitude of the noise and made it similar to that of the simulated signal

From this table we can see that, the moving average over about six steps removes the discrepancy. Subsequently we simulated the model again using the parameters estimated from the signal after the filtering (see Fig. 4. and compare with Fig. 3).

It can be seen that the high-frequency noise present in the experimental data has been removed and appears neither in the filtered nor simulated trajectory. After the signal was filtered, the estimates of the parameters for each detected ISI were calculated according to formulas (7–9). From now on, by "the data" we mean the filtered original data.

The differences in estimates of σ using formula (9) or (11) were negligible. For example, on the interval (20.4201, 20.54955); we found $\hat{\sigma}' = 0.0115$ [V/$\sqrt{s}$] using (11), and $\hat{\sigma} = 0.0114$ [V/$\sqrt{s}$] using (9). Therefore for the noise amplitude only estimate (9) was used.

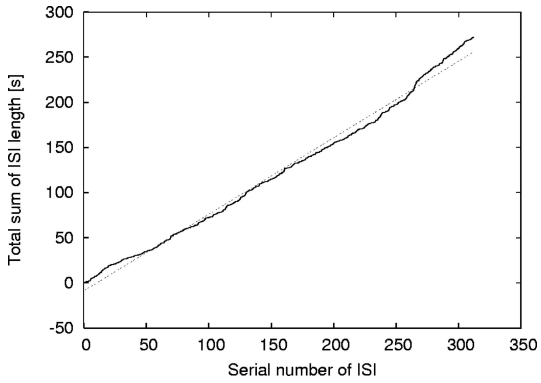

Fig. 5 Dependency of the sum of the ISIs length on the serial number of the ISI. The dotted line corresponds to the constant firing rate

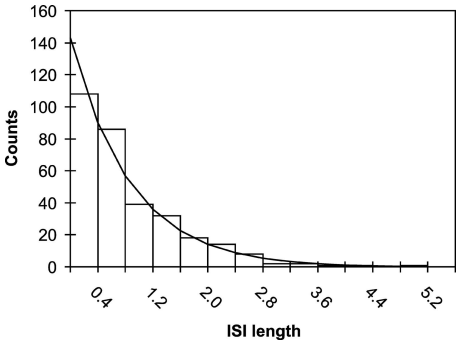

Fig. 6 Histogram of ISIs together with the corresponding density of exponential distribution normalized on the number of ISIs

Results

Parameters of the input and the membrane time constant

Using the above described procedure we identified all ISIs and estimated the parameters for each of them. In total, 312 ISIs were analyzed and before estimating the parameters of the model, we applied simple standard statistical procedures on them. The ISIs appear stable in time (see Fig. 5), which means that there is no trend in their length.

The corresponding statistical characteristics are median 0.585 [s], average 0.872 [s] and coefficient of variation 0.883. The shape of histogram of ISIs (Fig. 6) suggests that the ISIs are generated in accordance with the exponential distribution. Kolmogorov-Smirnov test does not reject the hypothesis of exponentiality, at 5% a significance level. Also the other test for normality of the estimates are at 5% significance level.

The parameters of model (1) were estimated by both methods for all the ISIs and by using the estimates in schema (6)

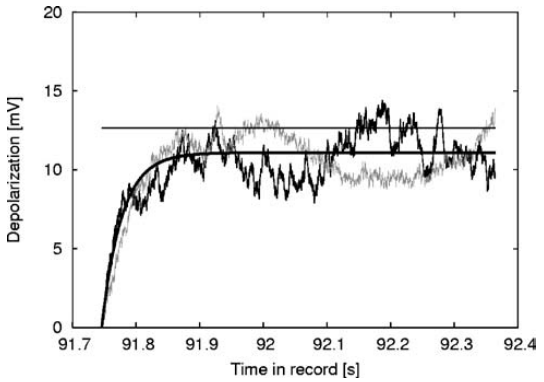

Fig. 7 Three curves: gray—data; fluctuating black—simulated model with parameters estimated by maximum likelihood method from the data; smooth black—mean value (model without noise). The horizontal line represents the estimated threshold S

the simulated depolarizations were plotted. An example is in Fig. 7.

From the simulations made with estimated parameters, it appears that the estimated asymptotical voltages, μ/β, coincide well with the data. On the other hand, in the first part of the trajectories, the real data is a bit faster in reaching the asymptote than simulated trajectory. This visual impression was confirmed by the following method which aimed to check the fit of the model to the data. For each ISI we have a vector of values of depolarization $\boldsymbol{x_i} = (x_{i0}, x_{i1}, \ldots, x_{in})$ a corresponding vector of depolarization, $\boldsymbol{y_i} = (y_{i0}, y_{i1}, \ldots, y_{in})$, obtained from simulating Eq. (1) by formula (6) using the estimated parameters. The differences $\boldsymbol{z_i} = \boldsymbol{x_i} - \boldsymbol{y_i}$ were calculated and their averages and standard deviations evaluated. These results are illustrated in Fig. 8 for both estimation methods. The main difference between the methods is in the period just after the spike generation. This could be due to a violation of the model assumptions (for example, hyperpolarization) and possibly the method of moments could be more robust against this violation.

Apparently the regression method works better. In both cases there is a systematic hump after the origin, but for the regression method it is much smaller.

An important question is dependency of the estimated parameters on the length of ISIs. The only dependency we can expect that, if the input to neurons changes with the experiment, then μ could get smaller for longer ISI. Otherwise, μ and β should keep stable and independent on the length of ISI. The results are illustrated in Fig. 9. We can see, that the results obtained by the regression method are independent of ISI ($corr(\hat{\mu}, ISI) = 0.016$ and $corr(\hat{\beta}, ISI) = 0.136$) which is not the case of the estimates obtained by the maximum

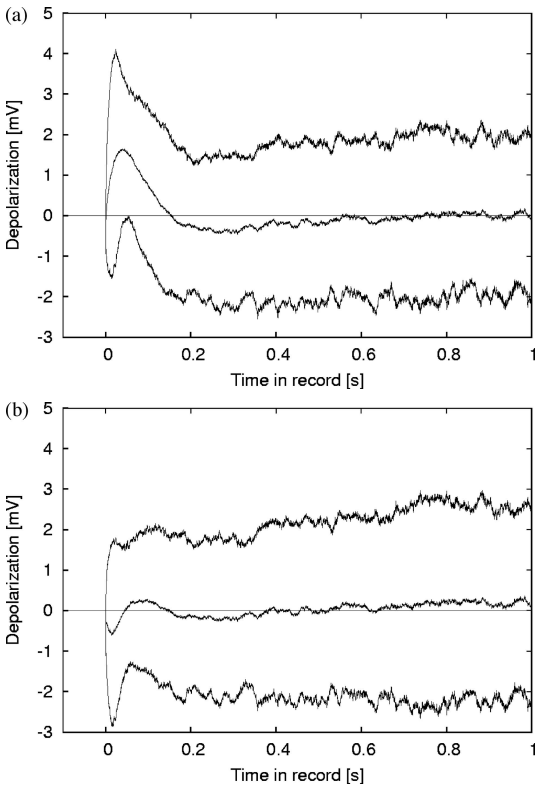

Fig. 8 Average difference between the data and simulated trajectory. (a) estimates obtained by maximum likelihood (b) estimates obtained by regression method. The region around the curves indicates $\pm 2 * standard\ deviations$

likelihood method ($corr(\hat{\mu}, ISI) = 0.663$ and $corr(\hat{\beta}, ISI) = 0.668$).

Similarly, we investigated the estimated value of σ and found it independent of the ISI length, ($corr(\hat{\sigma}, ISI) = -0.099$). As is apparent from the above analyses, the regression method was superior to the maximum likelihood method for estimation of μ and β (see Figs. 8 and 9), so the values from the regression are considered further on.

In Fig. 10 are presented histograms of estimated values of the input parameters μ, σ and of the inverse time constant β. We can see that the distributions are rather broad and quite symmetric resembling Gaussian density. This suggests the asymptotic normality of the estimates which can be used for future statistical inference. The Kolmogorov-Smirnov test rejected normality of $\hat{\mu}$ and $\hat{\beta}$, but not for $\hat{\sigma}$. The reason for the rejection in the case of $\hat{\mu}$ and $\hat{\beta}$ were the outliers on the right hand side of the histograms (see Fig. 10). After their removal the estimates also fit the normal distribution.

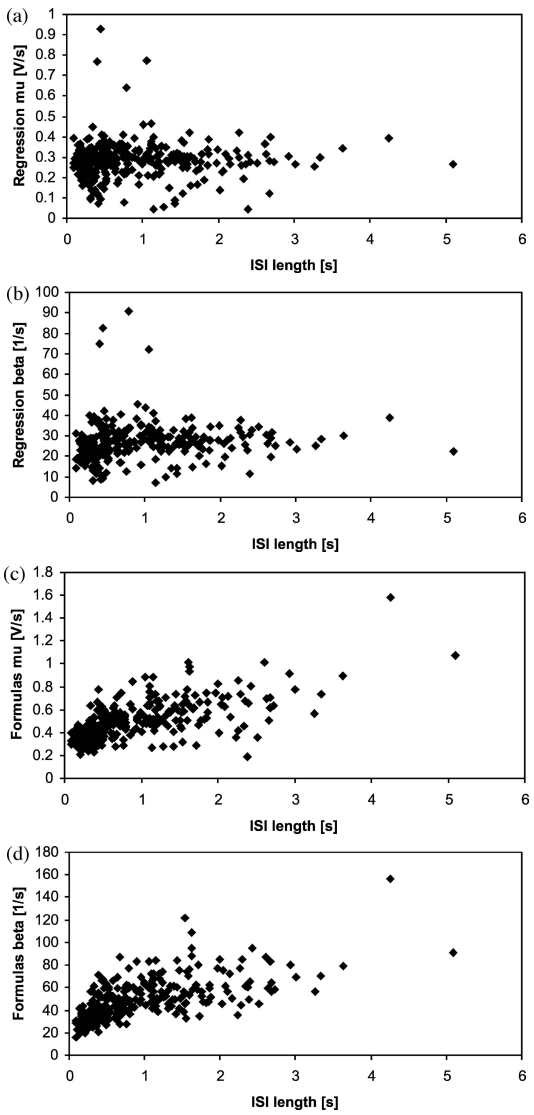

Fig. 9 Dependency of the estimated parameters (vertical axis) on the length of ISI (horizontal axis). In (Fig.9(a), and (b) are results obtained by regression method, (Fig.9(c), and (d) those obtained by the maximum likelihood method

Finally we calculated the central characteristics of the estimated parameters. Median value of the noise amplitude was $\hat{\sigma}_M = 0.013505\ [\mathrm{V}/\sqrt{s}]$. Median values of μ and β were by regression method, $\hat{\mu}_M = 0.2846$ [V/s], $\hat{\beta}_M = 25{,}8042$ [1/s], for the maximum likelihood method the obtained values were $\hat{\mu}_M = 0.4606$ [V/s], $\hat{\beta}_M = 43{,}5068$ [1/s]. Due to the symmetry of histograms, the averages and the medians were practically the same. We should notice that both methods give almost identical asymptotic depolarization

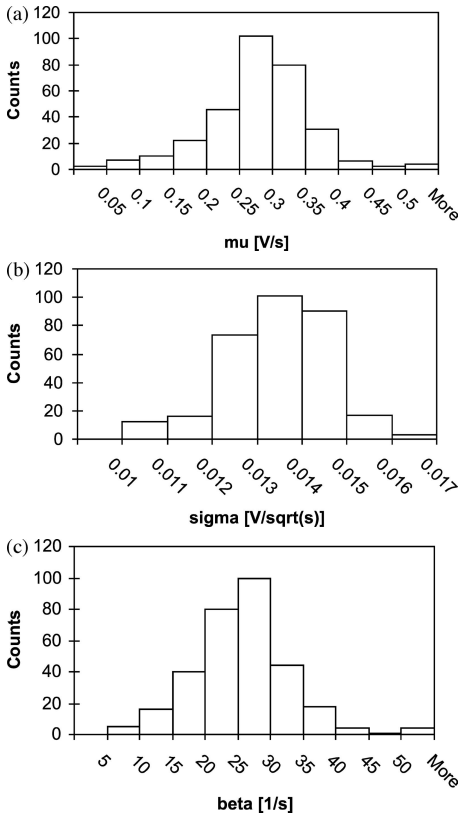

Fig. 10 Histograms of the estimated parameters. (a) the drift, (b) the noise amplitude, (c) the inverse membrane time constant

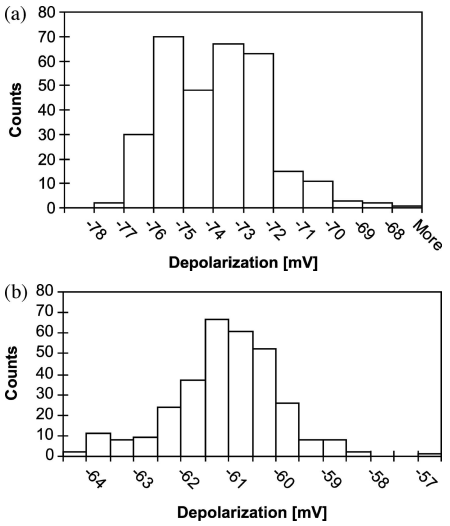

Fig. 11 Histograms of the membrane parameters. (a) initial membrane depolarization, (b) firing threshold depolarization

μ/β, for regression 0.0110 [V] and for maximum likelihood 0.0106 [V]. We can calculate the membrane time constant, which from the regression method yields after inverting the estimate of β, the value of 38.8 ms.

Reset, threshold and asymptotic depolarization

For each ISI we estimated the initial value of the depolarization after a spike and the firing threshold (the last value before the spike is generated), Fig. 11.

We see from comparison of Fig. 11(a) and (b) that the initial values were more variable than the thresholds S. The reason may be that the spike was not in principle generated at the time when the voltage was at its highest level during the ISI and this will be discussed later. The median value of the initial depolarization is $x_0 = -73.92$ [mV]. The median threshold value is $S = -61.0$ [mV]. It implies that, in average, the firing threshold is about 13 [mV] above the initial depolarization. It is larger than approximately 11 [mV] which is the level of asymptotic depolarization as it comes out from the parameters estimation. The normality of both determined parameters, x_0 and S, was rejected.

To illustrate the relationship between the firing threshold and the asymptotic depolarization we compare Fig. 12 and Fig. 11(b). Namely we can see that the estimated parameters predict subthreshold firing type, as from Fig. 12 we can see that the asymptotic depolarization is below the threshold even with respect to its variation.

Finally, to show that the neuron, as the estimation of the parameters suggests, is in the subthreshold (noise-driven) regimen, we compare directly the theoretical asymptotic depolarization and the corresponding firing threshold (Fig. 13). We can see that the difference between the threshold and the asymptotic depolarization is almost always positive (Fig. 13(a)). If we investigate some kind of two-standard-deviations envelope around the asymptotic depolarization, then we get below zero (Fig. 13(b)). The possible reasons for this result are presented in Discussion.

Discussion

This is mostly a methodological attempt to estimate the parameters of the Ornstein-Uhlenbeck neuronal model from the intracellular recordings and for an unknown input. We have to realize that only a single neuron in a single record was analyzed and thus the results are more a methodological illustration of how to deal with the problem than a statistically complete analysis.

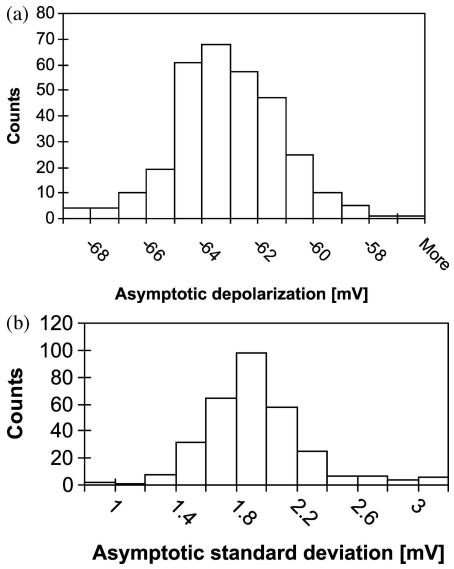

Fig. 12 Histograms of the asymptotic properties calculated from the parameter estimates. (a) asymptotic depolarization, (b) asymptotic standard deviation of the depolarization

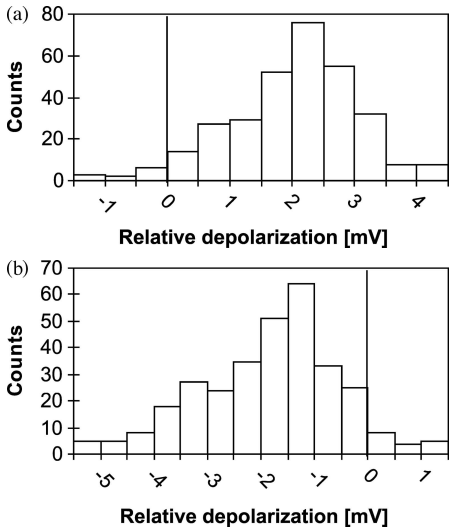

Fig. 13 Histogram of the pair wise differences between the estimated firing thresholds and the asymptotic depolarizations. (a) $\hat{S} - (\hat{x}_0 + \hat{\mu}/\hat{\beta})$, (b) $\hat{S} - (\hat{x}_0 + \hat{\mu}/\hat{\beta}) - 2\sigma/\sqrt{2\beta}$

Spontaneous activity

We selected for statistical treatment only the unstimulated activity of the neuron. The detected ISIs are exponentially distributed which suggests that they are generated in accordance with a Poisson process. The Poisson process as a model of spontaneous activity of a neuron was experimentally observed many times and on very different neuronal structures (e.g., Eggermont et al., 1993; Jones and Jones, 2000; Lin and Chen, 2000; Tateno et al., 2002). In sensory neurons, we showed in frogs (Rospars et al., 1994) and rats (Duchamp-Viret et al., 2005) that the spontaneous activity of olfactory receptor neurons can be described by a Poisson process. Theoretical arguments for the fact that the spontaneous activity is a low rate Poisson process can be found in Laughlin (2001). The spontaneous activity can be interpreted as the summation of two processes: (i) an intrinsic process which implies firing due to the noise, and (ii) an extrinsic process, which induces firing due to the uncontrolled occurrence of effects either from the environment or other neurons. Of course, Poisson process, as any other model, is an approximation which can be always questioned (Koyama and Shinomoto, 2005), in this case for example by the existence of the absolute refractory period, but such objections are marginal at this level of description.

From the point of view of the Ornstein-Uhlenbeck neuronal model, the Poisson process corresponds to the situation in which the signal is so weak that the asymptotic depolarization is far below the firing threshold, which has to be true with respect to the amplitude of noise. In other words, for model (1) and (2) this type of activity is predicted if the firing threshold S is far above the asymptotic depolarization, μ/β, given by Eq. (4) with respect the asymptotic variance (5), which is controlled by σ. We can see from Fig. 13(a), that the asymptotic depolarization is below the threshold. However, when we plot the asymptotic depolarization increased for two asymptotic standard deviations, we get above the threshold. This could break the exponentiality of ISIs distribution observed in our data. The reason why this has not happened may be that not every crossing of the voltage has induced a spike, in other words, that we had not recorded exactly the trigger zone depolarization. Namely, two-compartment version of the model would be closer to reality. Similar conclusion can be found in Jolivet et al. (2006).

Model assumptions

There are many assumptions of the model which are disputable and can be true only in idealization. First of all, it is the constancy of the input parameters μ and σ over each ISI. We selected the spontaneous activity as an experimental material, for which such a constancy can be expected. Another assumption is the Gaussian white noise on the neuronal input. This we found was not true for our data and the high-frequency noise was detected and eliminated. The source of this high frequency noise remains unclear to us. Next assumption, violated in our observations, was the first-passage time inducing the generation of a spike. Probably, we registered the membrane depolarization in other location than the spikes are generated. The traditional assumption of

the model is the fixed value of the reset depolarization (for the variants with random initial value see Lansky and Smith, 1989; Christodoulou and Bugmann, 2000). This assumption represents an oversimplification which was noticed as early as by Stevens (1964). We found that this assumption was also violated, but for the model performance the effect is negligible. Despite that any assumption of the model can be made questionable, as it is only a model, we may conclude that the data are consistent with the model. This was not the case in Stevens and Zador (1998) where model (1–2) in absence of noise was fitted to response of cortical neurons in vitro to injection of constant current. There the voltage approached the threshold as a concave curve, in contrast to Eq. (4), and our data. The authors of the paper solved the discrepancy by employing time-varying membrane resistance and time-varying membrane time "constant". In contrast to Stevens and Zador (1998), here the investigated trajectories shown the convex shapes, but it may happen that when a neuron is stimulated, this property is met.

Intrinsic parameters

Tuckwell and Richter (1978), who pioneered the estimation of the parameters in the stochastic neuronal models, classified the model parameters into two classes—intrinsic and input. Unfortunately, their results are based on different assumptions and thus not comparable with ours. In model (1–2) are three intrinsic parameters, β, S and x_0, and for different neurons have been reported different values of them, even without modeling concept. However, the intrinsic parameters were not in the center of our interest despite they play their important role for the model performance. Jolivet et al. (2006) analyzed spike response model which was claimed to be equivalent to the leaky integrate-and-fire model. However, their approach is not oriented on estimating the parameters μ and σ, but it is aimed on spike train prediction. The time-dependent threshold is considered in their paper, but the constant value is achieved in about 10 ms, which would not change our results as no ISI shorter of 10 ms was observed. In their Fig. 1(a) we can see, that the threshold reaches the value between -60 and -70 mV which corresponds to our results. In general, the values of intrinsic parameters obtained in this article are consistent with the values found in literature.

Input parameters

Completely different situation comes with the input parameters. The attempts to estimate them were up to now rare and based on additional assumptions. Inoue et al. (1995) analyzed spontaneous activity of the mesencephalic reticular formation neurons on the basis of ISIs. It should be noted that the term spontaneous activity has in central neurons different meaning than in the sensory systems. In the case of neurons investigated by Inoue et al. (1995) there were either in sleeping animals or in bird watching state, but there is no apparent difference in the activity or the parameters. We should keep in mind that the firing rates were higher than in our case and none of the neurons resembled Poissonian firing. There the firing threshold and the membrane time constants were selected a priory, S was set 15 [mV] above the reset value and the time constant was taken equal to 5 [ms]. The threshold obtained in this study (approx. 13 [mV]) is not so different from the value assumed by these authors. On the other hand, the membrane time constant we estimated was about seven times larger than that used by them. This fact corresponds well to the fact that our values of the drift parameter were estimated lower than in the cited paper. The estimated μ ranges in their paper from -6 to 3 [mV/ms], whereas in this study we obtained the values in much smaller range, around 0.28 [mV/ms]. Finally, the most striking at the first sight seems to be the difference in the amplitude of noise, which usually was found much larger than in this paper. However, it is indirectly clear that the values in Inoue et al. (1995) are in different units than in this paper ([mV/ms]). After rescaling, the values the difference becomes less apparent. It is an open question if the comparison of our results with Inoue et al. (1995) can be considered as a discrepancy, or if their results are so widespread that ours can be seen included in theirs. A possible source of discrepancy between these two papers is probably difference in applied method and the overall activity of the neurons.

Another attempt to compare the Ornstein-Uhlenbeck model with ISI data was done by Shinomoto et al. (1999) with a negative result. Their method is not based on direct estimation of the model parameters but on studying mutual relationship between coefficient of variation and the skewness coefficient. They concluded that the model is not adequate to account for the spiking in cortical neurons. These authors did not estimate the membrane time constant and considered for it several optional values. This complicates the comparison of their results with ours. However, they claimed that the reason for inconsitency of their data with the Ornstein-Uhlenbeck process was mainly due to anomalous long ISIs. In our case the parameters were found in the subthreshold region and thus the long ISIs represent no problem for the fit of the data to the model. On the other hand, in the case of the stimulated activity such a situation can arise.

Both these attempts (Inoue et al., 1995; Shinomoto et al., 1999) were based on ISIs statistics. It means that for estimation of the parameters a sample of several hundreds of ISIs is necessary. Our method permits to estimate the input parameters in a short time window (in a single ISI). It appeared that the regression method was superior to the maximum likelihood. There might be several reasons for this effect. The first one can be the above mentioned violation of the model

assumptions and thus that the maximum-likelihood may be more sensitive to these discrepancies between the model and the data. The second reason is that the maximum likelihood estimates are discretized version of continuous sampling theory. The asymptotic depolarization μ/β was estimated very well by both methods, better than the parameters μ and β separately. The reason is that the membrane potential was almost permanently at the asymptotic level and in this situation the estimation of individual parameters is less precise (Lansky et al., 1988). The distinction on input and intrinsic parameters fails for more realistic leaky integrate-and-fire models (e.g., Lansky and Lanska, 1987; Richardson and Gerstner, 2005). There the membrane time constant becomes input dependent. The change is only formal at the level of description applied in this article.

Noise

The results suggest that our neuron was firing in the noise activated regimen, in other words, that in the absence of the noise it would remain silent. This corresponds very well to the fact that the driving signal is small and the neuron fires only due to the stochastic fluctuation of the membrane depolarization. Theoretical prediction of the Poissonian firing in the subthreshold regime of the Ornstein-Uhlenbeck neuronal model is well known for a long time (Nobile et al., 1985) and here the prediction and data estimation fits perfectly together. The values of the estimated noise amplitude (Fig. 10(b)) seems to be quite small, but this is only an illusion as what has to be considered comes out of Eq. (6), and it is the asymptotic standard deviation of the depolarization, $\sigma\sqrt{2\beta}$.

Conclusions

We estimated the parameters of the Ornstein-Uhlenbeck neuronal model in spontaneous neuronal activity. The achieved results are consistent with the conclusions which can be obtained from the statistical analysis of the ISIs. The neuron fires in subthreshold regimen and thus the activity is Poissonian. The advantage of the applied method is that it permits to judge quantitatively the input to the neuron within a single ISI. This property will appear more important in presence of stimulation and comparison of neuronal activity under different conditions.

Acknowledgments The authors thank to P.W.F. Poon for initiating and permanent support for this work and to P.E. Greenwood for stimulating discussions. This work was supported by Academy of Sciences of the Czech Republic Grant (Information Society, 1ET400110401), AV0Z50110509, Center for Neurosciences LC554.

References

Brillinger DR, Segundo JP (1979) Empirical examination of the threshold model of neuron firing. Biol. Cybern. 35: 213–220.
Christodoulou C, Bugmann G (2000) Near poisson-type firing produced by concurrent excitation and inhibition. BioSystems 58: 41–48.
Dayan P, Abbot LF (2001) Theoretical Neuroscience. MIT Press, Cambridge, MA.
Ditlevsen S, Lansky P (2005) Estimation of the input parameters in the Ornstein-Uhlenbeck neuronal model. Phys. Rev. E 71: Art. No. 011907.
Duchamp-Viret P, Kostal L, Chaput M, Lansky P, Rospars J-P (2005) Patterns of spontaneous activity in single rat olfactory receptor neurons are different in normally breathing and tracheotomized animals. J Neurobiol.
Eggermont JJ, Smith GM, Bowman D (1993) Spontaneous burst firing in cat primary auditory-cortex—Age and depth dependency and its effect on neural interaction measures. J. Neurophysiol. 69: 1292–1313.
Feigin P (1976) Maximum likelihood estimation for stochastic processes—A martingale approach. Adv. Appl. Probab. 8: 712–736.
Gardiner CW (1983) Handbook of Stochastic Methods for Physics, Chemistry and the Natural Sciences. Springer, Berlin.
Gerstner W, Kistler W (2002) Spiking Neuron Models. Cambridge University Press, Cambridge.
He J (2003) Slow oscillation in non-lemniscal auditory thalamus. J Neurosci. 23: 8281–8290.
Inoue J, Sato S, Ricciardi LM (1995) On the parameter estimation for diffusion models of single neurons' activities. Biol. Cybern. 73: 209–221.
Johnson DH (1996) Point process models of single-neuron discharges. J. Comput. Neurosci. 3: 275–300.
Jolivet R, Rauch A, Lüscher H-R, Gerstner W (2006) Integrate-and-fire models with adaptation are good enough: Predicting spike times under random current injection. In: Y Weiss, B Schölkopf, J Platt, eds. Advances in Neural Information Processing Systems 18, MIT Press, Cambridge MA.
Jones TA, Jones SM (2000) Spontaneous activity in the statoacoustic ganglion of the chicken embryo. J. Neurphysiol. 83: 1452–1468.
Keat J, Reinagel P, Reid RC, Meister M (2001) Predicting every spike: A model for the responses of visual neurons. Neuron 30: 803–817.
Kistler WM, Gerstner W, van Hemmen JL (1997) Reduction of the Hodgkin-Huxley equations to a single-variable threshold model. Neural Comput. 9: 1015–1045.
Kloeden PE, Platen E (1992) Numerical Solution of Stochastic Differential Equations. Springer, Berlin.
Koch C (1999) Biophysics of Computation: Information Processing in Single Neurons. Oxford University Press, Oxford.
Koyama S, Shinomnoto S (2005) Empirical Bayes interpretation of random point events. J. Phys. A: Math. Gen. 38: L531–L537.
La Camera G, Rauch A, Luscher HR, Senn W, Fusi S (2004) Minimal models of adapted neuronal response to in vivo-like input currents. Neural Comput. 16: 2101–2124.
Lansky P (1983) Inference for the diffusion models of neuronal activity. Math. Biosci. 67: 247–260.
Lansky P (1997) Sources of periodical force in noisy integrate-and-fire models of neuronal dynamics. Phys. Rev. E 55: 2040–2043.
Lansky P, Lanska V (1987) Diffusion approximation of the neuronal model with synaptic reversal potentials. Biol. Cybern. 56:19–26.
Lansky P, Giorno V, Nobile AG, Ricciardi LM (1998) A diffusion neuronal model and its parameters. In: LM Ricciardi, ed. Proceedings of International Workshop Biomathematics and related Computational Problems. Kluwer, Dordrecht.

Lansky P, Lanska V (1994) First-passage-time problem for simulated stochastic diffusion processes. Comp. Biol. Med. 24: 91–101.
Lansky P, Smith CE (1989) The effect of a random initial value in neural 1st-passage-time models. Math. Biosci. 93: 191–215.
Laughlin SB (2001) Energy as a constraint on the coding and processing of sensory information. Curr. Opin. Neurobiol. 11: 475–480.
Lin X, Chen SP (2000) Endogenously generated spontaneous spiking activities recorded from postnatal spiral ganglion neurons in vitro. Developmental Brain Res. 119: 297–305.
Nobile AG, Ricciardi LM, Sacerdote L (1985) Exponential trends of Ornstein-Uhlenbeck 1st-passage-time densities. J. Appl. Prob. 22: 360–369.
Paninski L, Pillow J, Simoncelli E (2005) Comparing integrate-and-fire models estimated using intracellular and extracellular data. Neurocomputing 65: 379–385.
Paninski L, Pillow JW, Simoncelli EP (2004) Maximum likelihood estimation of a stochastic integrate-and-fire neural encoding model. Neural Comput. 16: 2533–2561.
Pinsky PF, Rinzel J (1994) Intrinsic and network rhythmogenesis in a reduced Traub model for CA3 neurons 1: 39–60.
Prakasa Rao BLS (1999) Statistical inference for diffusion type processes. Arnold, London.
Rauch A, La Camera G, Luscher HR, Senn W, Fusi S (2003) Neocortical pyramidal cells respond as integrate-and-fire neurons to in vivo-like input currents. J. Neurophysiol. 90: 1598–1612.
Ricciardi LM, Lansky P (2003) Diffusion models of neuronal activity. In: MA Arbib, ed. The Handbook of the Brain Theory and Neural Networks, (2nd edn.) MIT Press, Cambridge, MA.
Richardson MJE, Gerstner W (2005) Synaptic shot noise and conductance fluctuations affect the membrane voltage with equal significance Neural Comput. 17: 923–947.
Rodriguez R, Lansky P (2000) Effect of spatial extension on noise enhanced phase-locking in a leaky integrate-and-fire model of a neuron. Phys. Rev. E 62: 8427–8437.
Rospars J-P, Lansky P, Vaillant J, Duchamp-Viret P, Duchamp A (1994) Spontaneous activity of first- and second-order neurons in the olfactory system. Brain Res. 662: 31–44.
Segev I (1992) Single neurone models: Oversimple, complex and reduced. TINS 15:414–421.
Shinomoto S, Sakai Y, Funahashi S (1999) The ornstein-uhlenbeck process does not reproduce spiking statistics of neurons in prefrontal cortex. Neural Comp. 11: 935–951.
Stein RB (1965) A theoretical analysis of neuronal variability. Biophys. J. 5: 173–195.
Stevens CF, Zador AM (1998) Novel Integrate-and-fire-like Model of repetitive firing in cortical neurons. Proceedings of the 5th Joint Symposium on Neural Computation, UCSD, La Jolla CA.
Stevens CF (1964) Letter to the editor. Biophys. J. 4: 417–419.
Tateno T, Kawana A, Jimbo Y (2002) Analytical characterization of spontaneous firing in networks of developing rat cultured cortical neurons. Phys. Rev. E 65: Art. No. 051924.
Tuckwell HC (1988) Introduction to Theoretical Neurobiology. Cambridge Univ. Press, Cambridge.
Tuckwell HC, Lansky P (1997) On the simulation of biological diffusion processes. Comput. Biol. Med. 27: 1–7.
Tuckwell HC, Richter W (1978) Neuronal interspike time distribution and the estimation of neurophysiological and neuroanatomical parameters. J. theor. Biol. 71: 167–183.
Xiong Y, Yu YQ, Chan YS He J (2003) An in-vivo intracellular study of the auditory thalamic neurons. Thalamus Related Sys. 2: 253–260.
Yu YQ, Xiong Y, Chan YS He JF (2004) Corticofugal gating of auditory information in the thalamus: An in vivo intracellular recording study. J. Neurosci. 24: 3060–3069.

Journal of Physiology - Paris 104 (2010) 160–166

Contents lists available at ScienceDirect

Journal of Physiology - Paris

journal homepage: www.elsevier.com/locate/jphysparis

Effect of stimulation on the input parameters of stochastic leaky integrate-and-fire neuronal model

Petr Lansky [a,*], Pavel Sanda [a], Jufang He [b]

[a] Institute of Physiology, Academy of Sciences of the Czech Republic, Prague, Czech Republic
[b] Department of Rehabilitation Sciences, The Hong Kong Polytechnic University, Hung Hom, Kowloon, Hong Kong

ARTICLE INFO

Keywords:
Interspike interval
Ornstein–Uhlenbeck
Intracellular recording
Estimation of parameters

ABSTRACT

The Ornstein–Uhlenbeck neuronal model is specified by two types of parameters. One type corresponds to the properties of the neuronal membrane, whereas the second type (local average rate of the membrane depolarization and its variability) corresponds to the input of the neuron. In this article, we estimate the parameters of the second type from an intracellular record during neuronal firing caused by stimulation (audio signal). We compare the obtained estimates with those from the spontaneous part of the record. As predicted from the model construction, the values of the input parameters are larger for the periods when neuron is stimulated than for the spontaneous ones. Finally, the firing regimen of the model is checked. It is confirmed that the neuron is in the suprathreshold regimen during the stimulation.

1. Introduction

Spiking activity is the basic mode of the information transfer within the nervous system. The sequences of spikes (action potentials) are generated and sent along an axon to other neurons. These action potentials are considered to be none-or-all events with shapes irrelevant for the information they convey. Formally, they are taken in the limit as Dirac delta function and the complete sequence of them as a realization of a stochastic point process. The application of the theory of stochastic point processes in description of spike trains is very common and the phenomenological models of single neurons predicting properties of these point processes are often investigated (Tuckwell, 1988; Gerstner and Kistler, 2002; Dayan and Abbott, 2001). The models are build to generate interspike intervals (ISIs) and they are often based on the first-passage-time principle for so called integrate-and-fire models which mimic accumulation of the incoming signal and the final generation of the spike is replaced by instantaneous reset of the generator to the initial level (Brunel and van Rossum, 2007).

Attempts to compare the experimental data with the models is very common for so called biophysical models of neurons, but considering the phenomenological models, they are more frequently compared qualitatively, and the researchers are satisfied if they perform in a similar way to the real neurons. Burkitt (2006) reviewed the integrate-and-fire neuron models and mathematical techniques to analyze them. We can see from this review that with exception of a few theoretical attempts, the comparison of the models with data has been rather neglected. Only recently the phenomenological models are confronted with experimental data, for a review see Lansky and Ditlevsen (2008).

Stochastic diffusion integrate-and-fire neuronal model (the Ornstein–Uhlenbeck process) describes the membrane potential as a continuous-time stochastic process. Along the introduction of this model there have been given many arguments why this treatment of the integrate-and-fire model is appropriate. Leakage of the neuronal membrane, it means the current which flows through the membrane due to its passive properties, was one of the first specification of the integrate-and-fire neuron model. It is a crucial property of the integrate-and-fire models and thus it is inherent for practically all the variants of the model. Generalizations were recently introduced aiming to improve flexibility of the model and its predictive power (Clopath et al., 2007; Jolivet et al., 2006).

The model investigated in this paper has parameters of two types. The first are the parameters which can be measured by indirect electrophysiological methods, deduced from the properties of other neurons or from measuring the membrane potential fluctuations. If these parameters are known, one can check how well the model predicts spiking activity under the condition of an input identical with the input to a real neuron. The second set of parameters, investigated in this paper, is identified with the signals impinging upon the neuron. Knowledge of these parameters can be used either to deduce unknown signal coming to a neuron or to check whether we are able to read correctly an artificially delivered signal.

* Corresponding author. Address: Institute of Physiology, Academy of Sciences, Videnska 1083, 142 20 Prague 4, Czech Republic.
E-mail address: lansky@biomed.cas.cz (P. Lansky).

0928-4257/$ - see front matter © 2009 Elsevier Ltd. All rights reserved.
doi:10.1016/j.jphysparis.2009.11.019

To estimate the input signal either the membrane depolarization or ISIs have to be at our disposal. As mentioned, the previous attempts to identify the model parameters were based on observation of ISIs. Such a task is complicated and leads to rather difficult numerical and mathematical problems (Inoue et al., 1995; Shinomoto et al., 1999; Ditlevsen and Lansky, 2005, 2006, 2007; Koyama and Kass, 2008; Mullowney and Iyengar, 2008). In the study Lansky et al. (2006) estimation of five basic parameters the Ornstein–Uhlenbeck model was studied for the membrane depolarization data. The whole estimation procedure was based on the spontaneous-firing part of the intracellular recording. The primary aim of this study is to extend the results on the stimulation part of the recorded signal.

2. Model and its properties

The deterministic leaky integrate-and-fire model (Lapicque model, RC-circuit) can be derived from the assumptions that the membrane depolarization is described by a circuit with a generator, a resistor and a capacitor in parallel. It has to be stressed that while the electrical representation is related to a small isopotential patch of neuronal membrane, the voltage in the model reflects an abstract representation of a complete neuron; usually described as depolarization at the trigger zone. The trigger zone serves as a reference point and all the other properties of the neuron are integrated into it.

The Ornstein–Uhlenbeck model of membrane depolarization is a stochastic variant of the RC-circuit model and can be formally described by a stochastic differential equation,

$$\frac{dX(t)}{dt} = -\beta(X(t) - x_0) + \mu + \sigma\xi(t), \quad X(0) = x_0, \tag{1}$$

where β reflects the spontaneous decay of the membrane depolarization to the resting level x_0, μ represents the local average rate of displacement due to the neuronal input, σ reflects the variability of the membrane potential due to the neuronal input and $\xi(t)$ stands for Gaussian white noise. The spikes are not an intrinsic part of model (1) but are generated when the membrane depolarization $X(t)$ reaches the firing threshold S for the first time. So, S is an additional parameter. After firing, the depolarization is reset to the resting level, x_0, and the process of input "integration" starts anew. Also the reset level, x_0, represents a parameter of the model. The model is fully described by five parameters: β, μ, σ, S and x_0, which specify Eq. (1) together with its initial and boundary condition. More details on the Ornstein–Uhlenbeck neuronal model can be found, for example, in Tuckwell (1988) or Burkitt (2006). The parameters introduced above can be divided in two categories:

- Parameters depending on the membrane properties – β being the inverse of the membrane time constant, threshold S and resting level x_0.
- Parameters depending on the input signal – μ representing the mean signal and σ characterizing its variability. In this study we identify these parameters. As we focus on the changes in them brought by the stimulation, we are interested in comparing the values of these two parameters in spontaneous and stimulated parts of the data.

There can be posed serious questions whether β, S and x_0 are independent of the input. Actually, from the experimental data we directly found that, at least, x_0 changes in the presence of stimulation and we further take this fact into account.

The position of the asymptotic mean depolarization $E(X(\infty)) = x_0 + \mu/\beta$, as seen from Eq. (1) determines three basic regimes of firing of the Ornstein–Uhlenbeck model:

- The subthreshold regimen ($\mu/\beta \ll S - x_0$) with Poissonian firing. As the asymptotic mean depolarization does not reach the threshold the firing depends on the noise and without it the neuron would remain silent. It was shown in our previous article Lansky et al. (2006) that the spontaneous part of the recorded data fits mostly with subthreshold regimen characterization.
- The threshold regimen ($\mu/\beta \approx S - x_0$), where the distribution of ISIs is positively skewed and resembles for example Gamma distribution.
- The suprathreshold regimen ($\mu/\beta \gg S - x_0$), where the firing is almost regular and ISI histogram resembles normal distribution. The noise plays a limited role in this range of parameters.

As already mentioned in Section 1 two basic types of data can be used for the identification of the parameters of the Ornstein–Uhlenbeck model. If only the ISIs are available, the methods applicable in this situation are reviewed in Lansky and Ditlevsen (2008). In the second situation, which is investigated here, the membrane depolarization is recorded in between the spike generation. Some methods for estimation of the parameters under this sampling were compared for this type of data in Lansky et al. (2006) and now we apply only the selected ones.

3. Methods

3.1. Data collection

3.1.1. Animal preparation and data preprocessing

Guinea pigs served as subjects for the intracellular recording experiments. Throughout the recording, an electrocorticograph was monitored to assess the level of anaesthesia. A midline incision was made in the scalp and a craniotomy was performed to enable vertical access to the MGB in the right hemisphere (He, 2003; Xiong et al., 2006; Yu et al., 2004). The experimental procedures were approved by the Animal Subjects Ethics Sub-Committee of The Hong Kong Polytechnic University. Upon penetrating the membrane of a cell, the electrode detected the negative membrane potential. After amplification, the membrane potential as well as the auditory stimulus were stored in the computer with the aid of commercial software (AxoScope, Axon). Single neuron data were selected for this article. The membrane potential was recorded with time step $h = 0.00015$ s $= 0.15$ ms , for period 0–501 s. For further processing we make basic noise-filtering of the membrane potential by a moving average over six values, see Lansky et al. (2006) for details. The acoustic signal used for the stimulation of neuron has duration of 0.1 s and the series of the acoustic signals divided the record into the sections of stimulated and spontaneous parts. We compare the stimulated parts of the record with the unstimulated ones.

3.1.2. Detection of spikes

We detected and selected 86 stimulated parts in the record, which were used for the analysis. An example of a data can be seen in Fig. 1.

A typical neuronal response varies between two and three spikes during the stimulation. In the spontaneous part, the spikes appear rarely. As can be seen in Fig. 2 there is a substantial change of depolarization course after the second spike within the period of stimulation.

Because of this fact we need to distinguish between the first and the following ISIs within one stimulation. For this purpose we divide the periods of stimulation according to the number of ISIs in them. We got three periods of stimulation without any complete ISI, 68 periods of stimulation containing just one ISI, 14 periods of stimulation containing two ISIs and one period of stimulation

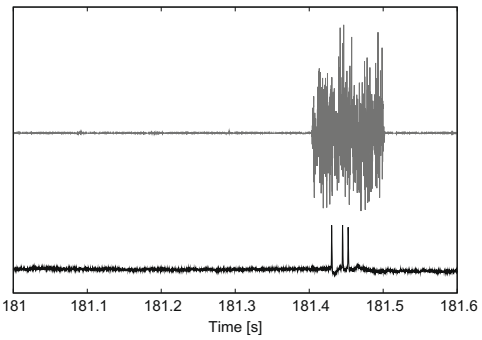

Fig. 1. Example of the acoustic signal (shaded curve) and the membrane depolarization (black curve). There are no spikes in the absence of stimulation and three spikes during the stimulation.

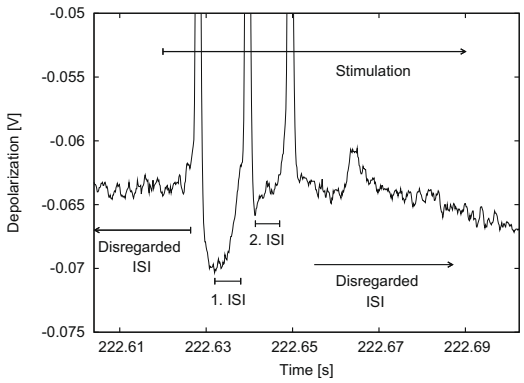

Fig. 2. An example of membrane depolarization course during the period of stimulation containing two ISIs.

containing three ISIs. It is obvious from this distribution, that for statistical evaluation only the first ISIs (68 + 14 + 1) can be used (the second and the third ISIs are too rare).

In the spontaneous part we got 312 complete ISIs and because the spike frequency in this part was substantially lower the shapes of membrane depolarization were similar and there was no need to distinguish serial number of ISIs in spontaneous part. Note that the comparison between stimulated and spontaneous records is based on ISIs which are completely within these specific periods and thus the ISIs which are partly in both periods are disregarded (see Fig. 2).

3.2. Precise detection of ISI

The membrane potential trajectories between spikes take a shape of valleys in the stimulated parts of the record (see Fig. 2). Firstly, we formulate a heuristic procedure how to detect these valleys in the record. As the estimation of the parameters is based on the membrane potential trajectory which is entirely outside the spikes, we have to determine carefully from what time and up to which time we consider the data. Then, these two time instances implicitly define the corresponding ISI.

For the detection of spike we fix the voltage level at -35.5 mV as in the previous study (Lansky et al., 2006). For the beginning of the valley we pose the *valley-detection* level at -50 mV. For the detection of the end of the valley we look for the maximum

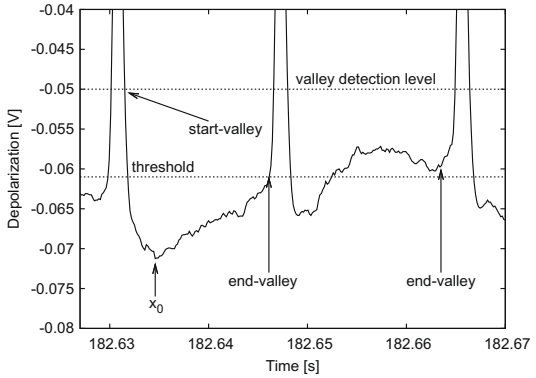

Fig. 3. ISI detection. We can see three spikes defining two ISIs within period of stimulation. The values of the membrane potential from x_0 to the end of the valley are used for the parameters estimation. See text for details.

of the last point with decreasing depolarization before the next spike or the last point when the threshold S is crossed before next spike. Both cases can be seen in Fig. 3.

Threshold S itself is not searched for in periods of stimulation, as the heuristic method used in the spontaneous part failed. Here the depolarization often goes from the valley after spike straightly (almost linearly) towards next spike without crossing any specific point, which can be clearly marked as the threshold (see Fig. 2). Model (1) considers the threshold as the membrane property and thus we take its value $S = -61$ mV as derived from the spontaneous part of the data (Lansky et al., 2006). In the same way, for the inverse of the membrane time constant we fix $\beta = 25.8\ 1/\mathrm{s}$ as it was estimated from the spontaneous activity.

After detecting the valley we can detect the corresponding ISI. We identify reset potential x_0 as the minimal voltage value in the valley and it is the only intrinsic parameter determined in this paper, see Section 4.2.3. The ISI is defined as interval between the time when $X(t) = x_0$ and the end of the valley. The period from the spike to the beginning of ISI can be identified as the refractory period. For a recent review of methods for determination of refractory period from ISI data, see Hampel and Lansky (2008). Here we do not investigate this problem, but we complement the picture by giving the values derived from the depolarization but not the ISIs, see Section 4.2.4. We should note that the current procedure applied to the data is slightly different from that used in our previous paper. In this study the valley has to be defined in a more complex way as the lengths of ISIs are very short and the shapes of membrane potential are much more variable (see details in Fig. 3).

3.3. Parameters estimation

There are two parameters of model (1) driven by the incoming signal to the neuron – μ and σ. In Lansky et al. (2006), the regression method appeared to be more appropriate than the likelihood method for estimating the parameter μ. To apply the regression method we minimize the functional

$$L(\mu) = \sum_{j=1}^{N} \left(x_j - x_0 - \frac{\mu}{\beta}(1 - exp(-\beta jh)) \right)^2 \qquad (2)$$

with respect to the parameter μ, where h stands for time step and x_j are individual measured values of membrane depolarization for the total time $T = Nh$. What is minimized in Eq. (2) is the distance between observed values of the membrane potential and the mean depolarization in the absence of the threshold. There are two draw-

backs of the method. At first, it is the fact, that the predicted values are those expected in the absence of the threshold. We investigated this fact deeply in Bibbona et al. (2008) and the effect on the estimation is not substantial. At second, the observed values of the membrane depolarization are not independent realizations of random variables and it restricts the conclusions made on the basis of the regression. Nevertheless, in our experience, the method is an acceptable compromise between the tractability and efficiency.

For estimation of the noise amplitude we use the formula obtained by the maximum likelihood method

$$\widehat{\sigma^2} = \frac{1}{T}\sum_{j=0}^{N-1}(x_{j+1} - x_j + x_j h\beta - h\hat{\mu})^2, \tag{3}$$

and also the formula established by Feigin (1976), which is independent of the other parameters estimation:

$$\widehat{\sigma^2}' = \frac{1}{T}\sum_{j=0}^{N-1}(x_{j+1} - x_j)^2. \tag{4}$$

In this way for each ISI a pair of estimated $\hat{\mu}_i, \hat{\sigma}_i$ is computed.

4. Results and discussion

We investigate the effect of stimulation in two directions. At first, we compare simulations of model (1) based on the estimated parameters with the experimental record. Secondly, we compare the stimulated ISIs and their respective μ, σ parameters to ISIs and the parameters from the spontaneous part of the record.

4.1. Model and data comparison

As already stated, we have 83 ISIs which are the first ones and completely contained in the stimulation periods. For i-th ISI $(i = 1, \ldots, 83)$ we have a vector of values of depolarization $\boldsymbol{x_i} = (x_{i0}, x_{i1}, \ldots, x_{in})$, where n depends on the length of the ISI. Corresponding vector of mean depolarization, $\boldsymbol{y_i} = (y_{i0}, y_{i1}, \ldots, y_{in})$ was obtained from simulating Eq. (1) using the estimated parameter $\hat{\mu}_i$ and $\sigma_i = 0$. The differences $\boldsymbol{z_i} = \boldsymbol{x_i} - \boldsymbol{y_i}$ were calculated and their average and standard deviation evaluated. The results are shown in Fig. 4. We can see that model based on the estimated parameters does not show any systematic error in the course of membrane depolarization.

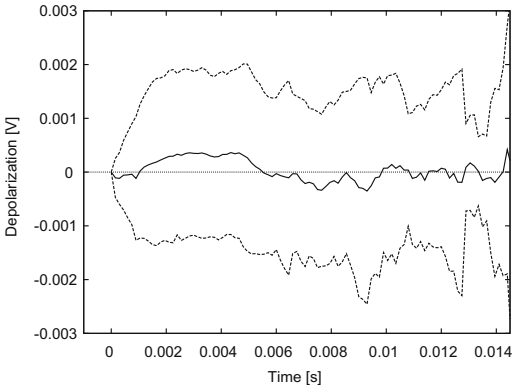

Fig. 4. Comparison of experimental data with the model. The central solid curve is an average of the differences z_i, dotted curves indicate $\pm 2 * \textit{standard deviations}$. See text for details.

4.2. Comparison of the parameters

4.2.1. Parameter μ

It can be clearly seen in Fig. 5 that the estimates of μ have much broader distribution with median around 1.1 V/s in the stimulated part than in the spontaneous part, where the distribution is located around the value of 0.3 V/s. The fact that for stimulated part all the estimated values of μ are higher than in the spontaneous one corresponds with the interpretation of μ in the Ornstein–Uhlenbeck model. The lower variability of μ in the spontaneous regime corresponds to the fact that their values are lower, see Table 1, but the relative variability, as reflected by CV, is higher for the spontaneous data.

4.2.2. Parameter σ

In Fig. 6 we can see that the situation for σ is analogous to the case of μ. The estimate of the variance σ has broader distribution with median around $0.026\,\mathrm{V}/\sqrt{s}$ in the stimulated parts than in the spontaneous parts, where σ has more narrow range with significantly higher peak around the value of $0.013\,\mathrm{V}/\sqrt{s}$. The results are also documented in Table 2, where we can realize that Eq. (3) gives slightly lower values of estimates than Eq. (4).

In correspondence with Lansky and Sacerdote (2001) there is higher σ for the stimulated ISIs. This is the first experimental confirmation of our results originally achieved on entirely theoretical basis. To get a better picture of the relationship between μ and σ different levels of the stimulation would be necessary.

4.2.3. Reset potential x_0

It is apparent from the data and illustrated in Fig. 2 that the reset value is influenced by the stimulation. This can be interpreted in such a way, that the accumulation of the incoming signal takes place during the reset of the membrane potential, resp., during the refractory period. Obviously, for the second ISI within one stimulation period, there are additional reasons why x_0 changes. Thus the

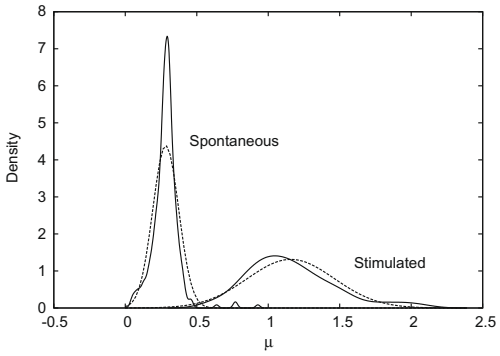

Fig. 5. Distribution of the estimates of the parameter μ: left curves – spontaneous, right curves – stimulated. Dotted lines are fitted normal distributions $f(\mu) = \frac{1}{s\sqrt{2\pi}} e^{\frac{(\mu - m)^2}{2s^2}}$, $m_{stim} = 1.158$, $s_{stim} = 0.304$ and $m_{spont} = 0.283$, $s_{spont} = 0.091$.

Table 1
Descriptive statistics for the estimates of parameter μ.

$\hat{\mu}$ [V/s]	Stimulated	Spontaneous
Min	0.6046	0.04665
Max	2.0840	0.92737
Median	1.1061	0.28460
Mean	1.1580	0.28324
CV	0.2645	0.32156

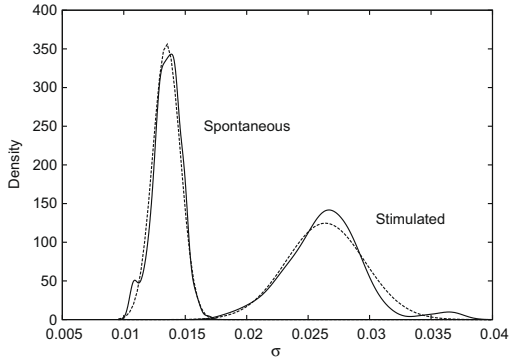

Fig. 6. Distribution of the estimates of the parameter σ: left curves – spontaneous, right curves – stimulated. Dotted lines are fitted normal distributions $f(\mu) = \frac{1}{s\sqrt{2\pi}} e^{-\frac{(\mu-m)^2}{2s^2}}$, $m_{stim} = 0.0264$, $s_{stim} = 0.0032$ and $m_{spont} = 0.0135$, $s_{spont} = 0.0012$.

Table 2
Descriptive statistics for the estimates of parameter σ.

$\hat{\sigma}'$ [V/$\sqrt{s}$]	Stimulated	Spontaneous	Stimulated ($\hat{\sigma}$ from Eq. (3))
Min	0.01843	0.01043	0.01576
Max	0.03686	0.01681	0.03166
Median	0.02646	0.01351	0.02262
Mean	0.02640	0.01348	0.02215
CV	0.12218	0.08310	0.12566

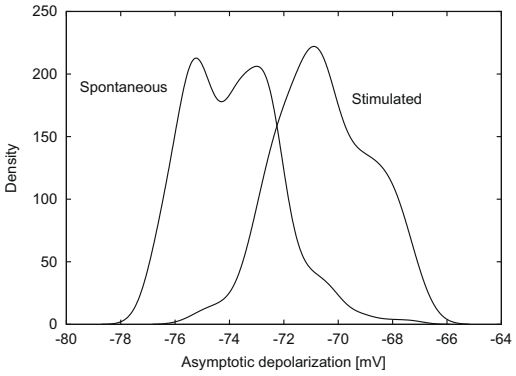

Fig. 7. Distribution of the reset potential x_0: left curve – spontaneous, right curve – stimulated.

last parameter which we determine is x_0. We can see in Fig. 7 that the shapes of the densities of the estimates do not differ and the range remains around 10 mV for both cases. The median value is lower in the case of spontaneous record. As mentioned, this can be explained by the fact, that the input signal contributes to the membrane potential during the refractory period. See Table 3 for the descriptive statistics of x_0.

4.2.4. Time to reach the resting potential

We also measure how much time it takes for the membrane potential to reach the resting level after the spike. It is not a parameter of model (1), but such knowledge could help to judge how realistic the model is. In particular we take the interval which

Table 3
Descriptive statistics for parameter x_0.

$\hat{x_0}$ [mV]	Stimulated	Spontaneous
Min	−74.92	−77.25
Max	−67.08	−67.33
Median	−70.58	−73.92
Mean	−70.52	−73.90
CV	−0.024	−0.023

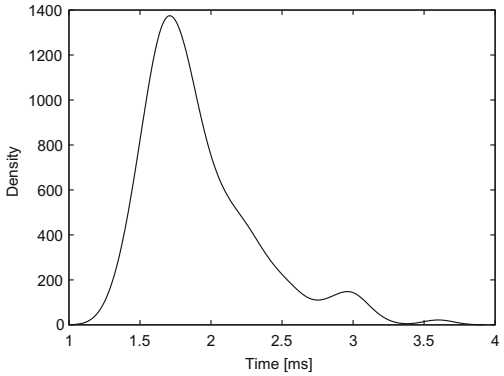

Fig. 8. Distribution of the time from the peak of the spike to the resting potential, 169 (=3 + 2 ∗ 68 + 2 ∗ 14 + 2 ∗ 1 – two first spikes taken, if possible) spikes were regarded.

Table 4
Descriptive statistics for the time to reach the resting potential.

Time to reach the resting potential [ms]	
Min	1.35
Max	3.6
Median	1.8
Mean	1.9
CV	0.21

starts on the top of the spike and calculate the time till the first local minimum in the membrane depolarization after the spike. This procedure has the advantage that we can take both the first and the second spikes in stimulated region for statistical evaluation – as it follows from the previous section, it is not generally possible to define x_0 after the second spike. The density estimation of the time till x_0 is reached is in Fig. 8 and summary statistics in Table 4.

These results practically coincide with the estimation of the refractory period based on ISIs only, which was estimated around 3 ms (Hampel and Lansky, 2008), taking into account that the refractory period should be longer than the time to the minimum depolarization.

4.2.5. Firing regimen

As mentioned in Section 2, the key issue for the behavior of model (1) is the mutual position between $S - x_0$ and μ/β. To check the threshold regime we compute $S - x_0$ and $\hat{\mu}/\beta$, where for $\hat{\mu}$ we take the vector of estimated values, S, β are medians of the estimates taken from the spontaneous part of the data and x_0 from the corresponding part (spontaneous or stimulated). In Fig. 9 we see that asymptotic mean depolarization is always higher (median is 43 mV) than threshold value in the case of stimulated data, which is in a good agreement with our expectation.

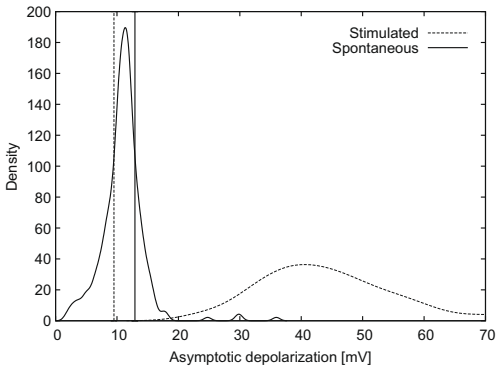

Fig. 9. Estimations of the densities of the asymptotic depolarization with regard to the threshold: left curve – spontaneous, right curve – stimulated. The values (vertical lines) of $S - x_0 = 13$ mV for the spontaneous case and 9.5 mV for stimulated case divides the supra and subthreshold regimen.

4.3. ISI distribution

Using the methods described above we got 83 first ISIs completely within the stimulated parts and 312 ISIs in the spontaneous parts. In Fig. 10 we compare their distributions. The empirical density of the spontaneous ISIs suggests that they are generated in accordance with the exponential distribution (Kolmogorov–Smirnov test does not reject the hypothesis of exponentiality at 5% significance level), which may imply the Poissonian firing regime. The shape of the density for the stimulated ISIs suggests gamma distribution (Kolmogorov–Smirnov test does not reject the hypothesis of gamma distribution at 5% a significance level).

Table 5
Descriptive statistics for ISIs.

ISIs [ms]	Stimulated	Spontaneous
Min	3.900	88.5
Max	24.750	5090.4
Median	8.400	584.6
Mean	9.033	871.9
CV	0.345	0.883

The descriptive statistics of the ISIs are in Table 5. We can see that there is a clear distinction between the spike frequency for stimulated part $f_{stim} = 110$ Hz and for spontaneous part $f_{spon} = 1.14$ Hz, for median the values are $f_{stim} = 119$ Hz, $f_{spon} = 1.71$ Hz.

4.3.1. Comparison of experimental and theoretical distribution

To compare experimental ISI distributions with the Ornstein–Uhlenbeck first-passage-time distribution, we simulated model (1) with estimated parameters. The results are in Fig. 11.

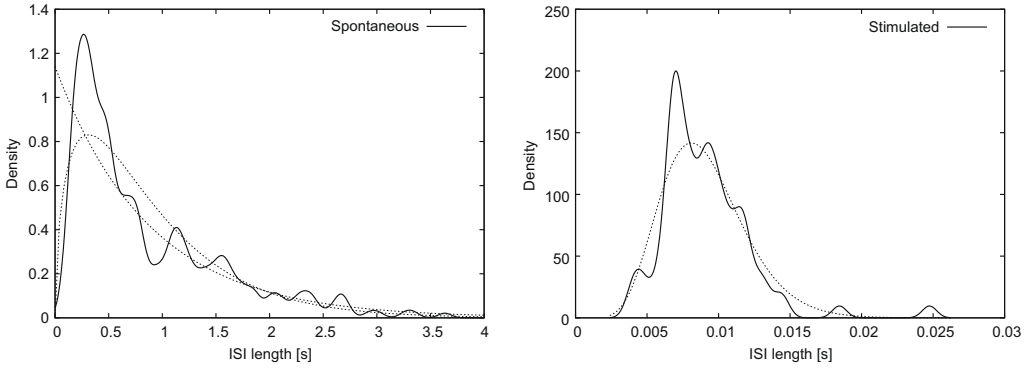

Fig. 10. Distributions of ISIs lengths: the left panel – spontaneous ISIs, the dotted line represents the fitted exponential ($f(x) = \lambda e^{-\lambda x}$, $\lambda = 1.14$) and gamma ($f(x) = x^{\alpha-1}\frac{\beta^\alpha e^{-\beta x}}{\Gamma(\alpha)}$, $\alpha = 1.56$, $\beta = 1.79$) distribution; the right panel – stimulated ISIs, the dotted line represents the fitted gamma distribution ($\alpha = 9.45$, $\beta = 1043.3$).

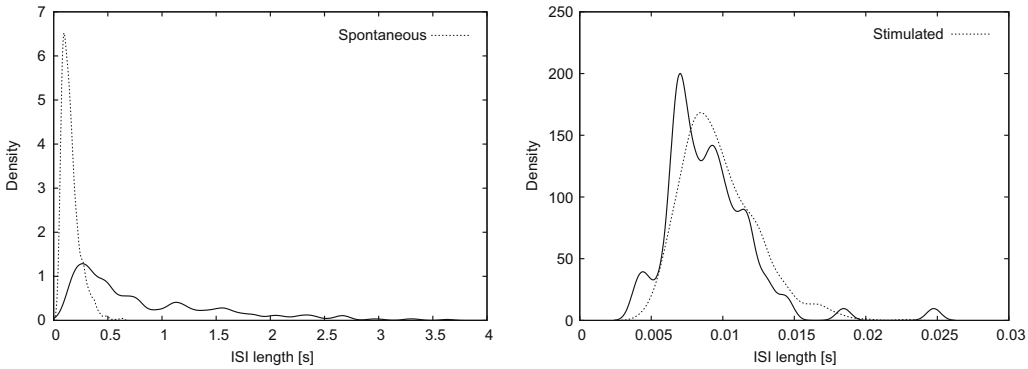

Fig. 11. Distributions of the first-passage-times obtained from Eq. (1) with parameters estimated from the trajectories: the left panel – spontaneous, the right panel – stimulated. The solid lines are estimated densities of experimentally obtained ISIs (histograms), the dotted lines are estimated densities from the simulation of first-passage-times of model (10^3 runs).

The fit of the observed lSIs to the model is perfect for the stimulated activity. It is not the case for the spontaneous activity, where from the model we obtained distribution which is more narrow and shifted in direction of short lSIs. At this moment we are not able to explain this discrepancy.

Acknowledgments

AV0Z50110509, Center for Neurosciences LC554, Grant Agency of the Academy of Sciences of the Czech Republic – Project IAA101120604.

References

Bibbona, E., Lansky, P., Sacerdote, L., Sirovich, R., 2008. Errors in estimation of the input signal for integrate-and-fire neuronal models. Physical Review E 78, 011918.

Brunel, N., van Rossum, M., 2007. Lapicque's 1907 paper: from frogs to integrate-and-fire. Biological Cybernectics 97, 1–3.

Burkitt, A., 2006. A review of the integrate-and-fire neuron model: I. Homogeneous synaptic input. Biological Cybernetics 95, 1–19.

Clopath, C., Jolivet, R., Rauch, A., Lüscher, H., Gerstner, W., 2007. Predicting neuronal activity with simple models of the threshold type: adaptive exponential integrate-and-fire model with two compartments. Neurocomputing 70, 1668–1673.

Dayan, P., Abbott, L., 2001. Theoretical Neuroscience. MIT Press, Cambridge, CA.

Ditlevsen, S., Lansky, P., 2005. Estimation of the input parameters in the Ornstein–Uhlenbeck neuronal model. Physical Review E 71, 11907.

Ditlevsen, S., Lansky, P., 2006. Estimation of the input parameters in the Feller neuronal model. Physical Review E 73, 61910.

Ditlevsen, S., Lansky, P., 2007. Parameters of stochastic diffusion processes estimated from observations of first-hitting times: application to the leaky integrate-and-fire neuronal model. Physical Review E 76, 41906.

Feigin, P., 1976. Maximum likelihood estimation for continuous-time stochastic processes. Advances in Applied Probability 8, 712–736.

Gerstner, W., Kistler, W., 2002. Spiking Neuron Models. Cambridge University Press, New York.

Hampel, D., Lansky, P., 2008. On the estimation of refractory period. Journal of Neuroscience Methods 171, 288–295.

He, J., 2003. Slow oscillation in non-lemniscal auditory thalamus. Journal of Neuroscience 23, 8281–8290.

Inoue, J., Sato, S., Ricciardi, L., 1995. On the parameter estimation for diffusion models of single neuron's activities. Biological Cybernetics 73, 209–221.

Jolivet, R., Rauch, A., Luscher, H., Gerstner, W., 2006. Integrate-and-fire models with adaptation are good enough: predicting spike times under random current injection. In: Weiss, Y., Schölkopf, B.P.J. (Eds.), Advances in Neural Information Processing Systems, Vol. 18. MIT Press, Cambridge MA, pp. 595–602.

Koyama, S., Kass, R., 2008. Spike train probability models for stimulus-driven leaky integrate-and-fire neurons. Neural Computation 20, 1776–1795.

Lansky, P., Ditlevsen, S., 2008. A review of the methods for signal estimation in stochastic diffusion leaky integrate-and-fire neuronal models. Biological Cybernetics 99, 253–262.

Lansky, P., Sacerdote, L., 2001. The Ornstein–Uhlenbeck neuronal model with signal-dependent noise. Physics Letters A 285, 132–140.

Lansky, P., Sanda, P., He, J., 2006. The parameters of the stochastic leaky integrate-and-fire neuronal model. Journal of Computational Neuroscience 21, 211–223.

Mullowney, P., Iyengar, S., 2008. Parameter estimation for a leaky integrate-and-fire neuronal model from ISI data. Journal of Computational Neuroscience 24, 179–194.

Shinomoto, S., Sakai, Y., Funahashi, S., 1999. The Ornstein–Uhlenbeck process does not reproduce spiking statistics of neurons in prefrontal cortex. Neural Computation 11, 935–951.

Tuckwell, H., 1988. Introduction to Theoretical Neurobiology. Cambridge University Press, New York.

Xiong, Y., Yu, Y., Fujimoto, K., Chan, Y., He, J., 2006. An in vivo intracellular study of auditory thalamic neurons. Thalamus and Related Systems 2, 253–260.

Yu, Y., Xiong, Y., Chan, Y., He, J., 2004. Corticofugal gating of auditory information in the thalamus: an in vivo intracellular recording study. Journal of Neuroscience 24, 3060–3069.

BRAIN RESEARCH 1434 (2012) 257–265

Available online at www.sciencedirect.com

SciVerse ScienceDirect

www.elsevier.com/locate/brainres

BRAIN RESEARCH

Research Report

Stochastic interpolation model of the medial superior olive neural circuit

Pavel Sanda[a,c,d,*], *Petr Marsalek*[b,c,d]

[a]*Institute of Physiology, Academy of Sciences of the Czech Republic, Videnska 1083, 142 20, Praha 4, Czech Republic*
[b]*Institute of Pathological Physiology, First Medical Faculty, Charles University of Prague, U Nemocnice 5, 128 53, Praha 2, Czech Republic*
[c]*Max Planck Institute for the Physics of Complex Systems, Noethnitzer Str. 38, 011 87, Dresden, Germany*
[d]*Faculty of Biomedical Engineering, Czech Technical University of Prague, Nam. Sitna 3105, 272 01, Kladno, Czech Republic*

ARTICLE INFO

Article history:
Accepted 19 August 2011
Available online 27 August 2011

Keywords:
Coincidence detection
Directional hearing
Interaural time delay
Sound azimuth
Interpolation model

ABSTRACT

This article presents a stochastic model of binaural hearing in the medial superior olive (MSO) circuit. This model is a variant of the slope encoding models. First, a general framework is developed describing the elementary neural operations realized on spike trains in individual parts of the circuit and how the neurons converging onto the MSO are connected. Random delay, coincidence detection of spikes, divergence and convergence of spike trains are operations implemented by the following modules: spike generator, jitter generator, and coincidence detector. Subsequent processing of spike trains computes the sound azimuth in the circuit. The circuit parameters that influence efficiency of slope encoding are studied. In order to measure the overall circuit performance the concept of an ideal observer is used instead of a detailed model of higher relays in the auditory pathway. This makes it possible to bridge the gap between psychophysical observations in humans and recordings taken of small rodents. Most of the results are obtained through numerical simulations of the model.

1. Introduction

A model of the mammalian MSO circuit which localizes the direction of the sound source in the horizontal plane (azimuth) at low frequency range is presented here. This model is based upon the *interpolation* of the direction in question using the firing rate code of the MSO binaural neurons. This is proposed as an alternative mechanism for low frequency sound localization in mammals, as the precise mechanism in mammals is not known to date (Dean et al., 2008; Joris et al., 1998, 2006; Karino et al., 2011). The *interpolation model* differs from the model proposing an *array of delay lines* (Jeffress, 1948). In the Jeffress model, the sound direction is encoded using a spatial code which includes the position of peak neural activity within the array. In the interpolation model, the binaural neuron encodes the sound direction using its firing rate. Firing of this neuron constitutes the ITD (interaural time difference) curve. The sound direction is read out by interpolation from this curve.

McAlpine et al. (2001), Brand et al. (2002), Grothe (2003) and others have proposed an ITD readout mechanism which en-

* *Corresponding author at:* Institute of Physiology, Academy of Sciences of the Czech Republic, Videnska 1083, 142 20, Praha 4, Czech Republic. Fax: +420 241 062 488.
E-mail address: sanda@biomed.cas.cz (P. Sanda).

Abbreviations: AN, auditory nerve; AP, action potential; EE, excitatory–excitatory; EI, excitatory–inhibitory; EPSP, excitatory post-synaptic potentials; IPSP, inhibitory post-synaptic potentials; ITD, interaural time difference; MSO, medial superior olive

0006-8993/$ – see front matter © 2011 Elsevier B.V. All rights reserved.
doi:10.1016/j.brainres.2011.08.048

codes the sound direction through the maximal slope of the response function. This function has the ITD as its argument and the firing rate as its output. In line with the terminology used previously, we can call this mechanism *slope encoding*. Our interpolation model is a variant of this slope encoding mechanism. One of the crucial experimental findings is that abolishing of inhibitory inputs by strychnine moves the maximum slope out of the operational range (Brand et al., 2002). Based on this observation, the slope encoding model has, as one of its key elements, an inhibitory input to the MSO.

Our model reproduces the MSO computations at the level of abstract neural circuit description. Biophysical interactions of the excitatory and inhibitory postsynaptic potentials (EPSPs and IPSPs) at the postsynaptic membrane are not modeled in detail. Concerning the interaction of the IPSP with the EPSP, their time order is important. The IPSP must precede the EPSP to exceed the threshold (Grothe, 2003; Pecka et al., 2008). The PSPs from the two sides have to meet within a given coincidence detection time window. The window size is one of the key parameters in our model. We stress this aspect of the model because the rise and decay time constants of postsynaptic voltage dependent currents determine the coincidence detection window size. The subcellular details are abstracted in this paper. In vitro experiments conducted in the search for the subcellular mechanism responsible for the sub-millisecond precision show the plurality of underlying biophysical mechanisms. To name only two of these one particular mechanism which contributes to setting the duration of the coincidence detection window is implemented by the voltage-activated potassium current at the postsynaptic membrane (Mathews et al., 2010). Another mechanism by which the order of the IPSP and EPSP is distinguished is the post-inhibitory rebound mechanism (Brand et al., 2002).

We also use the ergodic assumption of indistinguishable time and population ensemble encoding of the signals by spike trains. The ergodic assumption in physics was originally introduced in statistical mechanics of gases by Boltzmann in the nineteenth century. According to this assumption the average of a selected quantity is the same for the time average and for the statistical ensemble average (Papoulis, 1991). In other words, it assumes that the same result is obtained when observing a process over a long period of time as when sampling a given number of shorter independent realizations of the same process. This approach is applied in the neural coding description as follows. To receive information about the sound source direction, one can either wait for a given period of time and measure all the

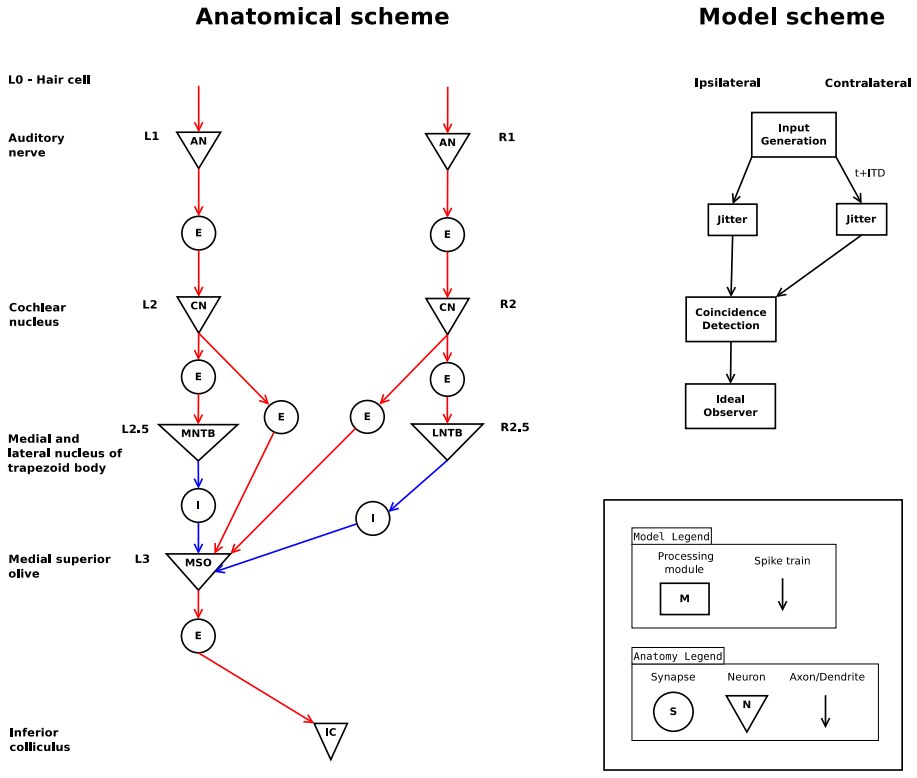

Fig. 1 – Schemes of the MSO circuit anatomy and the interpolation model. The anatomical scheme (left) shows branches of the binaural circuit (only one half of the symmetrical circuit is shown). L1, L2,..., R1, R2 are left and right neurons. The direction from the auditory periphery to the auditory center is oriented top-down. Each neuron is denoted by its nucleus abbreviation (expanded in the left-hand column). Synapses are either excitatory (E) or inhibitory (I). The model scheme (right) employs neural circuit simplifications without losing the implementation of the key mechanisms.

spikes in that period on an individual neuron, or one can observe a given number of neurons over a shorter time period and achieve the same precision. The number of spikes required for such a measurement was estimated using the Bernoulli process statistical model in Marsalek and Lansky (2005).

We propose a simple model where the basic processing stages of the neural circuit have been replaced by four modules operating in succession (see Fig. 1): a spike generator that represents the input from the auditory nerve (AN), a jitter generator that adds jitter and delays, occurring in the pathway up to the MSO, a coincidence detector that represents the first binaural neuron in the MSO, and an ideal observer module. The detailed description of these modules can be found in Section 4.

2. Results

2.1. *Effects of inhibition*

For the basic set of parameters (see Table 1), we obtained the ITD curve shown in Fig. 2. It was checked that disabling the asymmetric rule in the coincidence detector affects the output of the circuit. We consider this to be our counterpart of inhibition suppression in the physiological model (see Section 2.3). The result was as expected: in the purely excitatory case, i.e., with no inhibition, there is a higher firing frequency and, due to the symmetric processing of excitatory spikes, the curve peaks at $D_{ITD}=0$. In all other simulations we used the asymmetric coincidence detection rule only.

2.2. *Effects of varying time parameters*

After testing the basic parameter set, let us move to exploring the parameter space, beginning with the timing jitter and input sound frequency. When the ITD curves for increasing input frequency f_{in} are generated, it can be observed that the firing rate grows and the ITD curve changes from flat in lower frequencies to steep in higher frequencies (Fig. 3, left). Similar rise of the firing rate with rising input frequency is observed with the use of more detailed Meddis model, with markedly lower output firing rates (Fig. 3, right). Furthermore, the distance between the ITD peaks becomes smaller with increasing f_{in} as the input sound period decreases. The curve offset around the $D_{ITD}=0$ does not shift while changing f_{in}.

As jitter decreases, the firing rate in the ITD curves increases accordingly. See Fig. 4, right. This is due to the fact that the smaller jitter helps spikes to occur in the same coincidence window. For $T_J \rightarrow 0$, we would obtain a rectangular pulse, which is unusable for interpolation. If the jitter becomes larger than the sound period, this would render the response flat (not shown, effects of higher jitter values on ITD curve are thoroughly demonstrated by simulations in Supplementary information). Thus, the feasible jitter values are bounded on both sides. Changes in jitter T_J values in the jitter generator do not affect the ITD curve shift.

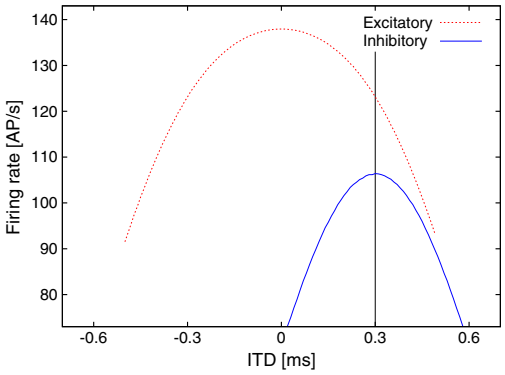

Fig. 2 – ITD curves for the basic set of parameters. This shows a detailed view of the peak with inhibition shifted out of the point, where $D_{ITD}=0$ as compared to the peak without inhibition. The relative distances of the two curves (30–50 Hz) are given in Grothe (2003). Further, the EE interaction has a higher maximum firing rate than the EI interaction. The basic ITD curve has shift of 0.25 ms, which is an emergent property with no free parameter tuning.

2.2.1. *Window width and ITD curve shift*

The ITD curve shift in our model is produced by the asymmetric coincidence rule but its particular size is affected by the parameters of the circuit. Therefore each parameter of our circuit was studied to determine which parameters influence the ITD peak shift. As a result of the simulations, it was possible to observe that the parameter that changes the peak shift considerably is the coincidence detection window width w_{CD}. See Fig. 4. Other parameters of our model did not affect the peak shift significantly. See vertical lines in Figs. 3, 4.

2.3. *Ideal observer*

The ideal observer module is connected to the output of the coincidence detector. For interpolation from the firing rate back to the D_{ITD} value a previously fitted ITD function is used. The ITD readout slope can be fitted to a sine function: $y = \frac{1}{2}A(1 + sin(Bt + C) + D)$, where A is the multiplicative constant setting up the maximum firing rate, B is dependent on the input frequency, C is the phase shift and D is the spontaneous activity. See Fig. 5.

The shape of this function used for interpolation determines how precise the computation of D_{ITD} encoded in the incoming spike train is. As shown in previous sections, two features are important. The first feature is the unambiguous assignment of the unique D_{ITD} value from the firing rate. It is the asymmetric rule together with w_{CD} that plays an important role in determining the readout curve whose fit is shown in Fig. 5. The second feature is the slope of the interpolation curve obtained as the difference $\Delta_{ITD}=\Delta D_{ITD}/\Delta t$ and output range of the ITD curve. Both are decisive for accuracy (or speed) of ITD estimate by the observer. As the output range increases, we obtain a more precise azimuth estimate, which is influenced by all the parameters, with jitter T_J being the main factor, as shown above.

2.3.1. *Asymptotic times*

Up to now we have looked only at the circuit output in the terms of the firing rate. At the end, the information contained in the output spike train is used in higher stages of the

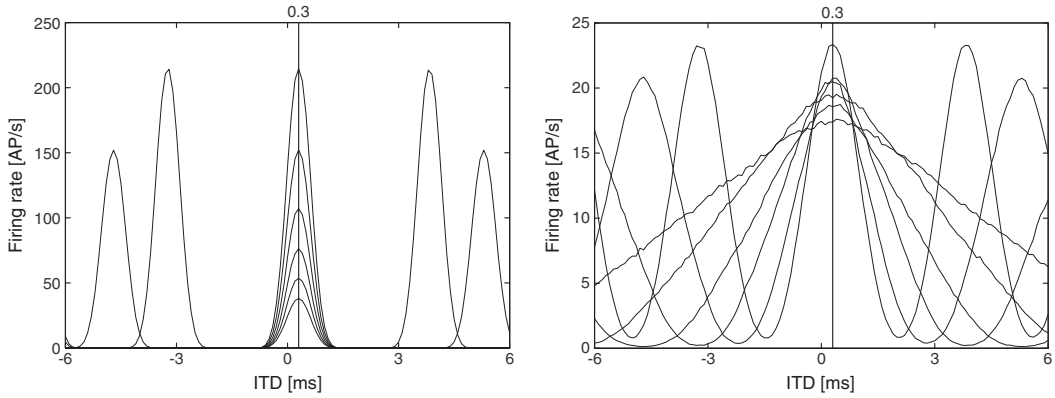

Fig. 3 – ITD response curves for different input frequencies f_{in} directly delivered to the circuit (left-hand panel) and delivered through the Meddis model (right-hand panel). For increasing the sound frequencies with step $\sqrt{2}$ (50, 71, 100, 141, 200, 283 Hz), the maximum firing also increases. In both cases, the period of the ITD curve decreases as the input frequency increases. If cochlear filtering is used, it can be seen that the width of a single peak increases as the input frequency decreases. Secondly, the output firing is approximately ten times lower with the Meddis model involved. For each sound frequency shown, the Meddis model was used with the same characteristic frequency. For cut-off frequencies see Supplementary information.

auditory pathway to estimate the azimuth. Since we do not model higher stages of auditory processing, we use the observer module, which sequentially collects information from the circuit output and predicts resulting ITD from the information given. Naturally, the longer the spike train is measured for, the more accurate the estimate of the source's D_{ITD} which can be assessed. Thus in order to investigate the overall estimate performance of our model circuit, we fed it with a longer input and estimated the time T_A needed for the ideal observer to achieve accuracy 4°, in the head-on direction (Mills, 1972). Fig. 6 shows fast asymptotic convergence towards the source D_{ITD} value when basic jitter value (T_J=1 ms) is applied (left), and a comparison of the asymptotic times for different parameter sets (right). In all cases shown here we set D_{ITD}=0. A comparison between a pure tone and a noisy input produced by the Meddis model was added to the Supplementary information.

The time to reach the asymptotic values T_A, which range from 0.5 s up to 5 s (see Fig. 6), would be too long compared to the typical reaction time. The human minimum integration time is discussed in Middlebrooks and Green (1991) as a range of values: while a stimulus of 50 ms duration is detected with

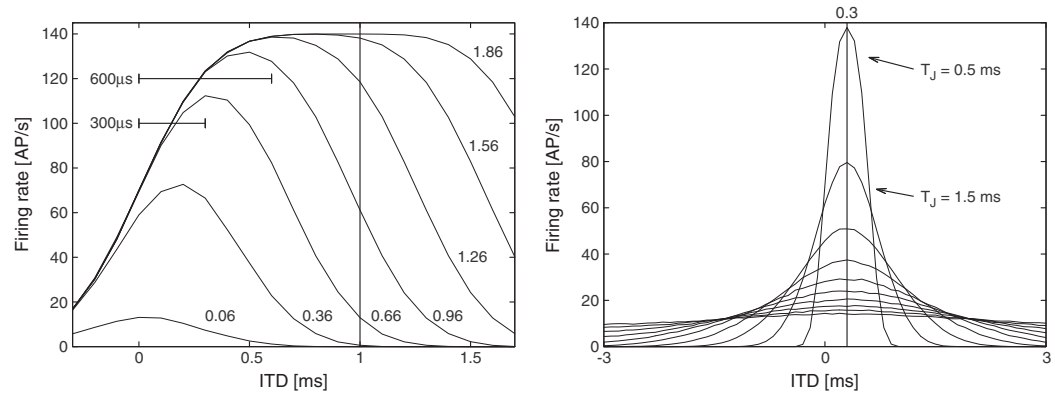

Fig. 4 – Dependence of ITD peak shift on the coincidence detection window width w_{CD} (left-hand panel) and different values of jitter T_J (right-hand panel). Peaks do not exceed 140 Hz due to the input frequency f_{in}=140 Hz in the basic set of parameters. In the left-hand panel a shift of the peak towards higher ITDs can be seen as the window size increases from 60 μs towards 2 ms (with step 300 μs). The two top left intervals show physiologically relevant range in a domestic cat (300 μs) and in a human (600 μs), respectively. From around w_{CD}=0.6 ms, and above that value, the maximum slope is observed and the shape of the ITD function in physiologically relevant range does not change. For further notes about physiological relevance of this observation see the Discussion section. Right-hand panel: larger jitter causes lower output dynamic range and wider curves. The presence of high jitter values renders the response curve flat. The response increases as the magnitude of jitter decreases towards zero.

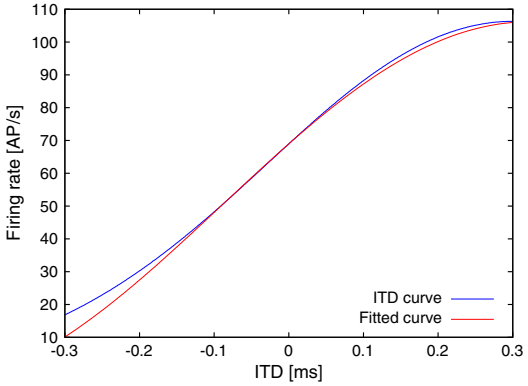

Fig. 5 – The interpolation ITD curve in the physiologically relevant range of values. The ITD curve is shown together with the fitted sinus function used for interpolation in the ideal observer. This function is fixed for the set of parameters which would correspond to the fixed tuning of the neural circuit for selected input signals. In this example, we used the ITD curve, which results from simulation of the circuit for the basic set of parameters. Note that the period of this slope corresponds to the fundamental sound period.

errors, typical azimuth integration time ranges from 150 to 300 ms of sound duration. However, the pathway from the AN to the MSO is highly parallel and consists of up to a few hundred neurons. When the ergodic hypothesis is used, as discussed in Section 3.4, T_A can be divided by the number of neurons. The time thus obtained corresponds to the theoretical minimum time required by human listeners to determine the D_{ITD}, when the entire brainstem circuit is working in parallel and cooperating on the ITD estimation. When the basic set of parameters is used we obtain that approximately 4 parallel neurons would be needed in order to achieve the 150 ms integration time.

3. Discussion

3.1. *Type of neuronal coding*

Jeffress (1948) proposed a theory of how sound is localized by a particular neural circuit. According to this concept, neural representation divides the whole azimuthal space into distinct sections. Each section is handled by a specific neuron and the fact that the sound originates from a given direction is represented by higher firing activity of the corresponding neuron. Jeffress suggested that this circuit is anatomically realized by an array of delay lines. Indeed, experimental evidence supporting this hypothesis was later found in the circuit of the nucleus laminaris of birds by Carr and Konishi (1988).

The responses of higher nuclei such as the colliculus inferior in both birds, Wagner et al. (1987, 2007) and mammals, Joris et al. (1998, 2006) have been systematically studied until recently. This is because the colliculus inferior is more accessible to recordings and its binaural response is analogous to that of the nucleus laminaris or the MSO, respectively. In the MSO, which is a mammalian anatomical counterpart of the avian circuit, there is little supporting evidence for the existence of a structure similar to such an array of delay lines, Grothe (2003), but see also

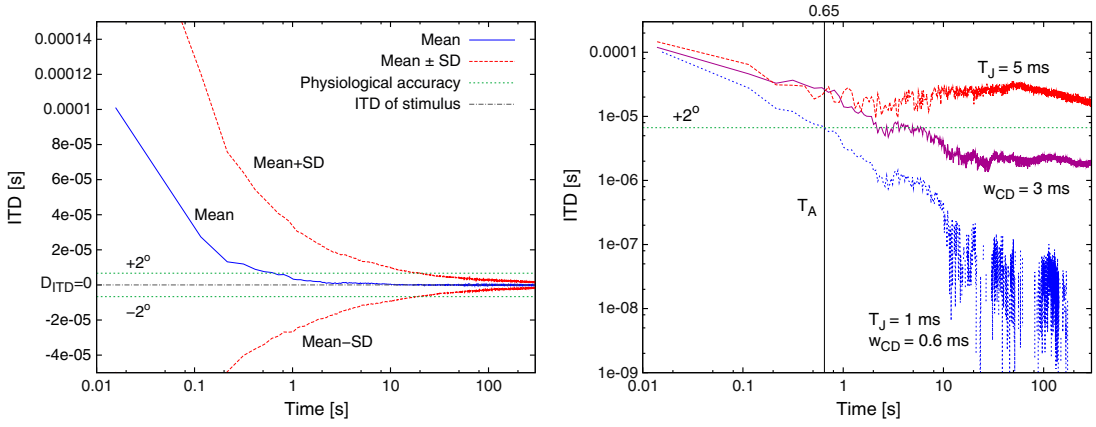

Fig. 6 – Time required to reach a reliable estimate (with a given precision) of azimuth T_A by a single binaural neuron. The x-axis shows time and the y-axis shows the ITD. Note the logarithmic scales used. In the left-hand panel, the middle solid line represents the mean value obtained for 1000 simulation runs, while the dotted lines show standard deviation. The three dotted horizontal lines show D_{ITD} original source and margins of azimuth difference ±2° respectively. In the right-hand panel, the top line shows mean convergence when using larger jitter (T_J=5 ms), the middle line shows how convergence improves when using a wider window (w_{CD}=3 ms), which is different from the basic parameter set, and the bottom line shows faster convergence for the basic set of parameters (T_J=1 ms). The horizontal lines show the precision obtained in the psychoacoustical experiments. At the point in time T_A (T_A=0.65 s for basic set of parameters) when the mean value crosses the precision line, enough information has been obtained for our model to be able to report the azimuth with average precision corresponding to that of human listeners ([−2°;2°]).

Joris et al. (1998). This raises the question of whether such a type of neural coding is also to be found in the mammalian brain stem. Various alternatives have been proposed, for example, delays of the cochlear traveling wave (Jennings and Colburn, 2010; Joris et al., 2006; Shamma et al., 1989). Previous experiments have shown that ITD peaks occur out of the relevant physiological range (McAlpine et al., 2001) and further reproductions of mammalian experiments similar to those have led to the development of a theory showing that the mammalian localization mechanism is different from that of the avian. The importance of the role of synaptic inhibition was also experimentally discovered by Brand et al. (2002). The shift of the ITD curve peak is somewhat counter-intuitive when we assume that the Jeffress model is employed, and thus the slope (rate) coding model has been proposed instead. In this paper a circuit based on the slope coding scheme is studied.

3.2. *Asymmetric rule for coincidence detection*

The excitatory and inhibitory effects in the sound localization circuit have been extensively discussed in experimental literature. Classical electrophysiological works by Goldberg and Brown (1969) and others have distinguished between the EE and EI type of binaural unit response. The EE (excitatory– excitatory) abbreviation labels units where the sound level increment at both sides has an excitatory effect, while EI stands for the excitatory effect of one side and inhibitory effect of the other side. However, this is a phenomenological classification and does not imply the synaptic mechanisms.

In the mammalian MSO circuit, other inhibitory inputs besides those from the MNTB (Medial Nucleus of Trapezoid Body) are involved. Each sensory pathway, including the auditory pathway, also contains local inhibitory interneurons and often other inhibitory circuits, like, for example the indirect pathway of the basal ganglia. In all these synaptic circuits, the role of inhibition is to dynamically set up the gain of the circuit via feedback connections. Other inhibitory synapses in the MSO circuit contribute to setting the gain, adaptation, and perhaps to further unknown functions of the circuit.

Our model follows anatomical connections of the feedforward sound localization pathway. Although throughout the paper excitatory and inhibitory synapses are referred to according to their anatomical and functional classification, we have shown that instead of synapse polarity, it is possible to use a timing rule for coincidence detection. Thus, we have been able to describe the circuitry independent of the synapses polarity in more abstract and simple terms. We have also demonstrated that our results are in line with the experimental results related to inhibition blocking (Brand et al., 2002; Pecka et al., 2008).

3.3. *Properties of the circuit*

Having studied the parameters that affect important properties of the ITD curve, we have found that the parameter significantly affecting peak position is the coincidence window width. One consequence of shifting the peak by employing a wider window is a steeper ITD function in the physiological range of ITDs. Bringing steepness to its maximum value would require $w_{CD} \approx 0.6$ ms which is higher than the observed values (Jercog et al., 2010). Using smaller jitter values proved much more effective in increasing the output range and steepness of the ITD curve. As noted in Section 4.3, on the one hand, jitter plays a positive role for more subtle differentiation of azimuthal space, but on the other hand, higher jitter reduces coding efficiency. This indicates the possible existence of an optimal jitter value which merits further research.

Asymptotic behavior of the sound direction "ideally observed" by the model was also investigated. This gives us overall precision and time performance for the whole circuit. It could be seen that an ideal observer located on a single fiber performs in the range of seconds, which is acceptable considering that the auditory pathway works in parallel using tens to hundreds of neurons. Using an ergodic assumption for the ideal observer, we obtain a hundreds of milliseconds time range. This allows us to connect physiological and psychoacoustical observations, which are normally two separate areas of research.

Besides the regular input, the Meddis (2006) model of the auditory periphery was used to compare the performance of the two input models. Generally, the Meddis model causes a fall in the firing rate delivered as the input to our model, compared to the regular spiking input we used. In addition, only phase-locked spikes will be registered by coincidence detection. This reduces both the available dynamic range of values of the ITD curve and the computational performance of the circuit. The question remains how closely this model corresponds to the real input to the MSO, since the model produces only the spike train occurring at the auditory fiber. The cochlear nucleus can improve the phase-locking due to summation of more AN fiber inputs.

The timing jitter also plays a role in deteriorating the phase-locking precision. Most of the auditory processing stages blur the phase locking. The comparison with the Meddis model indicates that introducing more processing stages into the circuit does not necessarily blur the spike trains beyond the state when the circuit would no longer function and would no longer possess a functioning coincidence detection mechanism. Indeed, Reed et al. (2002) have shown that the phase locking in a model neuron within a neural circuit can deteriorate, can be sharpened, or can stay unaltered, depending upon the connection divergence and other simple properties of the neuron as a relay within the sensory pathway.

3.4. *Ergodic assumption*

The performance of a single binaural neuron has been shown for several parameters and inputs. Time (T_A) to reach the estimate of D_{ITD} by single neuron is higher than in psychoacoustic experiments. It is known that the auditory pathway uses AN fibers and subsequent neurons in parallel so the brainstem contains several parallel circuits cooperating on the computation of azimuth. We used the ergodic hypothesis to divide T_A by the number of parallel neurons. This hypothesis used in interpretation of Fig. 6 states that the same result is obtained when counting spikes for a long time as when sampling them across a given number of parallel fibers. This is also consistent with the actual ITD processing in the MSO reported in several species, which produced the same ITD tuning curves by several repeats of sound stimulus, as shown, for instance by Goldberg and Brown (1969).

The exact number of circuits which work in parallel is difficult to estimate. It concerns not only the number of the binaural MSO neurons but also the number and connectivity of the spherical bushy cells of the cochlear nucleus. About 7000 of these cells connect to the MSO in a domestic cat. Since their axons branch, the average number of connections to the MSO is difficult to obtain with the current methodology (P.X. Joris, personal communication). Next, the exact spectral content of incoming acoustic stimuli affects the number of involved fibers due to the tonotopic organization. For example the broadband stimuli would be expected to perform better than pure tone stimuli due to higher number of parallel fibers transmitting the signal. All these problems were not studied deeper in the current paper but they pose interesting open questions for further work.

3.5. *Stochastic coding of ITD*

Finally, we would like to point out the use of the built-in random number generator in our model. By means of these stochastic simulations we have obtained realizations of a random variable, namely of the timing jitter. The results obtained for the ideal observer are shown together with their statistical description. A previous paper by Marsalek and Lansky (2005) presented a stochastic model of a coincidence detector and theoretically calculated average detection times. In this paper a further step has been taken, as the entire MSO model circuit has been studied. The precision of the ITD detection assessed by our model requires further verification by future experiments employing psychoacoustical data.

4. Experimental procedures

4.1. *Spike generator*

In some simulations a constant frequency spike train was used as the input, with two spikes generated in each cycle — one to one side, the other delayed by the ITD (this variable is denoted by D_{ITD}) to the other side.

While the regular spiking input is suitable for analysis of circuit parameter properties, a more biologically plausible model of spike generation was also included. Specifically, the first part of the computational model of the auditory periphery as described in Meddis (2006) was used. Here, the complex acoustic stimuli are passed through successive stages of processing: stapes, basilar membrane, inner hair cell receptor potential, presynaptic calcium currents and transmitter release events, AN (auditory nerve) synapse and finally AN spiking response, including refractory effects. The output – spike train in the auditory nerve fiber with selected characteristic frequency – is subsequently used as an input to our circuit. An extensive overview of all the parameters can be found in the appendix under Meddis (2006). This model was then used without further modifications.

4.2. *Jitter generator*

In the next processing stage, jitter is generated and added to the spike times, simulating natural noise occurring in the neural spike transmission. Each spike is shifted in time by a small random delay value defined as $D = T_J(B(a,b) - 0.5)$, where $B(a,b)$ is a random variable from the beta distribution with parameters $a=2$, $b=4$ and T_J is the timing jitter magnitude. Values of $a=2$ and $b=4$ are the smallest nontrivial values resulting in a nonzero skewness of the beta probability density function, as discussed in Drapal and Marsalek (2010). Note the positive role of this type of noise in the circuit — it is because of this noise that more refined azimuth precision is achieved.

4.3. *Coincidence detector*

Whenever two spikes are detected within the short time window, the coincidence detector neuron fires. In the classical Jeffress (1948) model, coincidence detection is realized by the excitatory spikes converging on a binaural neuron from both sides simultaneously in a short time succession. The mere fact of coincidence determines the azimuth defined by the position of the neuron in a delay line. The interpolation model also introduces a short time window for detecting consequent spikes, while distinguishing between two EPSPs and a pair of one EPSP and one IPSP. The preceding application of the timing jitter is of essential importance to the circuit here as it allows a more subtle distribution of coincidences. Instead of a binary answer about two spikes being in the coincidence window, a probabilistic variable is obtained which, in turn, allows a finer distribution of recognized ITD values. Compared to the "all or none" output of the Jeffress model, this means that one single binaural neuron is already capable of determining D_{ITD}. However a longer spike train is needed to achieve the necessary precision of the estimate.

The important property of the ITD curve is its peak shift as observed in an experimental study of mammals (Brand et al., 2002). First, this leads to a shift of possible ITD values inside the physiologically relevant range. Second, it allows the unambiguous interpolation of a particular firing rate to a single ITD value. This is in contrast to the situation where the ITD curve has a peak at $D_{ITD}=0$ and the concave shape allows two possible ITDs to be selected. We show that in order to achieve this ITD curve shift, we need an "asymmetric" rule of EPSP and IPSP coincidence detection, allowing incoming spikes to trigger an output spike only if the inhibitory spike precedes the excitatory spike. This corresponds to the detailed biophysics of the PSPs. Pharmacological suppression of the inhibition is equivalent in our model to disabling this asymmetric rule and letting the symmetric coincidence detection operate on the incoming EPSPs only. By "asymmetry" we mean that the order of excitatory and inhibitory spikes matters — in contrast to the excitatory only situation.

4.4. *Ideal observer module*

Compared to the Jeffress model where the azimuth is determined by the position of the firing neuron in the delay line, the interpolation model relies on the value of a firing rate. The firing rate is realized by random variations in the input spike timings, and one way to eliminate this random component is to take an average of the firing rates over a given time. Because the input sound sequences may only last for a short period of time, we would like to know what length of

time intervals are needed in order to obtain an azimuth estimate. Our aim here is not to model the higher stages of spatial sound localization, but rather to estimate the information that is available after the MSO processing stage and to connect the physiologically relevant information (firing rate) with experimental azimuth measurements.

The concept of the ideal observer, originally also known as the ideal receiver, is frequently used in the signal detection theory and psychophysics (Tanner, 1961). By implementing the ideal observer module, we used this concept to describe a mechanism which represents the function of the next processing stages of the auditory pathway. It should be noted that this is not strictly an ideal observer analysis. Unlike previous modules, this module does not process the data. Instead, it simply extracts the available information encoded in the output spike train from the binaural neuron, and in particular it reads the sound source direction from the MSO neuron. This is done via the interpolation of the firing rates in the ITD curve. This lookup (calibration) function must be known beforehand and it can be approximated by a sine function $R_{ITD} \approx R_{max} sin 2\pi f_{in} D_{ITD}$. The meaning of the parameters of this approximation are listed in the Results section.

Since the ideal observer has complete access to perceptual information, the azimuth perception can be obtained. In psychophysics this precision is called the just noticeable difference, and in azimuthal sound localization in the head-on direction is 4° (angular degrees). This has been observed within a decade variation amongst distant animal species, in humans, Mills (1972), guinea pigs, McAlpine et al. (1996) barn owls, Moiseff and Konishi (1981) and even in parasitic flies *Ormia ochracea*, Miles et al. (1995). Here, different azimuths are distinguished as distinct points on the ITD curve along its slope. Thanks to interpolation the just noticeable difference is obtained from the difference between two spike train firing rates elicited by two stimuli (azimuths) φ_1 and φ_2. The firing rates of spike trains in response to stimuli φ_1 and φ_2 denoted as R_1 and R_2 can be described as random variables with means μ_1 and μ_2 and standard deviation σ (we assume $\sigma_1 = \sigma_2$). Detection distance is defined as: $d = (\mu_2 - \mu_1)/\sigma$. When $t \to \infty$, firing rates converge to their means, $R_1 \to \mu_1$ and $R_2 \to \mu_2$. The computational precision performance of the circuit is dependent upon speed of this convergence. Thus we measure the time to reach the direction estimate T_A. This variable is mainly dependent on the firing rate R_{ITD} and input sound frequency f_{in}, as well as other parameters.

4.5. *Simulations and parameters*

The model circuit was simulated numerically with exploration of plausible parameter space. Each of the circuit modules has its own set of parameters which together define the circuit parameters. A default value of jitter of $T_J = 1$ ms was assigned since the experimentally observed values of jitter do not exceed 1 ms as shown for example in the experiment involving the octopus type cells of the cochlear nucleus in a domestic cat (Oertel et al., 2000). The width of the coincidence window w_{CD} has been assigned as 600 μs. This is in agreement with the value used in a model part of Beckius et al. (1999). Briefly, their model performed well as long as the coincidence detection window was shorter than the period of the fundamental frequency. (We get $1/w_{CD} = 1667$ Hz, therefore it must be $f_{in} < 1667$ Hz.) This latter assumption is also frequently mentioned in other models. The subcellular experimental studies also measured values of relevant postsynaptic current- and voltage-dependent ionic current rise time. The values measured give window width in the sub-millisecond range close to this value (Jercog et al., 2010). Representative fundamental sound frequency in the following results is $f_{in} = 140$ Hz. Besides the fundamental frequency of spike generator f_{in}, we set the duration of most simulations to 500 s in order to reach a steady state. We select the parameters above as a *basic set*, summarized in Table 1. An extensive list of circuit parameters can be found in the Supplementary information. In all the simulations we use this basic set of the parameters unless stated otherwise.

Table 1 – The basic set parameters.

Parameter	Value
T_J	1 ms
w_{CD}	600 μs
f_{in}	140 Hz
T	500 s

The physiological range of D_{ITD} in humans when localizing sound source in one quadrant (0–90°) ranges from 0 to 600 μs. This can be calculated from the sound speed in the air and the distance between the ears. Differences in the ear distance of smaller animals have to be taken into account when interpreting the data recorded in various laboratory animals.

Supplementary materials related to this article can be found online at doi:10.1016/j.brainres.2011.08.048.

Acknowledgments

Supported by research initiatives MSM 0021620806 and MSM 6840770012 by the Ministry of Education, Youth and Sports, by MPO FR-TI3/869 by the Ministry of Industry and Trade of the Czech Republic, by P103/11/0282 by the Grant Agency of the Czech Republic, and by the Max Planck Society. Thanks to Philip Joris, Petr Lansky, David McAlpine and Raymond Meddis for discussions and to Deborah A. M. James, Martina Missikova and Linda Jayne Turner for copy-editing.

REFERENCES

Beckius, G.E., Batra, R., Oliver, D.L., 1999. Axons from anteroventral cochlear nucleus that terminate in medial superior olive of cat: observations related to delay lines. J. Neurosci. 19 (8), 3146–3161.

Brand, A., Behrend, O., Marquardt, T., McAlpine, D., Grothe, B., 2002. Precise inhibition is essential for microsecond interaural time difference coding. Nature 417 (6888), 543–547.

Carr, C.E., Konishi, M., 1988. Axonal delay lines for time measurement in the owl's brainstem. Proc. Natl. Acad. Sci. U S A 85 (21), 8311–8315.

Dean, I., Robinson, B.L., Harper, N.S., McAlpine, D., 2008. Rapid neural adaptation to sound level statistics. J. Neurosci. 28 (25), 6430–6438.

Drapal, M., Marsalek, P., 2010. Stochastic model shows how cochlear implants process azimuth in real auditory space. Chin. J. Physiol. 53 (6), 439–446.

Goldberg, J.M., Brown, P.B., 1969. Response of binaural neurons of dog superior olivary complex to dichotic tonal stimuli: some physiological mechanisms of sound localization. J. Neurophysiol. 32 (4), 613–636.
Grothe, B., 2003. New roles for synaptic inhibition in sound localization. Nat. Rev. Neurosci. 4 (7), 540–550.
Jeffress, L.A., 1948. A place theory of sound localization. J. Comp. Physiol. Psychol. 41 (1), 35–39.
Jennings, T.R., Colburn, H.S., 2010. Models of the superior olivary complex. In: Meddis, R., Lopez-Poveda, E.A., Fay, R.R., Popper, A.N. (Eds.), Computational Models of the Auditory System. Springer, New York, pp. 65–96.
Jercog, P.E., Svirskis, G., Kotak, V.C., Sanes, D.H., Rinzel, J., 2010. Asymmetric excitatory synaptic dynamics underlie interaural time difference processing in the auditory system. PLoS Biol. 8 (6), e1000406 1–9.
Joris, P.X., Smith, P.H., Yin, T.C.T., 1998. Coincidence detection in the auditory system: 50 years after Jeffress. Neuron 21 (6), 1235–1238.
Joris, P.X., Van de Sande, B., Louage, D.H., van der Heijden, M., 2006. Binaural and cochlear disparities. Proc. Natl. Acad. Sci. U S A 103 (34), 12917–12922.
Karino, S., Smith, P., Yin, T., Joris, P., 2011. Axonal branching patterns as sources of delay in the mammalian auditory brainstem: a re-examination. J. Neurosci. 31 (8), 3016–3031.
Marsalek, P., Lansky, P., 2005. Proposed mechanisms for coincidence detection in the auditory brainstem. Biol. Cybern. 92 (6), 445–451.
Mathews, P., Jercog, P., Rinzel, J., Scott, L., Golding, N., 2010. Control of submillisecond synaptic timing in binaural coincidence detectors by K(v)1 channels. Nat. Neurosci. 13 (5), 601–609.
McAlpine, D., Jiang, D., Palmer, A., 1996. Interaural delay sensitivity and the classification of low best-frequency binaural responses in the inferior colliculus of the guinea pig. Hear. Res. 97 (1–2), 136–152.
McAlpine, D., Jiang, D., Palmer, A.R., 2001. A neural code for low-frequency sound localization in mammals. Nat. Neurosci. 4 (4), 396–401.
Meddis, R., 2006. Auditory-nerve first-spike latency and auditory absolute threshold: a computer model. J. Acoust. Soc. Am. 119 (1), 406–417.
Middlebrooks, J.C., Green, D.M., 1991. Sound localization by human listeners. Annu. Rev. Psychol. 42 (1), 135–159.
Miles, R., Robert, D., Hoy, R., 1995. Mechanically coupled ears for directional hearing in the parasitoid fly *Ormia ochracea*. J. Acoust. Soc. Am. 98 (6), 3059–3070.
Mills, A.W., 1972. Auditory localization. In: Tobias, J.V. (Ed.), Foundations of Modern Auditory Theory. Academic Press, New York, pp. 303–348.
Moiseff, A., Konishi, M., 1981. Neuronal and behavioral sensitivity to binaural time differences in the owl. J. Neurosci. 1 (1), 40–48.
Oertel, D., Bal, R., Gardner, S.M., Smith, P.H., Joris, P.X., 2000. etection of synchrony in the activity of auditory nerve fibers by octopus cells of the mammalian cochlear nucleus. Proc. Natl. Acad. Sci. U S A 97 (22), 11773–11779.
Papoulis, A., 1991. Probability, Random Variables, and Stochastic Processes. McGraw-Hill, New York.
Pecka, M., Brand, A., Behrend, O., Grothe, B., 2008. Interaural time difference processing in the mammalian medial superior olive: the role of glycinergic inhibition. J. Neurosci. 28 (27), 6914–6925.
Reed, M.C., Blum, J.J., Mitchell, C.C., 2002. Precision of neural timing: effects of convergence and time-windowing. J. Comput. Neurosci. 13 (1), 35–47.
Shamma, S., Shen, N., Gopalaswamy, P., 1989. Stereausis: binaural processing without neural delays. J. Acoust. Soc. Am. 86 (3), 989–1006.
Tanner Jr., W.P., 1961. Physiological implications of psychophysical data. Ann. N.Y. Acad. Sci. 89 (5), 752–765.
Wagner, H., Takahashi, T., Konishi, M., 1987. Representation of interaural time difference in the central nucleus of the barn owl's inferior colliculus. J. Neurosci. 7 (10), 3105–3116.
Wagner, H., Asadollahi, A., Bremen, P., Endler, F., Vonderschen, K., von Campenhausen, M., 2007. Distribution of interaural time difference in the barn owl's inferior colliculus in the low- and high-frequency ranges. J. Neurosci. 27 (15), 4191–4200.

Speeding Up the Algorithm for Finding Optimal Kernel Bandwidth in Spike Train Analysis

P. Šanda[1]
[1]Institute of Physiology, Academy of Sciences of the Czech Republic
Supervisor: Doc. RNDr. Petr Lánský, CSc.

Summary
One of the important tasks in the spike train analysis is to estimate the underlying firing rate function. The aim of this article is to improve the time performance of an algorithm which can be used for the estimation.
As there is no unique way how to infer the firing rate function, several different methods have been proposed. A popular method how to estimate this function is the convolution of the spike train with Gaussian kernel with appropriate kernel bandwidth. The definition of what "appropriate" means remains a matter of discussion and a recent paper [1] proposes a method how to exactly compute optimal bandwidth under certain conditions. For large sets of spike train data the elementary version of the algorithm is unfortunately too inefficient in terms of computational time complexity.
We present a refined version of the algorithm which in turn allows us to use the original method even for large data sets.
The achieved performance improvement is demonstrated on a particular results and shows usability of proposed method.

Keywords: action potential, spike train, neural coding, firing rate, convolution, Gaussian kernel, kernel bandwidth, Brent's minimization, parallel computing, MPI

1. Introduction

Many neurophysiological studies are based on the assumption that the majority of information flow between neurons is provided by spikes. Spike trains are believed to form a neuronal code and many coding models successfully predict experimental stimuli features when only the resulting spike train is given. It has been shown that important aspects of the stimuli are coded by the neuron's firing rate, however, the exact procedure how to obtain such a rate from the experimental data differs from paper to paper and various methods were proposed [2].

Here we consider the method based on the convolution of a spike train with a fixed (Gaussian) kernel, which in result leads to a smooth estimate of firing rate and has been widely used in the past decades [3], [4], [5], [6], [7], [8]. The most difficult part of this method is the selection of the kernel bandwidth, because it affects substantially the "quality" of the estimate, while there is no obvious clue how the optimal bandwidth should be chosen. In [1] authors propose a kernel density estimator based on the mean integrated squared error principle (MISE) and formulate a precise algorithm how to infer optimal (fixed) kernel bandwidth.

For larger sets of recorded spike trains the time complexity of the straightforward version of the algorithm increases, so that it becomes unusable for online queries when studying the features of the method. Here we provide a solution, which improves the time complexity of the implementation. That at the end allows us to work with experimental data in a reasonable manner. It is also worth to note that the proposed solution does not interfere with the actual result of the original method - for the properties and comparison with other methods look in the original paper [1].

2. Methods

2.1 Original method

The firing rate is a non-negative function λ for which the integral $\int_b^a \lambda(t)dt$ gives the expected number of spikes during the time interval $[a,b)$. In the experimental recording we get only one or more trials of spike train data. The problem is how to assess the firing rate $\hat{\lambda}$, which will be as close as possible to the original λ, which is believed to stand in the background of spike discharges. The method is to convolve the spike train with a specific kernel, thus obtaining a smooth estimate of λ, for example see Fig. 1. In this case we use fixed Gaussian kernel

$$k_w(t) = \frac{1}{\sqrt{2\pi w}} \exp\left(-\frac{t^2}{2w^2}\right)$$

and the problem is reduced to the question how to select the optimal bandwidth w, so that the difference between λ and $\hat{\lambda}$ is minimal. The method itself is beyond the scope of this article, for details see [1]. What is important here is that the core of computation can be summarized in the following statement: find w^*, such that the formula (1) is minimal:

$$C(w) = \frac{1}{n^2}\sum_{i,j}\psi_w(t_i,t_j) - \frac{2}{n^2}\sum_{i\neq j}k_w(t_i - t_j) \quad (1),$$

where t_i is the time of i-th spike, n is the number of trials,

$$\psi_w(t_i,t_j) = \int_b^a k_w(t-t_i)\,k_w(t-t_j)\,dt, \quad [a,b]$$

defines the time range of the record and k_w is as the kernel used. Since we will study the Gaussian kernel the equation (1) can be rewritten as

$$2\sqrt{\pi}n^2 C(w) = \frac{N}{w} + \frac{2}{w}\sum_{i<j}\left(e^{-\frac{(t_i-t_j)^2}{4w^2}} - 2\sqrt{2}e^{-\frac{(t_i-t_j)^2}{2w^2}}\right) \quad (2),$$

where N is the number of spikes. Note that the term $2\sqrt{\pi}n^2$ is constant and has no effect on w^*. Let us denote the inner term of the sum in (2) as $E(w, t_i, t_j)$. We will denote $\mathcal{W}$ the set of possible values of w, in which we are searching. We denote the size $W = |\mathcal{W}|$ and assume that its points are equidistant.

The straightforward implementation will find the minimum value via evaluating this term in three nested loops:

(11) for $w \in \mathcal{W}$
(12) for $j \in [1,...N]$
(13) for $i \in [1,...,j-1]$
$Tmp = E(w, t_i, t_j)$
$if\ (min > tmp)\ min = tmp\ ,\ w^* = w$

thus obtaining the time complexity $O(N^2W)$. The selection of $\mathcal{W}$ is dependent on the interval $[a, b)$ and required precision of the optimal value. In a typical case $w^* << b - a$ we can select the upper bound of $\mathcal{W}$ to $log(b - a)$, in the case of bisection (see below) the upper bound is not so vital.

2.2 Bisecting

Now we will use that in a typical case where C forms an unimodal function, see Fig 2., though this cannot be asserted in general (such a problem can, for example, occur when searching for bandwidths is smaller than the sampling resolution of input data). Having the unimodal function and a sensible estimate of lower and upper bounds we can use any of the extremum search algorithms based on sectioning the domain. This will reduce loop ($I1$) time complexity from a linear to a logarithmic factor and as a result we obtain the complexity of $O(N^2log(W))$. As hinted above while this method helps a lot certain attention needs to be paid before its use.

2.3 Parallelization

Because the evaluation of $E(w, t_i, t_j)$ is independent of the previous computations, it is a natural target for parallelization.

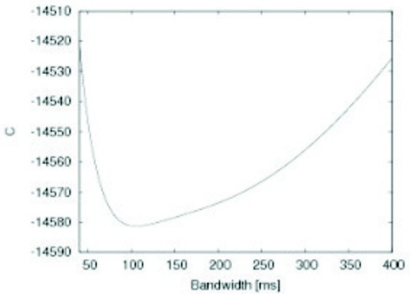

Fig. 2. Typical shape of the function for experimental spike train data.

Splitting the task for the parallel execution at the loop ($I1$) level will not allow us to use parallelization in case of the bisection run, thus we will split the task on p parts at the level ($I2$). That will give us the final estimate for the time complexity of $O(N^2log(W)/p)$.

Let us stick with the implementation details now.

2.3.1 Splitting

Since the upper bound in the loop ($I3$) is not constant, trivial splitting of ($I2$) will produce p subtasks $[1,...,N/p),[N/p,...,2N/p),...,[(p-1)N/p,...,N]$ with increasing time complexity of subtasks. At the end this would produce a situation where the first subtasks are completed having the relevant CPUs idling while the last subtasks would still be in computation.

There are more ways how to solve it - (1) move the splitting of task into ($I3$), (2) splitting p tasks in ($I2$) in a proportional way, so that each subtask has the same computational cost or (3) split ($I2$) into many small subtasks which are successively distributed to CPUs according to their load. In real-life implementation we have chosen (3) because (1) tends to produce high overhead of the parallelization engine and (2) assumes that the underlying CPUs are equivalent in performance and accessibility (that breaks in many distributed environments).

3. Results

3.1 Tuning parameters

The algorithm was implemented based on the sections above, allowing all the strategies - exhaustive search or bisecting both in sequential and parallelized versions. The language used was C++, for parallelization openMPI implementation [9] of MPI standard was chosen, for bisection we used Brent minimization algorithm [10]. In order to find the proper splitting of the subtasks we analyzed measured time demands for a different fragmentation of the tasks, see Fig. 3.

We ran the optimality search for two sets of 1000 and 18000 spikes. In the case of the larger set we could see that taking any value below $f = 500$ gives approximately the same time demands. On the very beginning there is a visible peak caused by the growth of the load by the parallelization maintenance (i.e. the cost of distributing subtasks starts to be larger than computation of subtasks themselves). From $f = 500$ we could see gradual growth caused by the insufficient fragmentation (i.e. some CPUs are needlessly idle and waiting for other unfinished subtasks).

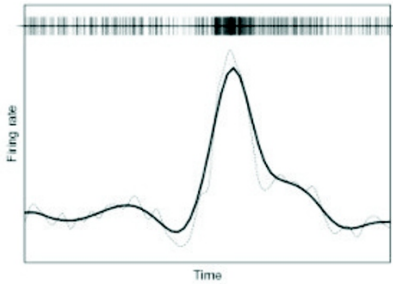

Fig.1. Illustration of the problem. The thick line is the original λ, the top line shows experimentally measured spike train generated from this function, the thin line is firing rate $\hat{\lambda}$, which we try to optimize.

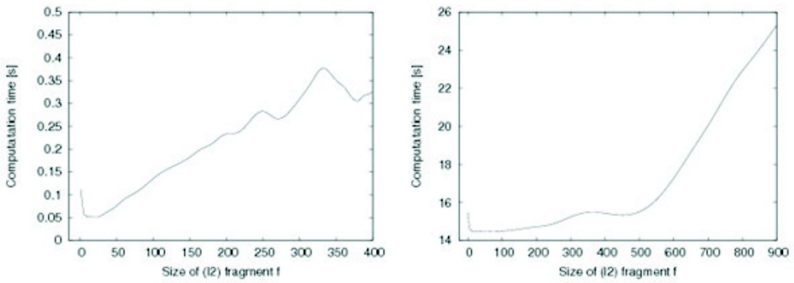

Fig. 3. Figure shows how splitting affects time performance of the computation. The left panel presents the case, where the input data were 1000 spikes, while the input for the right panel was 18000 spikes. Both sets were taken from the real experimental data, bisection was used in this case. f is the size of one (fixed) subtask, that is the number of (I3) iterations.

Tab. 1. Comparison of time demands.

Method	Time (min:sec)
Sequential search	58:41
Parallel search	4:14
Sequential bisection	2:43
Parallel bisection	0:09

As the number of spikes in the input set will decrease, this value will also decrease, as the results for the set of 1000 spikes show. Here we could see similar properties as far as the shape is concerned, but the total time needed for computation is now negligible.

This leads to the final choice of f = 100, which will be always sufficient for any larger input sets. As it can be seen in the left panel of Fig. 3, it is a reasonable value even for small sets, but that is not so important due to small total time demands. This value is, of course, dependent on the particular computational setting - in our case all tests have been done on a small cluster with 20 CPU cores.

3.2 Real time demands

For the comparison of real-time improvements we offer the table below. The input data and parameters were the same for all the tasks: 18000 spikes, [1;400] ms range for bandwidth, precision of 1 ms (W=400/1).

4. Discussion

We have proposed and implemented a parallel algorithm for optimal kernel bandwidth search which has better time performance than its "straightforward" version. Moreover when the function (1) is unimodal on the given range, we can use the bisecting version, which reduces the time even more drastically. To check the reasonable ranges, one can do the first trial run which uses only few sampling points (and in fact cannot be omitted even in normal case).

This performance boost does not play an important role in the case of small input sets of spikes, however, it is significant in case of large sets. The whole work was motivated by real demands, when experimental sets of ~20000 spikes were evaluated and, moreover, their subsets also needed to be evaluated the approximate knowledge of the function (1) shape reduced the need for a slow version of the algorithm.

At the end we proposed tuning parameters for an example cluster configuration and provided actual results of the performance improvement.

Acknowledgments

The work was supported by the grant SVV-2010-265 513.

References

[1] Shimazaki H., Shinomoto S:. Kernel bandwidth optimization in spike rate estimation. Journal of Computational Neuroscience 2010; 29: 171182.

[2] Cunningham J.P., Gilja V., Ryu S.I., Shenoy, K.V.: Methods for estimating neural firing rates, and their application to brain-machine interfaces. Neural Networks 2009; 22 (9): 12351246.

[3] Sanderson A.C.: Adaptive Filtering of Neuronal Spike Train Data. IEEE Transactions on Biomedical Engineering 1980; 27 (5): 271 274.

[4] Richmond B.J., Optican L.M., Podell M., Spitzer H.: Temporal encoding of two-dimensional patterns by single units in primate inferior temporal cortex. I. Response characteristics. J Neurophysiol 1987; 57 (1): 132146.

[5] Richmond B.J., Optican L.M., Spitzer H.:. Temporal encoding of twodimensional patterns by single units in primate primary visual cortex. I. Stimulus-response relations. J Neurophysiol 1990; 64 (2): 351369.

[6] Paulin M.G.: Digital filters for firing rate estimation. Biological cybernetics 1992; 66 (6): 525531.

[7] Paulin M.G., Hoffman L.F.: Optimal firing rate estimation. Neural Networks 2001; 14 (6-7): 877 881.

[8] Nawrot M., Aertsen A., Rotter S.: Single-trial estimation of neuronal firing rates: From single-neuron spike trains to population activity. Journal of Neuroscience Methods 1999; 94 (1): 81 92.

[9] Gabriel E., Fagg G.E., Bosilca G., Angskun T., Dongarra J.J., Squyres J.M. et al:. Open MPI: Goals, Concept, and Design of a Next Generation MPI Implementation. In: Proceedings, 11th European PVM/MPI Users' Group Meeting 2004; 97104.

[10] Brent R.P.: Algorithms for minimization without derivatives. Dover Pubns; 2002.

Contact
Mgr. Pavel Šanda
Institute of Physiology,
Academy of Sciences of the Czech Republic
Vídeňská 1083
142 20 Prague 4
Czech Republic
e-mail: ps@ucw.cz

Jitter Effect on the Performance of the Sound Localization Model of Medial Superior Olive Neural Circuit

Pavel Šanda[1,2]

[1]Institute of Physiology, Academy of Sciences of the Czech Republic

[2]3rd Medical Department, First Faculty of Medicine, Charles University in Prague, Czech Republic

Abstract

Objectives: Additional properties of the stochastic neural circuit model suggested in [1] were studied.
Methods: The performance of the whole circuit when the system employs a different jitter was studied by extensive simulations. By performance we mean the time needed to obtain a reliable estimate of ITD.
Results: It was found that the relation between jitter and performance is nonlinear and we estimated a plausible range of jitter values for the model.
Conclusion: To conclude, there exists an upper bound of the timing jitter since the number of neurons needed to compensate the injected noise grows exponentially and above certain jitter values becomes unrealistically high.

Mgr. Pavel Šanda

Keywords

Medial superior olive (MSO), stochastic model, timing jitter, interaural time difference (ITD)

Correspondence to:

Mgr. Pavel Šanda
Institute of Physiology, Academy of Sciences of the Czech Republic
Address: Videnska 1082, 142 20 Prague 4, Czech Republic
E–mail: sanda@biomed.cas.cz

EJBI 2011; 7(1):51–54
recieved: September 10, 2011
accepted: October 31, 2011
published: November 20, 2011

1 Introduction

The way mammalian brain localizes sound azimuth remains a matter of discussion. The current textbook view is based on the theory of delay lines proposed a long time ago by [2].

Although there is a strong experimental evidence that delay lines implemented by the branching pattern of neuronal fibers are present in the Nucleus Laminaris in birds [3], experimental evidence for such branching pattern in the Medial Superior Olive (MSO - counterpart of bird's NL) in mammals remain weak [4] and alternative theories have been proposed [5].

In a specific variant of the slope-encoding model [6] proposed in [1] the interaural time difference (ITD) is encoded by the firing rate of the first binaural neuron. This rate is driven by coincidence detection of the action potentials coming from time locked ipsi- and contralateral inputs shifted by ITD and additional jitter added to the system. Under certain conditions each ITD value corresponds to a unique value of the firing rate, thus the imaginary observer monitoring output of such a neuron is able to estimate ITD only by interpolation from its firing rate.

The role of noise in this model is ambiguous. On the one hand it allows a finer distribution of recognized ITD values, on the other hand higher values deteriorate the estimation performance of the circuit.

This performance decline was indicated in [1] for two circuits with different jitter. The aim of this report is to extend the previous result and show quantitatively how jitter affects performance of the whole range of circuits defined by different jitter values.

2 Methods

The circuit operates at an abstract level of description without explicit membrane potential regarding spikes as single time point events and consists of several consecutive processing stages (see Fig. 1):

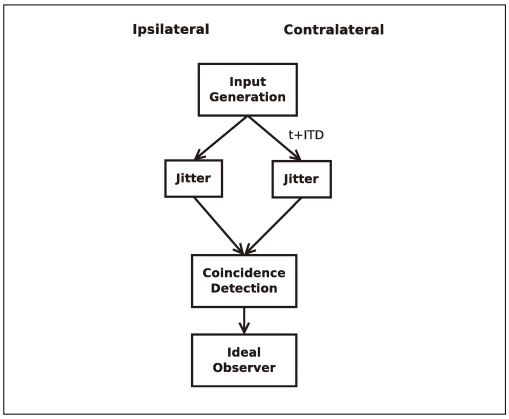

Figure 1: Scheme of successive processing stages of the circuit.

- A generator of action potentials simulates time-locked inputs, impulses from the contralateral side are shifted in time by ITD value. The frequency of generation is set to 140 Hz as in the previous study.
- A jitter generator which represents noise occurring in the circuit during the signal transmission along the auditory pathway. It is parametrized by a single value. It should be noted that each different parameter value defines a different circuit since it changes the characteristic ITD *interpolation curve* used for interpolation. Together with the spike generator they can be considered as a very simplified counterpart to the auditory pathway up to the MSO (where the signal from the left and right ear used for sound localization based on low sound frequencies converges). In this stage each spike is shifted in time by small random jitter Δ which is parametrized by jitter magnitude J, more precisely $\Delta = J(B(2,4) - 0.5)$, where $B(a,b)$ is a random variable from the beta distribution with parameters a, b.
- A coincidence detector representing the first binaural neuron. It generates a new spike only in case two input spikes occur within a short time window and in a specific order when contralateral spike precedes the ipsilateral one.
- An observer which collects output of the previous processing stages and estimates the ITD value computed by the circuit. It can be seen as a counterpart of higher processing stages which measure how much information can, in principle, be obtained from the rate coded presented by a single binaural neuron.

Details of the stages above are identical to those in [1] except for one important feature. Fixed parameters of the circuit define the ITD interpolation curve as seen in Fig. 2. In our previous study this curve was carefully fitted to a fixed sinusoidal function and the inverse of this function was used to interpolate ITD from estimated firing rate.

In Fig. 2 we can see how jitter J dramatically changes this curve. Since we will use the whole range of different jitter values we cannot rely on the fitted function anymore and we shall use directly this interpolation curve. Conceptually, this is not adding anything new, however, it leads to additional computational difficulties - for each jitter value a circuit ITD curve must be recomputed anew and an inverse mapping from firing rate to ITD must use a more elaborate interpolation mechanism since the curve is not locally strictly monotonous.

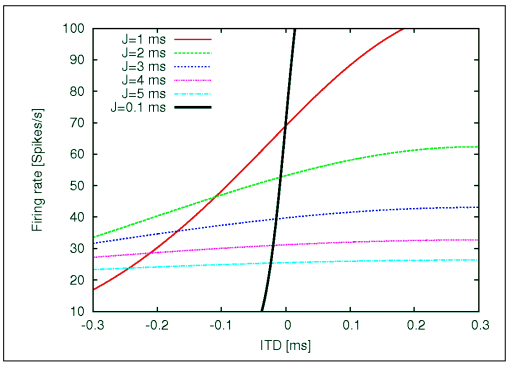

Figure 2: ITD interpolation curves for circuits with a different jitter value. Each firing rate value corresponds to an ITD value and is uniquely determined in case the function is strictly increasing in the ITD values under scrutiny. We see that increasing jitter leads to smaller slopes of the interpolation curve and we expect a deteriorated circuit performance for higher jitter values.

3 Results

Each jitter value defines a new circuit and after computing its interpolation curve we let the circuit estimate a single ITD value while observing how the estimate develops in time. This way we obtain asymptotic behaviour for each circuit, see Fig. 3.

From psychophysical experiments we know that the precision of azimuth estimation in a human is approximately 4° in the head-on direction [7]. We define that the time needed for reliable estimation of ITD is identical with the last-passage-time (LPT) of the 4° precision region, see the area delineated by horizontal dotted lines in Fig. 3.

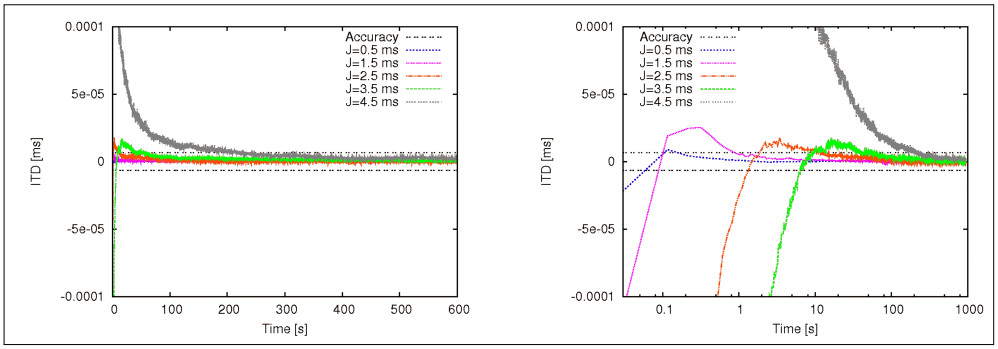

Figure 3: Asymptotic behaviour of ITD estimation produced by observer for selected values of jitter J. The original azimuth was selected as $ITD = 0$. Horizontal lines delineate the region when desired precision of ITD estimate was achieved ($\pm 2°$). For each line we can define the last passage time (LPT) when the function enters the region and remains inside of it. We see that increasing jitter leads to the increase of LPT value. Each line is an averaged function from 1000 simulation runs.

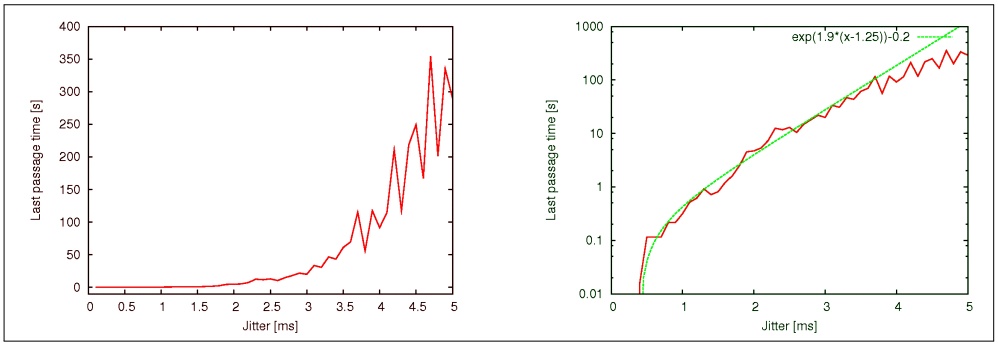

Figure 4: Dependence of last-passage-times on different jitter values. On the right hand side the same plot in logarithmic scale. We fit $f_{fit}(x)$ in such a way to be as close as possible in the interval of 0.1 - 10 s of LPT. This will be subsequently used for relating plausible jitter ranges, see text.

In this way we obtain unique LPT for each circuit with specific jitter value, as plotted in Fig. 4. As we can see, the functional dependence is nonlinear and can be approximately fitted by $f_{fit}(x) = e^{1.9(x-1.25)} - 0.2$.

Obtained circuit's LPT time t_A corresponds to the processing time of a single binaural neuron in MSO needed to estimate ITD. Because the auditory pathway consists of many parallel fibers and processing of the signal is simultaneous, we used the ergodic hypothesis in our previous study.

In short, we assume that when a single neuron of this type requires the time t_A, n neurons working in parallel need the time t_A/n to produce equivalent information subsequently used in higher stages of the pathway (represented by the concept of the observer).

The number of binaural neurons working in parallel is difficult to estimate but does not exceed hundreds of units. Next, we know from psychophysical experiments that the time t_A needed for azimuth estimation ranges around 150 - 300 ms in human subjects [8].

This allows us at least to connect specific jitter value J with the required number of neurons n in order to obtain t_A (let us fix $t_A = 0.2$ s). By employing the ergodic hypothesis we get $t_A = \frac{LPT(J)}{n}$ and from fitting $f_{fit}(J) LPT(J)$, hence

$$n = \frac{f_{fit}(J)}{t_A} = \frac{e^{1.9(J-1.25)} - 0.2}{0.2} \,. \qquad (1)$$

To sum up, we obtain that the physiologically plausible range of simultaneously working neurons $n \in [1; 100]$ corresponds to jitter range $J \in [0.7; 2.8]$, which also implies plausible jitter values for the canonical set of parameters of this model.

4 Discussion

Irregularities in spike timings observed in physiological recordings were originally thought to be the result of neuronal cells unreliability and it was assumed that the

firing-rate neural coding scheme is used because of its robustness against the noise present in neuronal activity. Later decades have shown that what was often considered as erratic behaviour was rather a misunderstanding of the transmitted code [9] and it turned out that neurons are capable of reliable and precise spike timing [10] needed for so-called temporal coding. Coincidence detection of precisely timed input spikes is an important concept in theories of binaural hearing and we suggested one variant of such a model in a stochastic neural circuit in [1].

This time we focused specifically on the role of jitter. In the previous study the jitter parameter was fixed to $J = 1$ ms which is in a good agreement with experimental findings [11]. Here we took a further step and estimated a range of possible values based on circuit performance. We should, however, note that this analysis is bound to the canonical set of basic circuit parameters. For example, the spike generator frequency also has an impact on the overall performance of the circuit; in the previous study we employed a more detailed model of the auditory periphery [12] and we could observe a decrease of overall performance of the circuit. This result cannot be, however, so easily incorporated since one processing stage (bushy cells layer) is missing. There are indications that this layer is able to provide better time locking and consequently improve coincidence detection in binaural neurons — that can be another example of a somewhat unexpected observation that higher processing stages of neural circuity increase the accuracy of phase locking [13].

Another problematic point is that the number of parallel circuits employed in ITD estimation is not experimentally known. This parallelism would have a strong impact on the overall performance as well, and we have at least shown the correspondence between jitter and the required number of neurons (or vice versa). By employing the ergodic hypothesis we can conclude that due to (1) the number of neurons needed to compensate the injected noise grows exponentially and above certain jitter values becomes unrealistically high. This gives us an approximate upper bound of jitter allowed for this type of circuit.

Acknowledgments

The work was supported by the grant SVV-2011-262 514 of Charles University in Prague.

References

[1] Sanda P, Marsalek P. Stochastic InterpolationModel of the Medial Superior Olive Neural Circuit. Brain Res. 2011;in press.

[2] Jeffress LA. A place theory of sound localization. J Comp Physiol Psychol. 1948;41(1):3539.

[3] Carr CE, Konishi M. Axonal delay lines for time measurement in the owls brainstem. Proc Natl Acad Sci USA. 1988;85(21):83118315.

[4] Grothe B. New roles for synaptic inhibition in sound localization. Nat Rev Neurosci. 2003;4(7):540-50.

[5] Jennings TR, Colburn HS. Models of the Superior Olivary Complex. In: Meddis R, Lopez-Poveda EA, Fay RR, Popper AN, editors. Computational Models of the Auditory System. Springer, New York; 2010. p. 6596.

[6] McAlpine D, Jiang D, Palmer AR. A neural code for low-frequency sound localization in mammals. Nat Neurosci. 2001;4(4):396401.

[7] Mills AW. Auditory Localization. In: Tobias JV, editor. Foundations of Modern Auditory Theory. New York: Academic Press; 1972. p. 303348.

[8] Middlebrooks JC, Green DM. Sound Localization by Human Listeners. Annu Rev of Psychol. 1991;42(1):135159.

[9] Barlow HB. Single units and sensation: a neuron doctrine for perceptual psychology. Perception. 1972;1(4):371394.

[10] Mainen ZF, Sejnowski TJ. Reliability of spike timing in neocortical neurons. Science. 1995;268(5216):15031506.

[11] Oertel D, Bal R, Gardner SM, Smith PH, Joris PX. Detection of synchrony in the activity of auditory nerve fibers by octopus cells of the mammalian cochlear nucleus. Proc Natl Acad Sci USA. 2000;97(22):1177311779.

[12] Meddis R. Auditory-nerve first-spike latency and auditory absolute threshold: A computer model. J Acoust Soc Am. 2006;119(1):406417.

[13] Carr CE, Heiligenberg W, Rose GJ. A time-comparison circuit in the electric fish midbrain. I. Behavior and physiology. J Neurosci. 1986;6(1):107.

